ABSTRACT

SURFACE-ENHANCED RAMAN DETECTION OF GLUCOSE ON SEVERAL NOVEL SUBSTRATES FOR BIOSENSING APPLICATIONS

by
Laila Alqarni

The small normal Raman cross-section of glucose is considered to be a major challenge for its detection by Surface Enhanced Raman Spectroscopy (SERS) for medical applications. These applications include blood glucose level monitoring of diabetic patients and evaluation of patients with other medical conditions, since glucose is a marker for many human diseases. This dissertation focuses on Surface-Enhanced Raman Scattering primarily for the detection of glucose. Some experiments also are carried out for the detection of the corresponding enzyme glucose oxidase that is used in electrochemical glucose sensors and in biofuel cells. This project explores the possibility of utilizing Surface Enhanced Raman Spectroscopy (SERS) with a variety of substrates (e.g., commercial gold substrates, nanocrystalline silver and gold nanoparticles, which are chemically assembled by citrate reduction on graphene-like sheets, silver nanoparticles on a commercial graphite sheet, and on electrochemically deposited polypyrrole conducting polymer) for glucose, rhodamine 6G (R6G) dye and glucose oxidase detection. These newly fabricated substrates can also be used for biosensing applications. The results of our study demonstrate that SERS is capable of detecting the molecules with high enhancement factor. This work reports the use of commercial multilayer graphene sheets as substrates on which gold nanoparticles are chemically assembled by citrate reduction. The results show that these substrates are capable of providing SERS enhancement factors of up to 10^{10} with a detection limit to 10^{-8} M in aqueous solutions of glucose. The SERS performance on graphene substrates are many orders of magnitude higher compared with results on gold-coated chemically

etched Klarite® commercial silicon substrates. Also, drop-coated Ag on Toray® graphite microfiber sheets with partition layers exhibit the best results; they yield an excellent enhancement for R6G and glucose detection limit to 10^{-16} M and 10^{-12} M of the dye and glucose molecules, respectively. Also, the results show for the first-time enhancement for glucose from a SERS substrate that consist of electrochemically fabricated polypyrolle (PP) on Toray® graphite microfiber sheets.

SURFACE-ENHANCED RAMAN DETECTION OF GLUCOSE ON
SEVERAL NOVEL SUBSTRATES FOR BIOSENSING APPLICATIONS

by
Laila Saad Alqarni

A Dissertation
Submitted to the Faculty of
New Jersey Institute of Technology
in Partial Fulfillment of the Requirements for the Degree of
Doctor of Philosophy in Chemistry

Department of Chemistry and Environmental Science

May 2019

APPROVAL PAGE

**SURFACE-ENHANCED RAMAN DETECTION OF GLUCOSE ON
SEVERAL NOVEL SUBSTRATES FOR BIOSENSING APPLICATIONS**

Laila Alqarni

Dr. Zafar Iqbal, Dissertation Co-Advisor	Date
Research Professor of Chemistry and Environmental Science, NJIT	

Dr. Tamara Gund, Dissertation Co-Advisor	Date
Professor of Chemistry and Environmental Science, NJIT	

Dr. Nuggehalli M Ravindra, Committee Member	Date
Professor of Physics, NJIT	

Dr. Yong I. Kim, Committee Member	Date
Assistant Professor of Chemistry and Environmental Science, NJIT	

Dr. Yuanwei Zhan **,** Committee Member	Date
Assistant Professor of Chemistry and Environmental Science, NJIT	

BIOGRAPHICAL SKETCH

Author: Laila Alqarni

Degree: Doctoral of Philosophy

Date: May 2019

Undergraduate and Graduate Education:

- Doctor of Philosophy in Chemistry,
  New Jersey Institute of Technology, Newark, NJ, 2019

- Master in Science in Chemistry,
  King Abdul Aziz University, Jeddah, Saudi Arabia, 2009

- Bachelor of Science in Chemistry,
  King Adul Aziz University, Jeddah, Saudi Arabia, 2006

Presentations and Publications:

Alqarni L., Leng B, &Zafar Iqbal (2018), Using partition layer to improve the
efficiency for Graphene like sheet substrate for glucose detection. American
Chemical Society(analytical chemistry). Under review

Alqarni, L., & Iqbal, Z. (2017). Surface-enhanced Raman spectroscopic sensing of
glucose. European Pharmaceutical Review, 22(6), 23-26.

Danthi Shivaram V., Liu R., Panchhi N, Alqarni L., Daroowalla R., Du S., Liu Y.,
Chow T. &Ravindra N. (2019), Magnetically Augmented Rotational Systems,
The Minerals Metals Materials Society Conference Proceedings.

Al-turkustani, A., Arab, S. T.,& Alqarni, L. (2010). The Use of Ruta Chalepensi as
Corrosion Inhibitor for Steel Corrosion in 2.0M Sulphuric Acid
Solution. Oriental Journal of Chemistry, 26(2), 437-454.

Al-Turkustani, A., Arab, S. T., & Alqarni, L. (2011). Medicago Sative Plant as Safe
Inhibitor on The Corrosion of Steel in 2.0 M H_2SO_4 Solution. Journal of Saudi

Chemical Society, 15(1), 73-82.

Alqarni L., Leng B., &Iqbal Z. (2017), Gold Nanoparticles Assembled on
Multilayer Graphene Sheets for Surface Enhanced Raman Spectroscopy of
Glucose. Material Research Society, Poster

Alqarni L., Leng B., & Iqbal Z. (2018), Nanoparticles Assembled on
Multilayer Graphene and Graphite Sheets for Surface-Enhanced Raman
Spectroscopy of Glucose, The Minerals Metals Materials Society, Poster

Alqarni L., Leng B. & Iqbal Z. (2018), Gold Nanoparticles Assembled on
Multilayer Graphene Sheets for Surface Enhanced Raman Spectroscopy of
Glucose and Related Organic Pollutants, 17th International Conference
on industrial Chemistry and Water Treatment (1671[th]of Conference Series LLC
Ltd),Poster

Alqarni L., Leng B. & Iqbal Z.(2018), Surface Enhanced Raman Detection
of Glucose on Different Substrate for Biosensing Applications, 256th American
chemical society national meeting, Poster

Leng, B., Alqarni, L., & Iqbal, Z. (2017). Biofuel Cells with Pressure-Immobilized
Enzymes on Carbon Nanotube Sheets. Bulletin of the American Physical
Society, 62.

I dedicate this dissertation to my beloved husband Khaled; my parents, Fatimah and

Saad, my brothers and my lovely kids, Mishaal and Lara . Without them, this

dissertation would have never been written. I am grateful to have them in my life.

ACKNOWLEDGMENT

I extend my deepest appreciation to those who have helped me, supported me and guided me to achieve my dream of obtaining a Ph.D.; you light up my life and leave behind wonderful memories. These memorable five years is a treasure for my future. Here, I feel honored to have the opportunity to appreciate the following people who made my life gorgeous.

I would like to express my sincere gratitude to my advisor ,Prof. Zafar Iqbal for the continuous support of my Ph.D. study and related research, for his patience, motivation, and immense knowledge. His guidance helped me in my research and writing of this dissertation. I could not have imagined having a better advisor and mentor for my PhD study. Besides my advisor, my thanks also go to the members of my committee: Prof. Tamara Gund for agreeing to serve as a co-advisor, Prof. Nuggehalli Ravindra, Dr. Yong I. Kim, and Dr. Yuanwei Zhan, for their insightful comments that improved the dissertation and content of this dissertation.

My sincere thanks also go to Prof.Ravindra, Dr.Wang, and Mr. Tien See Chow who provided me an opportunity to join their team as intern, and who gave me access to the laboratory and research facilities. Without their precious support, it would not have been possible to conduct this research.

Additionally, I want to express my warmest thanks to my team members, Bio Leng and El-Mostafa ben Shafique.

I would like to gratefully acknowledge Al-Baha University for the financial support throughout my Ph.D. study. Without this financial support, I would not have been able to achieve my goal.

TABLE OF CONTENTS

TABLE OF CONTENTS
(Continued)

LIST OF TABLES

LIST OF FIGURES

CHAPTER 1

INTRODUCTION

1.1 Objective

The primary goal of the research, conducted in this thesis, is to understand and develop Surface-Enhanced Raman Spectroscopy (SERS) for the detection of the biologically important glucose molecule. We have focused here on developing a SERS sensor for glucose detection using thin, cost-effective carbon-based substrates on which nanoscale gold and silver (for example, nanocrystalline silver and gold nanoparticles chemically assembled by citrate reduction on graphene-like sheets, silver nanoparticles deposited on sheets of graphitic fibers, and electrochemically prepared conducting polymer polypyrolle on gold coated sheets of graphitic fiber) are deposited and stabilized. For purposes of comparison, detection of the dye molecule Rhodamine 6G on the carbon-based substrates, and of glucose on commercial nanostructured gold-coated silicon substrates (Klarite®), were performed.

We have concentrated in this work on achieving glucose sensing to below 10^{-10} M for potential medical applications by the use of triethylene glycol (TEG) partition layers on the substrates to stabilize the metal nanoparticles, and used novel approaches for SERS, such as incorporation of conducting polymer polypyrrole, graphene-like and carbon microfiber sheets and plasma-treatment. In addition, we have initiated preliminary theoretical modeling to provide an understanding of the effect of TEG partition layers in SERS.

1.2 Background

SERS was discovered by Fleischmann, Hendra and McQuillan at Southampton University in 1974[1]. In the early experiments, the researchers discovered remarkably enhanced intensity of the Raman spectrum of pyridine on a silver electrode [1]. Subsequent work in the late 1970s by other researchers confirmed the discovery of SERS on a wide range of organic molecules [2, 3], showing enhancements of 5 to 6 orders of magnitude of the Raman cross-section. It was concluded that the enhancement is due to surface plasmons on a roughened, nanostructured metal surface [4, 5] on which the analyte molecules are adsorbed [6].

SERS typically occurs on nanoparticles of silver and gold, or on related nanostructures such as nanowires. It is , therefore, of vital importance in chemical sensing and analysis because it combines high detection sensitivity with the unique fingerprint capability of normal Raman spectroscopy. A major problem for SERS, however, is the lack of substrate reproducibility and uniformity.

As noted above, SERS arises from surface plasmons that are collective oscillations of the electron charge density in metals and originate from quantization of these oscillations in electron density relative to the fixed positive ions in the metal. Optical features associated with the plasmon frequency are transferred to the metals [7] via localized surface plasmon resonance (LSPR), which is an optical event that takes place following interaction of electromagnetic radiation with metal nanoparticles but is lower in intensity than that of the incident radiation. Hence, the stimulation of conduction band electrons is performed by the incident light electric field resulting in coherent localized plasmon oscillations with a

large frequency dependence on the geometry, composition, size, dielectric environment, and nanoparticle separation.

1.2.1 The SERS Mechanism

Enhancement of Raman intensities occurs as a result of the interaction of the molecular polarizability derivative with the incident electromagnetic field of the excitation laser. This scenario leads to two mechanisms. The first one involves the field intensity enhancements relevant to the excitation of plasmon resonance, and the second is concerned with the polarizability enhancement as a result of chemical influences, such as excited states with charge transfer [7-13]. The first mechanism covers the field intensity enhancements resulting from the excitations of plasmonic resonance as shown schematically in Figures 1.1a and b.
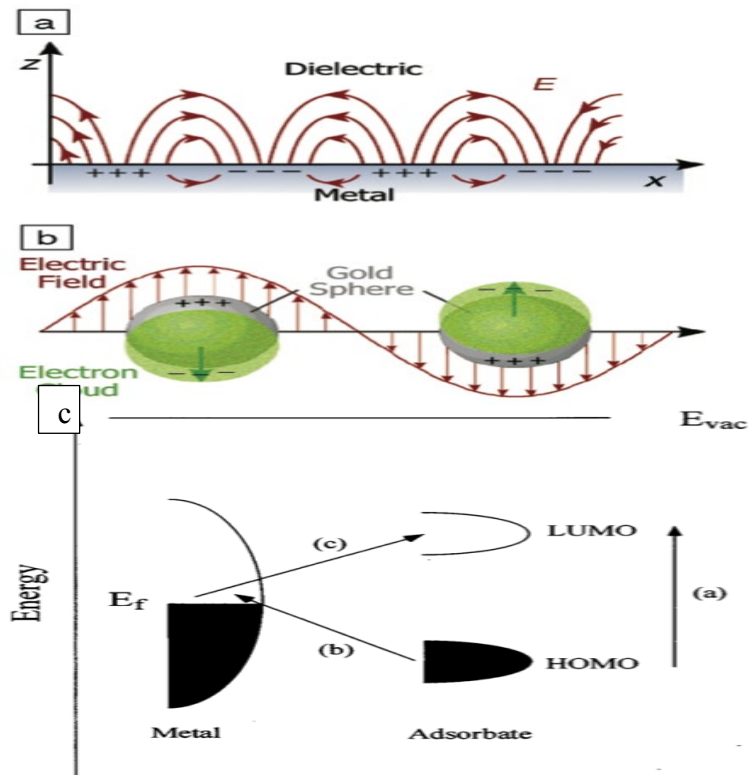
Figure 1.1 (a-c): Collective electron oscillations at metal-dielectric interfaces and metal-adsorbate band structure. More details are provided in the text.
Source: [14].

In Figure 1.1a, collective electron oscillations at a metal-dielectric interface is illustrated; in Figure 1.1b collective electron oscillations of nanoparticles of spherical metals are shown [14]; and collective electron excitation in the metal nanoparticle substrate conduction band is depicted in Figure 1.1c.

charge transfer between metal and adsorbate [15] is affected with electromagnetism which determines that the approximate value of E, the enhancement factor of one particle is:

$$E=|E(\omega)|^2 \, |E(\omega^1)|^2 \qquad (1.1)$$

where $E(\omega)$ is the local factor of the electric field enhancement at frequency ω and $E(\omega^1)$ is the local factor at the Stoke-shifted frequency (ω^1).

In the majority of SERS experiments, the average value of E is over the particles' surface area with possible adsorption of molecules for generating the enhancement. On the other hand, E_{max}, the maximum enhancement factor in a single SERS molecule has a significant value. E_{max} has greater magnitude than E. As for isolated homogeneous particles, it can be assumed that the enhancement factor is overestimated by a factor of three or more.

The second mechanism is related to the chemical effect which involves charge transfer in the excited states. There is a certain dependence of the electromagnetic enhancement on the roughness of the metal surface, which can be attained via the following methods: Lithography, oxidation and reduction reactions on the surface electrodes, metal colloids, deposition of metal particles on a substrate, deposition of polystyrene nanospheres, and others. Chemical enhancement is due to the modification of adsorbate electronic states by its chemisorption on the metal leading to a charge transfer process involving the excitation wavelength.

Researchers have studied SERS in various analytes after adsorption on noble and coinage metals Au, Ag, and Cu, or on reactive alkali surfaces of Na, Li, and K metals, followed by excitation in the visible region of the optical spectrum. In theory, most metals can exhibit surface enhancement; however, the best results are obtained when gold, coinage and alkali metals are used. Aggregation of analytes on SERS substrates is also known to lead to loss of SERS activity.

In the course of the past twenty years, the improvement of substrates has

experienced significant progress as a result of the technological success of nanotechnology that facilitated new types of fabrication approaches [16, 17]. SERS investigators use different dyes as standard molecules for trace level detection; for instance, they use crystal violet or Rhodamine 6G [18, 19] because of its intense Raman scattering properties related to resonance. Also benzenethiol has been used [16] because it can create SAMs or self-assembled monolayers on SERS active substrates.

There are a number of advantages of SERS. Because it is related to vibrational spectroscopy, the data provided by SERS regarding the local environment in condensed phases and molecular structure exceeds that provided by fluorescence or other electronic spectroscopy techniques. Significant quenching of interference due to fluorescence occurs as a result of SERS with the analyte present in the vicinity of the active metal or on it. This provides non-radiative ways for the decay of the excited states in some SERS experiments. Since Raman selection rules are unique, SERS data can provide unique molecular structural information. It is also possible to discern small changes in adsorbate orientation with SERS as slight changes in molecular orientation can give rise to measurable shifts in the SERS data. SERS can also be used to observe low frequency vibrations beyond the range detectable by IR spectroscopy provided that the instrumentation available is adequate [20]. The application of SERS can therefore be used for biomedical research investigations on tissues and cells in the body, identification of forbidden substances, biomedical processes, pharmaceutical research, and product authentication.

1.2.2 Hot Spot Model for SERS

SERS is the phenomenon in which the intensity of Raman scattering, emanating from molecules adjacent to metallic nanocrystals of a certain type, is enhanced by visible light excitation [21]. The optical transitions (plasmons) of gold (Au) and silver (Ag) electronic states, under the excitation of visible light, may be intense to an extent that the local electromagnetic field is intensified as illustrated in Figure 1.2.
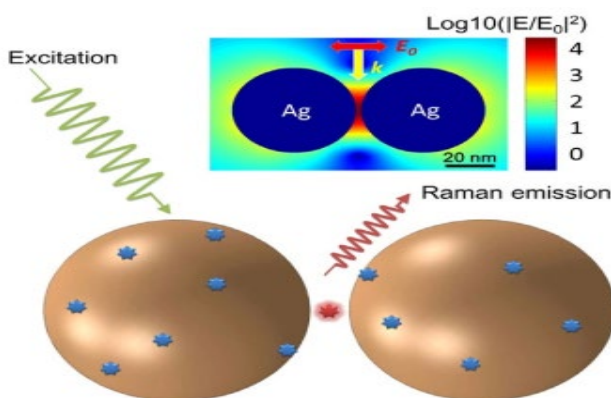
Figure 1.2 Schematic depiction of the hot spot mechanism of SERS.
Source:[22].

This property makes Au and Ag ideal antennas [23, 24] for enhancing Raman scattering. Rhodamine 6G (R6G) is one of the most commonly used dyes as a fluorescence tracer and also to substantiate uniaxial junction symmetry [23, 25]. Research shows that there is a significant correlation between two close nanocrystals to form the "hot spot" intensified electromagnetic field at the junction [26]. The analytical solutions to Maxwell's equations also illustrate that SERS amplification at the junction is increased to 10^{11} and beyond as the gap between 30 nm nanocrystals decreases to about 1 nm. This is an inherent case for SERS within the constraints that the two nanoparticles are almost in contact; thus,

there is only a limited space for few molecules within the same junction. Figure 1.3

illustrates three Ag nanocrystals with one junction containing a R6G dye molecule.
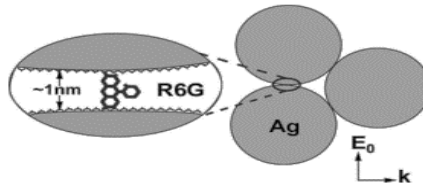
Figure 1.3 Schematic depiction of a nanocrystalline trimer with one junction containing a
R6G molecule.
Source: [23].

Trimers can exhibit a series of hot spots [27]. As mentioned by Brus (2008), as the

gap (*D*) between nanocrystals reduces, metallic polarization also amplifies on the metal

surface along the junction[23]. Figure 1.4 demonstrates metallic polarization density as a

function of the spacing between nanoparticles.
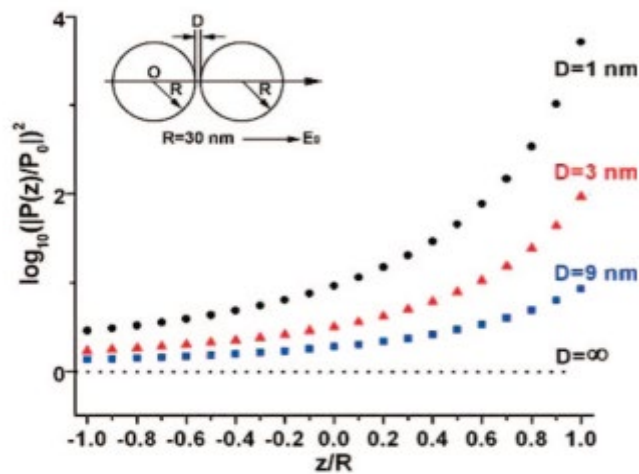
Figure 1.4 Logarithm of metallic polarization/cm^3 along the symmetry direction of the
dimer.
Source: [23].

Metallic polarization is constant when the nanocrystals are far apart. However, when the particles are very close, the polarization peaks on the nanoparticles' surfaces along the junction. According to Rycenga et al. [26], hot spots are located in the small inter-particle gaps in nano-particle aggregates. Moreover, coupling between the plasmons of the adjacent nano-particle in the dimer creates a large local electric-field enhancement along the inter-particle gap[28]. In the same context, the metallic polarization decays away from the junction towards the particle's back surface. Consequentially, the optically excited metallic polarization results in junction surface polarization. As the nanoparticles approach, the dipole P is excited along the junction. In that respect, adjacent particles excite other particles. Collectively, a surface polarization is created. In agreement with Brus (2008), Alonso-González, et al. (2011) demonstrated that the particle excitation as particles approach P is a quadruple moment around its center [29]. In other words, the scattering of light at the hot spot of effective optical antennae, such as Ag and Au, intensifies as the fourth power of the localized electromagnetic field. The underlying observation suggests that hot spot mechanism for both Raman (inelastic) and elastic scattering are the same. Figure 1.5 illustrates surface-enhanced light scattering, with (a) representing Raman scattering ($\omega_1 \neq \omega_2$) from an optical antenna (metal nanocrystal), and (b) illustrating an elastic scattering process where $\omega_1 = \omega_2 = \omega$.
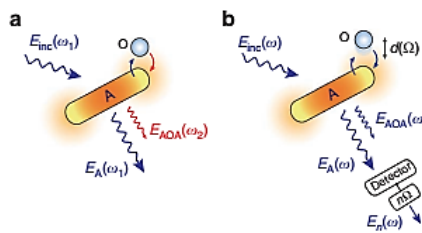
Figure 1.5 Illustration of surface enhancement of light scattering

Source:[29].

Noble metal nanostructures such as gold and silver can concentrate visible light into small volumes that significantly induced local electric fields on the junctions of the metal structures [30]. The amplified EM field becomes hot spots for SERS, which uses the enhanced field properties of the nano-particles to amplify the naturally weak Raman (inelastic) scattering signals. The excitation of metal particles can be differentiated from the excitation of molecules on the basis that the former have a stronger mutual particle interaction among its nanocrystals. In summary, as the distance between nanoparticles is reduced, the local electromagnetic field is intensified.

1.2.3 Raman Sensing of Rhodamine 6G Using Commercial Klarite® Substrates.

SERS investigators employ standard dye molecules such as the dye Rhodamine 6G (R6G) [19]. It is typically used because of its outstanding properties of strong resonance. The substrates comprise of photonic periodic crystal arrays of inverted pyramidal cavities of square shape with gold coating done by etching on a silicon wafer in order to ensure the inducing of Surface-Enhanced Raman Scattering. The previous research used SERS for the detection of low concentrations of R6G till to 10^{-9}M of R6G.

1.3 Summary

SERS remains one of the most sensitive and specific analytical chemistry techniques [27, 31]. It utilizes vibrational spectroscopy for the detection of analytes at very low concentrations. Other desirable characteristics include its interfacial generality and its ability to chemically analyze interfacial molecular species from the attomole, zeptomole mass to micro-molar and pico-molar concentrations [32, 33]. SERS is largely based on electromagnetic and chemical enhancements with the former being significantly dominant [34] . This is due to a surge in the local optical field which excites the molecule and the multiplying amplification effect coming off from the re-radiated scattered light [34]. For this to occur, the molecule has to be placed within a structured metal surface that supports electromagnetic resonance at a specific wavelength.

Chemical enhancement occurs due to the interaction of the metal surface and the adsorbent molecule and includes photon-induced charge-transfer enhancement, chemical bonding enhancement and resonance enhancement [35, 36]. Chemical enhancement commonly describes the optical resonance excitation occurring between adsorbate and the adatom [37, 38]. On the other hand, electrical enhancement is based on the interaction of both scattered and incident light with the substrate [34]. This results in the lightening rod effect referred to as localized surface plasmon resonance (LSPR) which has features that are common to SERS. According to Hammond et al. (2014) [34], LSPR provides the basis of SERS for biosensing. The frequency and strength of LSPR is influenced by substrate morphology, laser wavelength and the surrounding medium [39, 40] .

The Raman signal of the probe is commonly amplified via the LSPR excitation of the substrate which is normally in the form of metal particles [37, 41]. Consequently, the

magnitude of SERS is dependent on the substrate used (Sharma et al., 2013). Several factors have to be considered before choosing the optimal substrate to be used in SERS. First, the substrate must have higher SERS activity to ensure high sensitivity [35, 42-44] . This could be readily achieved through the tuning of interparticle distances between the nanoparticles to ensure that it matches the incident laser frequency as well as the coupling of nanoparticles. Substrates also need to be uniform with a minimum of deviations across the surface [45-48] . Other key factors defining substrates include reproducibility and good stability which is necessary in maintaining the electromagnetic enhancement [43]. The substrates are also required to be clean in order to adsorb both the strong and weak adsorbates as well as the unknown samples. Currently, there are few substrates that meet this criteria necessitating new methods for developing substrates [33, 49, 50]. Halloysite nanotubes which are used to form structured substrates [51] could also be used in SERS [52]. Layered aluminum halloysite is suggested to form a structured substrate [31, 36]. It also has no cap agent in the metal surface, making it well suited for SERS. Silver nano-arrays, prepared by vapor deposition, have also been identified as good substrates for SERS. Silver based substrates prevent any form of contaminant from binding into the surface in the process, resulting in increasing SERS features [53]. Graphene-gold substrates have been used in a number of applications including biosensors [43, 44]. Recently, graphene has become of one of the best substrate-based materials due to its inertness and compatibility with different metals during its use in SERS.

Development of biosensors is identified as one of the key areas where SERS has been applied. For example, the development of glucose based tests which show the varying levels of glucose in the blood could be detected through the use of a biosensor based on

the working principles outlined in SERS [32, 42, 54]. Electrochemical based sensors have moved from detection based on enzymatic reaction to changes detecting minute changes in the electrochemical levels. This quantitative form of monitoring is critical as it provides information on electrochemical changes occurring in blood. SERS allows for the development of glucose sensors which do not require any form of invasiveness to parts of the body. When gold or silver nano-spheres are used as the covering material for the substrate for SERS, the stability of the biosensor increases for about 14 days [43, 55]. Ideally, this indicates that SERS could be applied across a number of settings provided specific aspects related to the substrates are monitored frequently. Atomic layer deposition could be one of the methods used to deposit sequential self-limiting gaseous products to the substrate in a controlled manner. SERS can also be applied in the screening and identification of the different forms of cancers affecting an individual [51, 56, 57] . Therefore, the development of various substrates as well as the effectiveness of SERS could be used to develop effective diagnostics-based sensitive and specific tests.

1.4 Organization of the Dissertation

The dissertation is organized as follows:

Chapter 1 gives the characteristics of Raman spectroscopy in general and Surface Enhanced Raman spectroscopy in particular. It introduces the fundamental mechanisms of both conventional and Surface Enhanced Raman scattering, and it presents the characteristic features typical of the hot spot model for SERS. Furthermore, it gives an insight into the previous relevant studies in the literature.

Chapter 2 deals with the details of experimental techniques used in this dissertation. It gives explanations of the instrumentation used for Raman spectroscopy and the lasers used for SERS. Details of the surface enhancement factor and approaches to theoretical modeling of SERS are also discussed. In addition, other techniques used in this dissertation, such as cyclic voltammetry and scanning electron microscopy, are discussed.

Chapter 3 discusses results of SERS of glucose on spin-coated gold and silver nanoparticles, aggregated using calcium chloride. In addition, data of glucose placed on commercial nano-etched gold on silicon, referred to as Klarite®, is presented and interpreted.

Chapter 4 covers the results of SERS and subsequent discussion of glucose on drop-coated and chemically produced gold on graphene-like sheet substrate. The latter is used as the basis for conclusions made on the role of graphene enhancement from previous studies in the literature. The effectiveness of glucose sensing with the use of graphene-like sheet substrate is improved with the help of TEG partition layers. Further improvement of glucose detection is achieved by the use of plasma treatment of gold-coated graphene-like sheet with a TEG partition layer.

Chapter 5 presents the results of SERS and subsequent discussion of glucose on drop-coated chemically produced silver on Toray® graphite microfiber sheets in two variants: with the available partition layers and without them. The results of SERS and analysis of the role of glucose on drop-coated chemically produced gold on graphite microfiber sheets (Toray ®) with the use of partition layers are applied for the comparison with the relevant efficiency of using the same conditions and the same substrate with Ag

nanoparticles. Theoretical modeling is used to support the functions of the partition layers discussed in this chapter.

Chapter 6 presents the results of SERS on polypyrolle fabricated electrochemically by cyclic voltammetry on Toray® graphite microfiber sheets.

Chapter 7 summarizes the most important findings of the research and discusses potential applications in the biomedical area. In addition, guidelines and recommendations for future research are provided.

CHAPTER 2

FUNDMENTALS OF CONVENTIONAL AND
SURFACE-ENHANCED RAMAN SPECTROSCOPY

2.1 Raman Spectroscopy

Raman scattering is the inelastic scattering of photons by molecules in the solid, liquid and gaseous state that are excited to higher atomic vibrational or rotational energy levels. There is a wide range of applications where the role of Raman spectroscopy is crucial, for example, in biology, materials science, chemistry, condensed matter physics, and many other areas. The disadvantage of Raman scattering is its comparatively weak signal to noise ratio since it involves only approximately 10^6 -10^8 photons while the remaining photons give rise to Rayleigh scattering. Consequently, measurements of small sample amounts or dilute concentrations are challenging. Furthermore, useful Raman signals can be overwhelmed by fluorescence interfering with the scattering. One of the possible solutions is placing the analyte in the vicinity of nano-structured surfaces of silver, gold, or copper on that surface leading to enhancement of the Raman signal. This technique is referred to as SERS or surface enhanced Raman scattering[58] .

Raman scattering can be referred to as a phenomenon of light scattering or a secondary radiation which takes place in case of interaction of the light with subsequent scattering by molecules. The discovery of the mentioned phenomenon was done by Chandrasekhara Venkata Raman in 1928 [59]. Two years later, he was awarded with the Nobel Prize for this discovery in physics, and his name was given to the phenomenon of inelastic energy exchange between the matter and light.

The scenario of the Raman Effect has specific characteristics of light wavelength modification at the moment of deflection of a light beam by a molecule or a particle. Elastic or Rayleigh scattering can be presented as the light scattering effect of dominant characteristics that appears with the scattering of light off molecules without any exchange or shift in energy between the solid (molecules) and the light at the same frequency. Inelastic scattering or Raman light scattering is a relatively weak type of light scattering by crystal lattices or particles as a result of bond vibration. With the non-resonant interaction, this Raman scattering is known as spontaneous or anti-Stokes. Transfer of photon energy in Raman scattering is done in the framework of its interaction with molecules leading to the wavelength shift in the scattered light. Description of the interaction and scattering of light by molecules is done with the help of Rayleigh scattering and Raman light scattering theories.
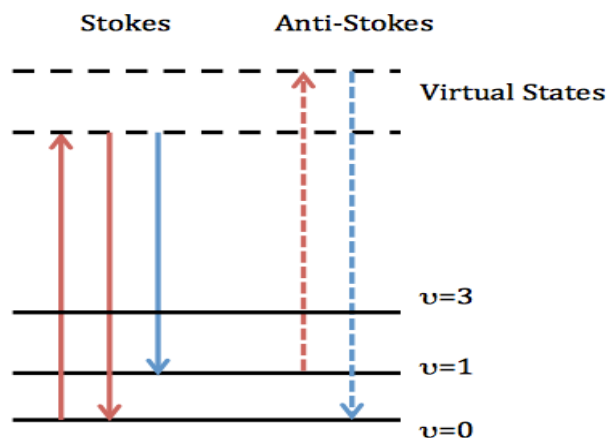
Figure 2.1.Various Types of Scattering The consequence of incident radiation is excitation into a virtual state that can be presented with the equation $E = h\nu_{ex}$. It is shown in Figure 2.1 with the help of a solid red line on the left. With the relaxation of the molecule and equality of the energy emitted by the photon to $E = h\nu_{ex}$, it is referred to as Rayleigh scattering (demonstrated with the second solid red line in Figure 1 on the left). The blue line of Stoke scattering has the energy of photons equal to $h(\nu_{ex} - \nu_v)$. It is required for the anti-Stokes scattering to have a molecule in the state of higher vibrational excitement; then, the energy of the emitted photon is the following: $E = h(\nu_{ex} + \nu_v)$.
Source: [59]

The described phenomenon can be referred to an event of low probability as inelastic scattering is experienced only by 1 out of 10^7. In the course of the interaction, the incoming photons carry the energy that causes the excitement of vibrational states in a solid or a molecule via the caused distortion of the clouds of electrons around intermolecular or molecular bonds in a solid. The consequence of the shifts that take place via the distribution of electron clouds is the alteration of the bond polarizability (α) and corresponding inducing of temporary dipole moment (P) with the excitement of solid or molecule into a virtual excited state with non-resonant interaction. As there is no infinite lifetime in the excited states, the time when the events are scattered is 10^{-12} seconds or even less; then,

there is the stage of relaxation of solid or molecules to the ground state back, with the photon emitted at the frequency (v_{vib}).

The difference in the energy available in the original state and the state of relaxation determines the modification of frequency in the light emitted from the incident light. Having relaxed to the state before the excitement, the solids or molecules cause the elastic scattering emitting the same light frequency (v). However, those solids or molecules which relax back to a vibrational state that differs from the previous one cause inelastic scattering emitting a photon that has a different energy. The shift in the frequency of generated photon is done by the amount which is related to the energy of a certain vibrational transition. In case the initial state is less energetic than the final state, there will be a shift in the emitted photon to a lower energy$(v - v_{vib})$. This change is referred to as a Stokes shift. In case the initial state is more energetic than the final state, there will be a shift of the emitted photon to a higher frequency $(v + v_{vib})$. The process leads to the anti-Stokes shift (see Figure 2.1). Inelastic photon scattering is caused by the explained shift in energy. There is a dependence of the difference in energy on the rotational, vibrational or, in case of solids, vibrational, molecule frequency within the states of liquids, gases, and solids; besides, it happens in case of vibrations between ions or molecules in a solid, being defined as Raman Effect.

The Raman effect is based on the theory suggested by Adolf Smekal, an outstanding Austrian physicist. It was developed five years earlier than the prediction of C. V. Raman about the availability of stray lines with the shifts in frequencies [60]. The inducing of dipole moments is done by an incident electromagnetic wave in the course of the interaction of light material. The dipole moment strength, P, is presented in the following:

$$P = \alpha E \qquad\qquad (2.1)$$

where α is the molecular polarizability tensor which ensures the measurement of the ease of distortion of the electron charge cloud around the molecular bond, while E is the electric field strength of the incident electromagnetic wave. Polarizability can be defined as the property of the material which relies on the incident electromagnetic radiation with the electrical field (E).

Taking into account the wave mechanics as the context for the molecule in the external electric field, the induced dipole moment can be presented as follows[61]:

$$P = \alpha_0 E_0 \cos(2\pi vt) \; (\frac{\partial \alpha}{\partial q})_0 q_0 E_0 \cos(2\pi(v+v_{vib})+ (\frac{\partial \alpha}{\partial q})_0 q_0 E_0 \cos(2\pi(v-v_{vib})t) \qquad (2.2)$$

Rayleigh   Anti-Stokes   Stokes

where $(\frac{\partial \alpha}{\partial q})_0$ is the change rate of α as related to q at the position of equilibrium. The study of the presented equation demonstrates that the creation of the induced dipole moments is done at such distinct frequencies as *v, (v - v_{vib}),* and *(v + v_{vib})*. The consequence is the scattered radiation taking place at the same three frequencies. There is correspondence of the scattered frequency number one to the incident frequency; thus, it results in elastic scattering, for instance Rayleigh or Mie. The other two types of frequencies experience the shift to higher or lower rates; thus, the processes are inelastic. In the latter two situations, the scattered light can be defined as Raman Scattering; the Stokes scattering refers to the longer wavelength and down-shifted frequency, while the Anti-Stokes scattering has the shorter wavelength and up-shifted frequency. Raman scattering can take place only in case of bond polarizability change as a bond length variation function in the course of vibration. It is ensured with the derivative of the

polarizability that is non-zero in case of a Raman-active vibration.

The signal in Raman scattering is generally weak as this event takes place rarely. Typically, Raman scattering covers merely 10^6-10^8 photons while the remaining protons undergo the Rayleigh type of scattering. As a result, there are certain problems with measurements in small amounts and dilute concentrations of sample. One more difficulty related to Raman scattering is the possibility of Raman signal to be overcome by the fluorescence. This limitation can be resolved with the enhancement of the Raman signal via setting the analyte near to the noble metal nano-structured surface made of silver, gold, or copper, or on that surface. This technique of measurement is known as SERS or surface enhanced Raman scattering [58].

The SERS implies the availability of enhanced intensity of Raman scattering by molecules on a nanostructured silver, gold or copper surface [6]. Nowadays, there are heated debates over the peculiarities of SERS mechanism; however, generally it is considered appropriate to ascribe it to a a combination of two mechanisms: charge transfer and electromagnetic enhancement mechanism, which contribute to a decrease in analyte molecules detection limit and corresponding increase in analyte signals [58]. The origin of EM, a key contributor to enhancement of Raman signals, is in the magnified electromagnetic field with the induction by a light-excited surface plasmon resonance [31]. A typical location of strong electromagnetic fields is in the nano-gaps between the metal nanostructures (so-called "hotspots") and at their the sharp corners [62]. Coexistence of CM with EM aims at a creation of a typical SERS system, on the basis of the transfer of charge between SERS substrates with an enhancement factor (EF) of approximately 10–100 and analytical molecules.

One of the functions of SERS technique is sensing molecules in trace amounts the area of biochemical and chemical analytics. Molecular fingerprint specificity is combined with potential sensitivity of a single molecule in the Raman spectroscopy (SERS) enhanced on the surface. Therefore, chemists use this powerful technique in a wide range of applications, in particular natural dye identification, trace analysis of pesticides [33, 61], analysis of glucose [61, 63-65], biosensors, etc. Moreover, SERS can be applied to implement immunoassay labeling [66, 67], identify bacteria [68] , Nucleic acid-based detection [69] ,and do genetic diagnostics [70]. Furthermore, the technique is applied for producing proteins as well as detecting energetic molecules and biomarkers in a number of pharmaceutical industry impurity analyses and homeland security applications.

2.2 The SERS Enhancement Factor (SERS EF)

The enhancement factor of SERS is defined as a ratio between the Raman signals produced by certain molecules in case the nanostructure is either present or absent. It strongly relies on the factors of shape and size of the relevant nanostructures. SERS enhancement has an average value of approximately 10^6 ; however, it is possible to achieve the peak of 10^{10} in the localized enhancement in case of using highly efficient sub-wavelength substrate regions [6]. It was concluded by the researchers that the efficiency of noble metal or nanoscale metallic junctions is the highest in case it is needed to achieve the high SERS enhancement factor. The measurement of Klarite substrate effectiveness is done via EF or enhancement factor measurement in the equation, as follows [71-74]:

$$\text{SERS EF [Raman Shift } (\text{cm}^{-1})] = \underline{(N_{vol} \cdot I_{SERS})} / (N_{SERS} \cdot I_{vol.}) \qquad (2.3)$$

The measurements done in the course of experiments present the calculations of the SERS-enhanced Raman intensity, in which normalization of I_{sers}, is done with the molecules binding of the metallic substrate , N_{sers}, with the subsequent division by the Raman intensity, $I_{vol.}$; the normalization of the latter done by molecules in the volume of excitation, $N_{vol.}$,

2.3 Molecular Docking

Molecular docking is a suitable tool for analyzing drug-biomolecular interactions required for the drug design. It is also essential in the placement of an element (ligand) into the desirable binding location of the target region [75]. Its primary objective is to achieve the desired ligand-receptor structure with the aim of gaining minimal binding energy (ΔG_{bind}), which is described in terms of ΔG_{hbond}, ΔG_{elec}, ΔG_{tor}, ΔG_{vdw}, ΔG_{desolv}, ΔG_{total} and ΔG_{unb} [76] . Determining the exact binding location enhances the docking process [77]. This process is illustrated below.
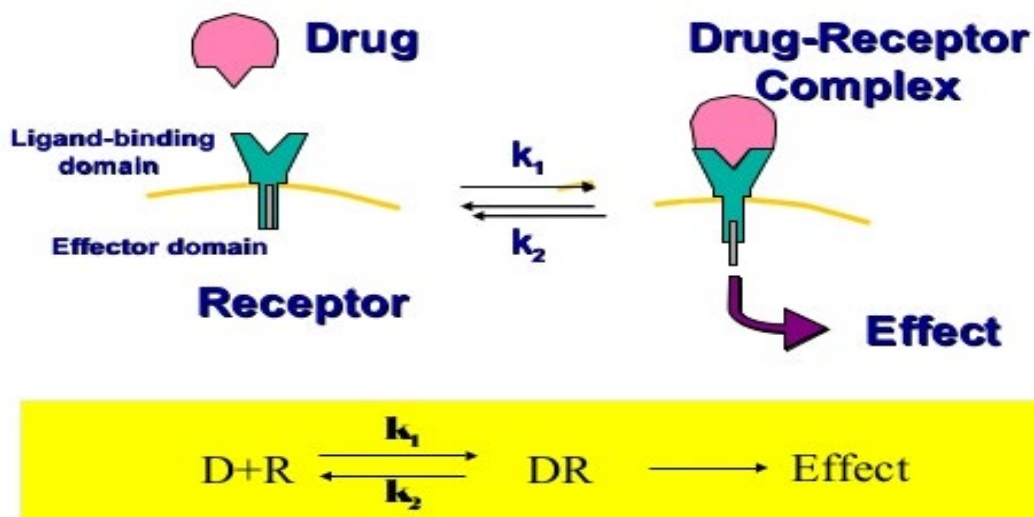
Figure 2.2 Molecular Docking.
Source[78].

Since the main concern of molecular docking is to provide a prediction of the ligand-receptor complex structure using computational methods, the underlying theory can be described using two interrelated steps, which are search designs and scoring algorithms [79] . Ideally, the search designs are mandated for reproducing the experimental binding mode [80]. Due to the expensive nature of this process, molecular dynamics, Monte Carlo, systematic, genetic and fragment-based algorithms are used for the docking analysis [81, 82]. Scoring functions are then used to predict the strength of the non-covalent bonds between the two molecules that have been docked [83]. Ideally, molecular docking must follow these interrelated steps to be a success.

Molecular docking is a robust means of forecasting the relationship between two molecules. It allows consideration of the size, charge distribution, shape, hydrogen bonding, and the hydrophobic interactions of the particles [84] . As such, it is possible to determine the nature and level of the mechanism of action between the molecules and hence

take the necessary precautions before docking. The applicability of the scoring function feature enables a selection of the best fit or the best combination of two molecules [84] .

Docking takes two general forms – rigid or flexible docking. Rigid ligand and rigid receptor method of docking considers only three rotational and three translational degrees of freedom, since the two molecules are regarded as rigid bodies [80]. On the contrary, the flexible molecule and rigid receptor docking is an enumeration on the rotations of one of the molecules[85] . To choose the most suitable pose in the end of the process, the surface cell occupancy and energy are measured calculated in every rotation.

There are two most common types of docking molecules. These are protein-protein docking and protein-ligand docking [76]. The first one is a simple procedure, which involves berthing two protein molecules; while the second one is used to forecast the location of an element when it is restrained on the receptor (protein) element [78] . These processes are achieved through the application of Sanjeevini, Schrodinger, AutoDock, Autolock Tools, Discovery Studio, and iGemDoc Software [78, 86] . The choice of the software should be based on the type of docking process.

This docking software are subtle in today's docking exercises. They yield data about the active spots of the protein. In doing so, they control the docking of the ligand in different locations of the receptor, thereby revealing data on the best possible binding location with the protein [85] . This minimizes the complexities of molecular docking.

2.4 Instrumentation and Techniques

2.4.1 Raman Instrumentation

There are two types of Raman spectrometers: interferometer systems that are used for the

sources of light in the infrared range and dispersive systems used for sources of light in the visible range and near-infrared spectral regions. Dispersive systems are applied more frequently. They are composed of an edge filter or a notch filter to reject Rayleigh scattering, a CCD (charge coupled device) array to detect photons, and a monochromator for scattered radiation dispersion, as it is shown in Figure 1.3 (a). A laser source excites a sample in the visible (Vis), ultraviolet (UV), or near-infrared (NIR) area. The required elimination of intense Rayleigh scattering is done by passing it through either a monochromator or a notch filter. Consequently, Raman signal obtained is forwarded to a CCD detector through a grating spectrometer.
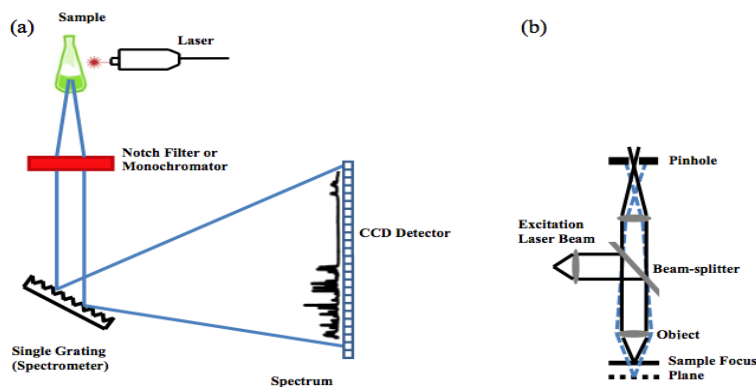
Figure 2.3 Raman spectrometers in: a) Fiber optic and (b) Confocal geometries.
Source:[87]

The speed of the Raman sampling process is high, and a spectrum is acquired in the course of only several seconds, thus providing numerous details related to the probed area structure and corresponding chemical composition. Sample sensing of standoff and remote types is possible by use of optical fibers as the latter are suitable for transport of both scattered and incident laser radiation. The design of a micro-Raman spectrometer is not done specifically for remote sampling; however, it can couple the source of incident light

and spectrometer to an optical microscope. As a result, Raman analysis can be conducted under the conditions of using a microscopic laser spot size that is suitable for both micron probes and probing sample features at the sub-micron scale.

A Raman microscope makes it possible to achieve spatial resolution at a sub-micron level and conduct the solid-state microstructure analysis as well as ensure spatial distribution of active particles and polymorphs in a composite. A composite sample chemical map can be created by using an automated stage with micro-Raman analysis [88]. Mapping allows for obtaining the complete Raman spectrum of a specimen for every image pixel. As every spectrum enables representation of chemical species fingerprint, it is possible to analyze the distribution of various materials along with their local features. Figure 1(b) shows how placing a small-size confocal pinhole in the microscope focal plane allows further improvement of axial resolution by collecting spectra from a sample volume and consequently establishing the depth profile of a sectioned specimen [89],[90]. Raman spectroscopy was performed in this work with a ThermoScientific DXR micro-Raman spectrometer (ThermoScientific Inc, Waltham, MA, USA). 532-nm and 782-nm laser excitation was used with spatial resolution equal to 10 μm and spectral resolution of 2 cm^{-1}.

Here the essential performance factors include high resolution, a small form factor, low rate of noise, and low consumption of power. It is a matter of crucial importance to have a proper photon detector, which depends on the type of laser excitation used. For instance, a standard charge coupled device (CCD) is appropriate for visible excitation; a CCD or photomultiplier tube (PMT) is used when UV excitation is used; while InGaAs or indium gallium arsenide is typically selected for NIR excitation.

2.4.2 Scanning Electron Microscopy (SEM)

SEM or Scanning Electron Microscopy engages the use of microscope of high resolution which applies high-energy electrons in a focused beam for the generation of different signals at the solid specimen surface to create a certain image. The mentioned technique discloses the data regarding the sample, in particular its texture or external morphology, crystalline structure, chemical composition, and material orientation of the sample. The narrow beam of electrons with a magnetic focus allows the recording of images by SEM in the range from micro-scale to nano-scale ones with the significant field depth; thus, the researchers use the most powerful microscopes and generate three-dimensional images with 5nm of spatial resolution. A normal SEM image ensures the surface structure visualization of nanoscale types and represents the morphology of composite and pure types of solids. SEM images in the present research were obtained with the use of field emission scanning electron microscope VP-1530 Carl Zeiss LEO (Peabody, MA). All non-conducting samples were set on stubs of aluminum with the use of carbon tape (double-sided) with further sputter-coating of carbon to prevent charging.

2.4.3 Cyclic Voltammetry

Voltammetry is one of the most important electrochemical methods of analysis, based on obtaining volt-ampere characteristics, i.e., the dependence of the current in the electrochemical system from an externally applied potential, changing in accordance with a specific law [91]. Cyclic voltammetry is a method in which the time variation of the current flowing through the system under study is recorded when a voltage is applied to it that varies in time according to the law of a triangle. Analysis of the main characteristic parameters of cyclic voltammograms allows obtaining important information on the

possible mechanisms of the electrochemical processes [92]. This method is one of the most complex electrochemical methods of analysis [93]. However, it is used quite often because it gives a rich experimental information on the kinetics and thermodynamics of many redox products systems. The main feature of the method is in the cyclic variation of the potential of the anode, and then to the cathode region or vice versa [94]. Cyclic voltammetry may be single-cycle or multi-cyclic, depending on the electrode, the process being studied, and the information required. In most cases, the first and last cycles are not identical. For quantitative measurements, multi-cyclic voltammetry is not used, since a quantitative theory of this method has not yet been developed [95]. Nevertheless, it is very useful in the study of complex processes. Cyclic voltammetry is one of the most common voltammetry methods. The wide use of this method is determined by its speed, simplicity and efficiency in the study of the properties of substances and the dynamics of electrochemical reactions [94]. Cyclic voltammetry can be applied in different areas of science and technology, as it is an effective method of research and analysis.

2.4.4 Plasma Treatment

The diagram of the plasma equipment used for the synthesis is represented in Figure 2.9. Nitrogen and argon were fed into the quartz tube through needle valve flow meters allowing control of the flow rate of the gas precursors. An adjustable radio frequency generator delivering up to 500 W is attached to an adjustable impedance matching box. Throughout this study, a power range of 65–100 W was maintained. Gas mixtures of 50% nitrogen and 50% argon were introduced into the deposition chamber where a quartz boat was used to hold a 2×2 cm^2 substrate. A vacuum pump was used to evacuate the deposition chamber to pressures below 1 Torr. Flow rates of 10–15 sccm (standard cubic centimeters

per minute) were preserved for each gas. The deposition time was typically between 2 and 3h, and at least 2h was required for optimal synthesis. The temperature of the substrate throughout each experiment was checked using a thermocouple even though external heat was not applied to the reactor. Temperatures of the plasma jet were in the 200–300 °C range and monitored using a thermocouple under floating potential inside the quartz tube [96].
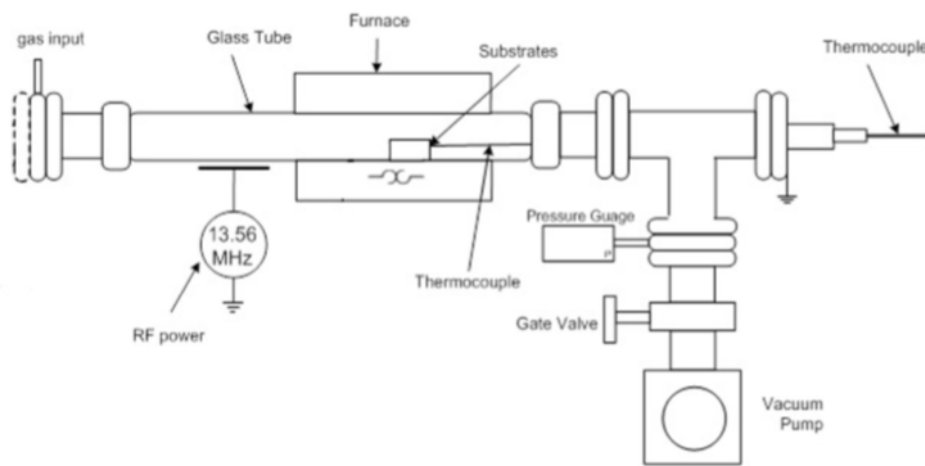
Figure 2.4 Schematic of plasma system used in this study.
Source: [96].

2.4.5 Attenuated Total Reflection Fourier Transform Infrared (ATR-FTIR) Spectroscopy

FTIR spectroscopy was examined on a Fourier Transform Infrared Spectrometer (Nicolet 560 FTIR) attached with an Attenuated Total Reflectance (ATR) accessory with a single reflection ZnSe crystal (MIRacle, Pike Technologies). Samples were measured in a range from 600 to $4000cm^{-1}$. The spectral resolution of FTIR spectra is at $4cm^{-1}$ and ratio against background interferogram, and the final spectrum stayed the average of 100 scans.

CHAPTER 3

SURFACE ENHANCED RAMAN SPECTROSCOPY (SERS) OF R6G AND GLUCOSE USING KLARITE® AND NANOCRYSTALLINE SILVER SUBSTRATES

3.1 Introduction

Nanoparticles (NPs) are nanoscale materials of various sizes ranging between 1 and 100 nanometers [97]. NPs are classified into various groups depending on their sizes, shapes and properties. The different groups include metal NPs, polymeric NPs and ceramic NPs. This chapter discusses the significance of NPs of gold and silver in SERS. From a chemical perspective, nanoparticles are more reactive since they have a larger surface to volume ratio than bulk materials. Gold and silver are widely used as antennas in SERS because of their optical transitions due to plasmons under visible light excitation are more intense than the local intensity of the electromagnetic field [22, 23, 98, 99].

Nanoparticles have a large surface area to volume ratio providing them with unique physical and chemical properties that are valuable building blocks of nanotechnology and nanoscience with applications in energy research, catalysis, sensors (in particular biological and chemical sensors [6] and drug delivery [7]. Metal nanoparticles such as gold and silver are obtained from pure metal precursors and are used in SERS because of their unique optical and electronic properties, such as their broad absorption in the visible.

3.1.1 Gold Nano-particles (AuNPs)

Gold nanoparticles synthesized at different nanoscale sizes shows different properties and colors, which is applicable in different bio-imaging applications [100]. Also, gold NPs exhibit different multicolor colloids that have bio-imaging applications [101].

Furthermore, AuNPs are used for coating samples for scanning electron microscopy (SEM) imaging by enhancing the electron beam critical to the generation of quality images [97].

3.1.2 Silver Nano-particles (AgNPs)

Silver NPs enhance surface plasmon resonance; hence, they are ideal for use on SERS substrates for the generation of intense Raman signals [101, 102]. As a tool, SERS is can be used to detect and monitor ecologically toxic substances in water and other aqueous solutions. Research shows that SERS employing silver NPs generates reproducible strong signals for detecting and monitoring toxic compounds [26, 103]. Higher silver NP density increases the sensitivity of the SERS substrate [104].

3.2 Klarite® Nanostructured Gold-coated Silicon Substrates

Klarite® SERS substrates consist of periodic square lattice of pits, having inverted square pyramidal form. It can be seen in Figure 3.1 (a) with the image made by scanning electron microscope. Pits result from the use of conventional photolithography with a mask of silicon dioxide on a silicon wafer of (100)-oriented type. Preferential etching of 111 planes was done with KOH to produce the inverted pyramidal pits in a periodic array. The range of periodic separation or pitch made by the pits was 0.7μm - 1.0μm. The spluttered gold layer of uniform 300nm on the wafer was made, after the process of etching was completed. It made the flat areas between the pits and the walls of the pits coated smoothly. The resonance between the Raman spectrometers with the excitation of the wavelengths of 632nm and 785nm in common use and the Plasmon bands of tunable type is enabled with the substrate design. It was possible to obtain the tapping mode image of substrate with gold coating with the use of AFM (Atomic Force Microscope) as Nanoscope III MultiMode

Microscope for Scanning Probes as can be seen in Figure 5.1 (b)). Investigation of the

SERS signal reproducibility across the active zone was done by Perney et al. [17]. (b)

Metallic SERS substrates of periodic, ordered, or uniform planer types, include the arrays

of metallic nanotextures with regular morphology formed on planer substrates with the use

of techniques of nano-lithography and other methods.

(a)
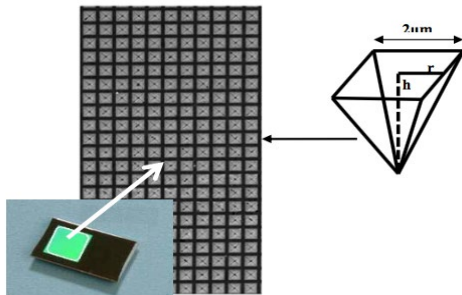
(b)
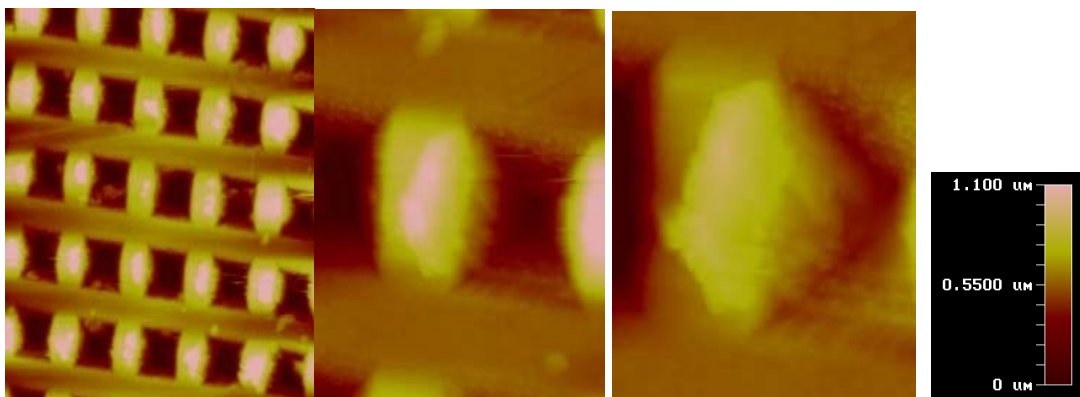
Figure 3.1 (a) Top view scanning electron microscope (SEM) image showing 2 μm wide inverted pyramids, and (b) A 10 mm wide atomic force microscope (AFM) image showing the inverted pyramidal pits of the photonic crystal SERS substrate with a 300 nm thick gold layer. Blow ups of the pits and the region between the pits are shown on the images to the right.
Source: [87].

3.3 Experimental Details

3.3.1 Raman Spectroscopy

Raman scattering experiments with Klarite® were carried out in segment using a Mesophotonics SE 1000 Raman spectrometer that was described in Chapter 2.

3.3.2 Preparation of Solutions

Rhodamine 6G (R6G) or Rhodamine 590 is an extremely fluorescent Rhodamine family dye. The R6G ($C_{28}H_{31}N_2O_3Cl$, molecular weight 479.02 g/mol) was purchased from Sigma Aldrich. The purity of the dye was 95% by mass percentage and was used without any further purification. The chemical structure of Rhodamine 6G (R6G) is reported in Figure 3.2.
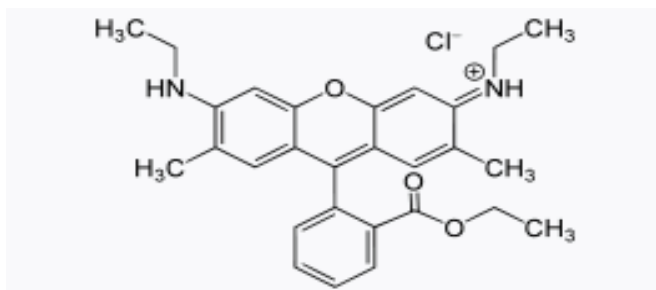
Figure 3.2 The structure of Rhodamine 6G.

R6G is a cationic dye with strong absorption and high fluorescence in the visible spectral range. Composition of the molecule comprises of two chromophores, xanthene (dibenzopyrenechomophore) and a group of a carboxyphenyl tilted to the xanthene ring by 90 ° (Figure 3.2). There is no conjugation of the π systems of the two chromophores of R6G. The maximum optical absorption in aqueous solution is at approximately 530 nm,

and the vibrionic shoulder is approximately at 470nm [105, 106]. The molar mass of R6G is 479.02 g/mole and the density is 1.26g/cm^3. The solubility in water is 20g/l at 25°C.

The range of concentrations for the aqueous R6G solutions was 10^{-2}-10^{-16} g/ml. At first, a concentrated solution was prepared followed by preparations of other samples via the dilution of stock solution with small volumes in distilled water. Additional samples were prepared to monitor the effectiveness of the substrate in identifying analyte concentrations between 10^{-2} and 10^{-16} g/ml in increments of smaller volumes: 1×10^{-4}, 1×10^{-6}, 1×10^{-8}, 1×10^{-10}, 1×10^{-12}, $10^{-14}\times$ and 1×10^{-16}g/ml.

Glucose A Klarite® substrate was used to detect different concentrations of glucose, from glucose stock solutions containing the following concentrations: 1 M, 0.5M, 10^{-3}M, 10^{-4}M and10^{-5}M, At the beginning, a glucose stock solution in different concentrations was deposited on several Klarite® substrates. After the glucose solution was deposited on the substrate, it was dried at 35° C in an oven. After that, the Raman spectra of the Klarite® substrates with glucose at different concentrations were each taken separately.

3.4. Methods

3.4.1 Preparation of the Substrate by Spin Coating

Figure 3.3 Diagram showing SERS substrate preparation.

The experimental set up for substrate preparation for this work is shown in Figure 3.3. The SERS substrate was prepared by adding nanocrystalline Ag on quartz, then spin coating

for 18s at 2 RPM, and 4 RPM for 60s, to produce a uniform layer of nanocrystalline Ag. Then, different concentrations of R6G are placed on the substrate and the spectra recorded using 780 nm laser radiation, and 15s acquisition time.

3.4.2 Preparing SERS Substrate by the Spin Coating Method with Aggregation Agent
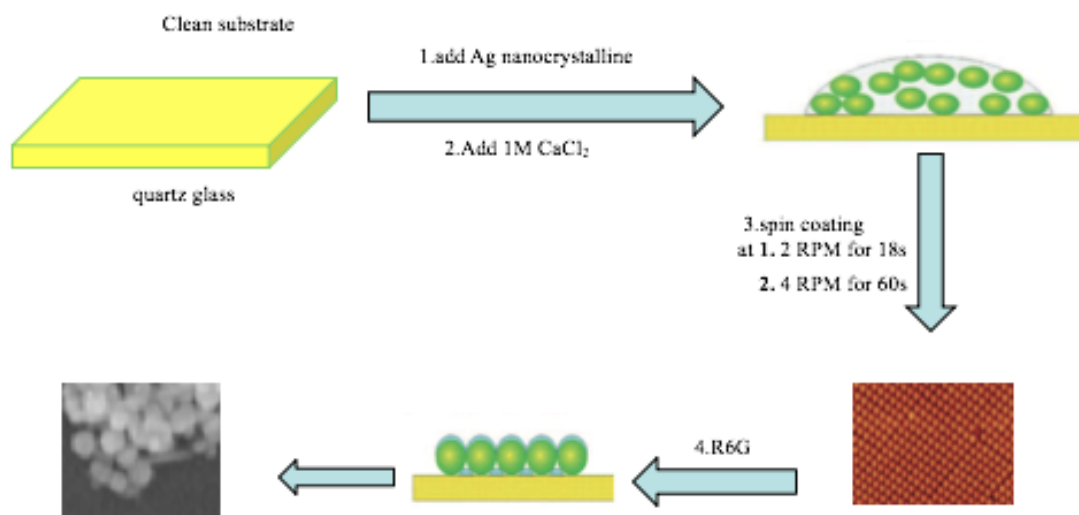
Figure 3.4 Diagram for SERS substrate preparation.

SERS substrate was prepared by adding nanocrystalline Ag with aggregation agent (1M $CaCl_2$) into quartz glass, then applying spin coating for 18s at 2 RPM of speed, then 4 RPM for 60s, to produce a uniform layer of nanocrystalline Ag. Then, different concentrations of R6G are dropped on the substrate. Finally, the spectra are taken by using 780 nm laser radiation and 15s acquisition time.

3.5 Results and Discussion

3.5.1 Klarite® SERS Substrates

Techniques of nanofabrication have considerably improved, and this factor has contributed to the preparation of numerous regularly ordered periodic nanostructures for surface-enhanced Raman spectroscopy [107, 108]. Despite these efforts, there are still certain problems and challenges, in particular in the area of reproducible and scalable production of reusable, rugged, and inexpensive SERS-active substrates. Initially, fabrication of a new type of substrate fabricated lithographically which has the architecture of photonic crystal voids with a periodic array able to support trapped plasmons was reported by Perney et al. [17] Later on, commercialization of the idea was done by Mesophotonics Ltd as Klarite® (later distributed by Renishaw Diagnostics Ltd). The surface plasmons employed in Klarite technology are obtained from structured metal surfaces comprised of inverted pyramids of square form coupled with the gold coating. There are still open questions in improving detection limits down to the single molecule level that requires further research and development of novel SERS substrates, such as those based on graphene and conducting polymers or their corresponding oligomers, and methods of isolating plasmon-generating metal particles deposited on the substrates, to further enhance the SERS signals.

3.5.2 Raman Sensing of R6G on a Klarite® Substrate

SERS investigators have used standard molecules for evaluating the detection of trace levels of analytes. One such molecule is Rhodamine 6G (R6G) dye which also provides strong resonance enhancement in addition to SERS. Klarite® substrates for SERS consist of periodic photonic crystal arrays of gold-coated inverted pyramidal cavities of square

shape formed by etching a silicon wafer. In previous research SERS was used to detect R6G down to 10^{-9} M concentration on Klarite®[87].

3.5.3 Raman Sensing of Glucose on a Klarite® Substrate

The small normal Raman cross-section of glucose (5.6×10^{-30}cm^2 molecule^{-1} sr^{-1}) [109] is a major challenge for its detection by SERS for medical applications, such as blood glucose level monitoring of diabetic patients and the medical evaluation of patients since glucose is a marker for many diseases. The work related to SERS analysis of glucose was performed with commercially available Klarite® substrates. The induction of SERS on the photonic crystal substrates was obtained by ensuring strong interaction of visible laser radiation (532 nm) with trapped surface plasmons in the cavity void architecture of the substrate. SERS with a high level of reproduction on the active substrates was achieved at a detection level down to 10^{-5} M. Figure 3.5 shows the SERS data with enhancement factor of 10^5 for glucose solutions on Klarite®. We propose to modify the substrate with a novel feature in order to achieve further enhancement of the SERS signal with detection levels down to extremely low concentrations.
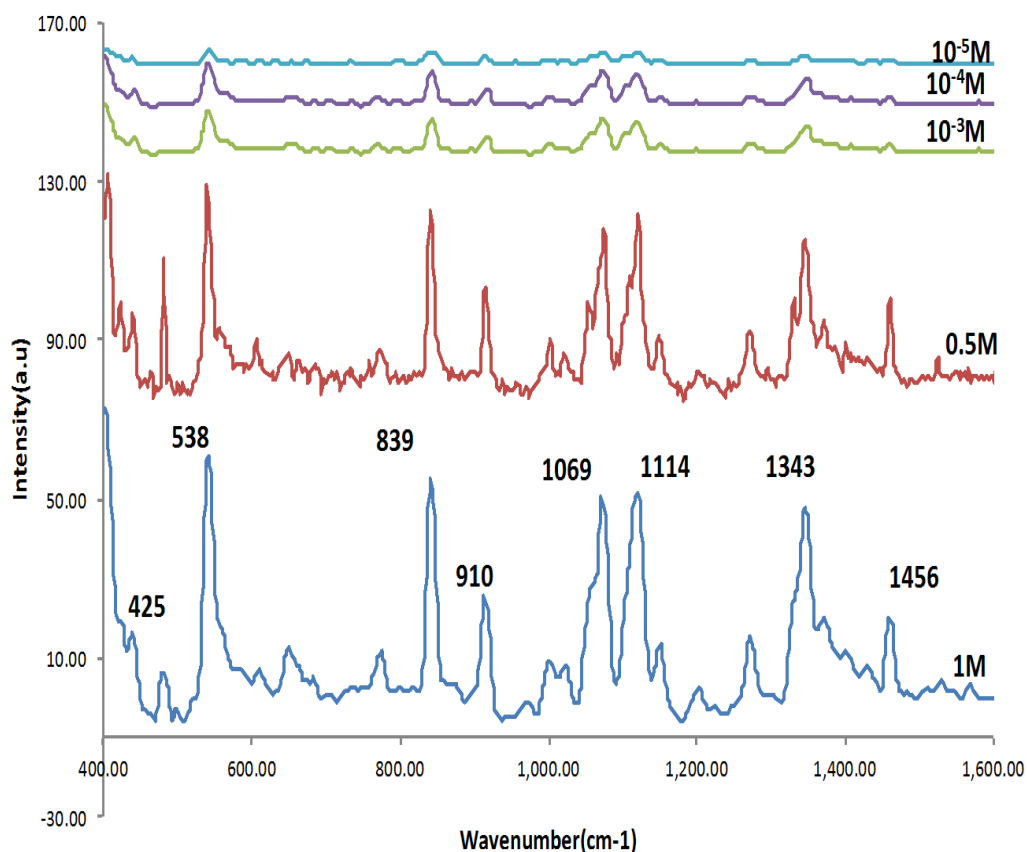
Figure 3.5 SERS for different concentrations of glucose on Klarite® with λ_{ex}=532nm, power =10 mW, acquisition time =10 sec averaged over 3 scans. Lines appearing in SERS at 425, 538, 839, 910, 1069, 1124, 1343 and 1456 cm^{-1} correspond to those in the normal Raman spectrum of crystalline glucose.

3.5.4 Nanocrystalline Silver as SERS Substrate for R6G Detection

The specific hot spots typical of metal colloid clusters coupled with the electromagnetic field serves as the key factors for SERS. SERS activities are affected by the following two factors: 1. Metal substrate plasmon excitation of the full surface, and 2. Closeness of the metal substrate surface to the probed atoms. It is difficult to observe SERS if the metal substrate surface is not suitable for analyte absorption. Therefore, it was considered on these grounds that the metal substrate surface chemistry is a key element for SERS activity. It is assumed that an analyte atom has to be located inside the electromagnetic field or 0–4

nm from the substrate surface to produce a significant SERS effect. Similarly, it is necessary for an atom to be attached non-covalently to the metal surface for the required SERS enhancement to occur. R6G, for example, is a common analyte used to test for SERS activity on Ag because it is difficult to observe it on Au substrates due to its lack of interaction with Au surfaces [108]. Therefore, using nanocrystalline Ag deposited on a glass or quartz substrate would be desirable for detecting R6G at low concentration levels as shown in Figure 3.6 .
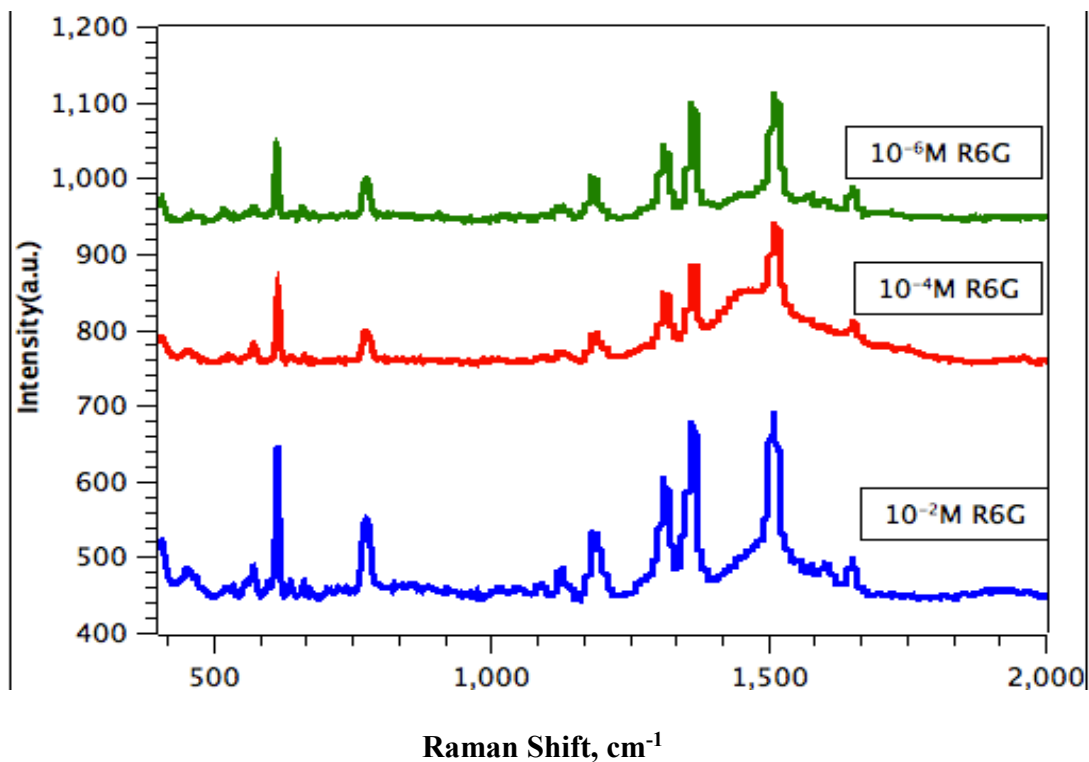
Figure 3.6 SERS for different concentrations of R6G from sample prepared by adding nanocrystalline Ag on quartz and then spin coating for 60s at low speed to produce a uniform layer of nanocrystalline Ag. The spectra were taken using 780nm laser radiation, 15s acquisition time, and 50x microscope objective.

3.5.5 Detection of R6G Using Nanocrystalline Silver with an Aggregation Agent

To further increase the efficiency for nanocrystalline silver substrates, SERS of R6G were directly determined after depositing a few drops of nanocrystalline Ag with some drops of the aggregation agent (1M $CaCl_2$) on to a quartz substrate.

As it was essential to ensure the increase in the nanocrystalline silver substrate efficiency, determination of SERS of R6G was done directly after deposition of nanocrystalline Ag on the quartz substrate together with drops of the aggregation agent (1M $CaCl_2$). Figure 3.7 clearly demonstrates strong SERS activity for R6G in particular lines at $1511cm^{-1}$, $1360cm^{-1}$, $1310cm^{-1}$, $1186cm^{-1}$, $770cm^{-1}$, and $610cm^{-1}$. The Raman lines at $1511cm^{-1}$, $1360cm^{-1}$ and $1310cm^{-1}$ are associated with high symmetry in-plane C-C R6G stretching vibrations.
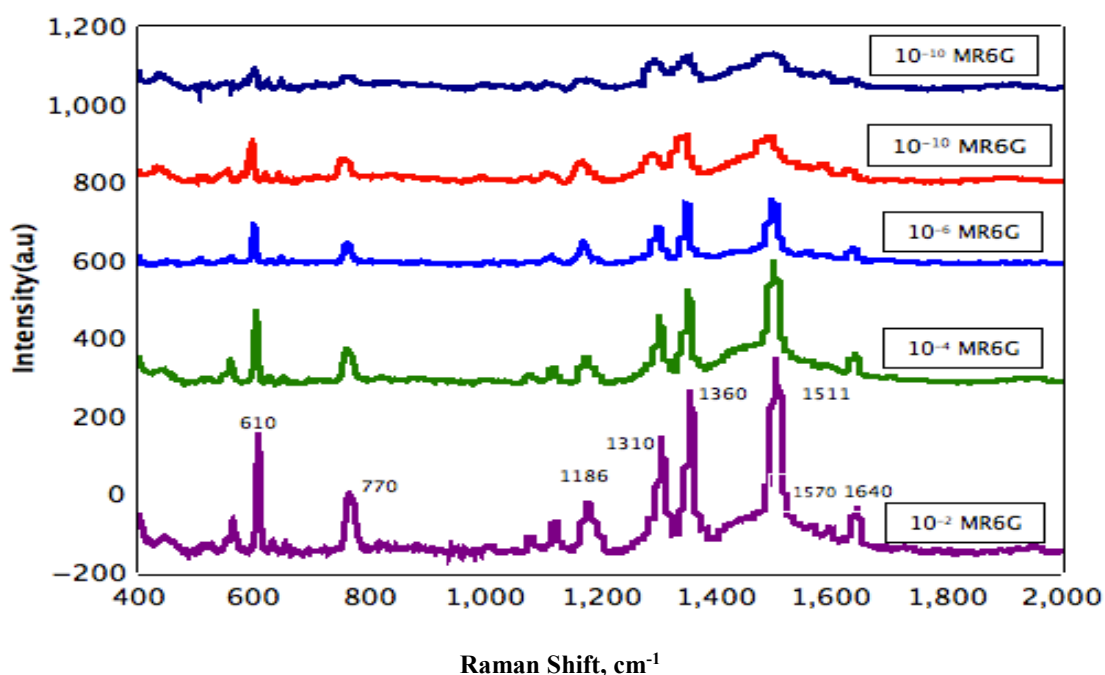
Figure 3.7 SERS for different concentrations of R6G from sample prepared by adding solution of aggregation agent (1M CaCl$_2$) on nanocrystalline Ag deposited on quartz and then spin coating for 60s at low speed to produce a uniform layer of nanocrystalline Ag. The spectra were taken using 780nm laser radiation with 15s acquisition time, and 50x microscope objective.

3.5.6 Sodium/Calcium Chloride Activated Aggregation

It is observed in the arranged series of experiments that the aggregation agent increases SERS activation in the R6G-Ag-glass system; the aggregation agent was done by the electrolyte calcium chloride. Typically, activation of the Ag-nanocrystalline aggregation is done with the use of such aggregation agents as sulfate salts, metal halide, or nitric acid as electrolytes [110-112]. Reduction of the gaps between the adjacent metallic nanostructures is done with the aggregation agent used also for producing hot spots; as a result, the efficiency of detection is increased, and the reproducibility of SERS is improved.

Conclusions

This chapter discusses the evaluation and selection of nanoparticles that are used for SERS of glucose and R6G. Some commercial nanoparticles were evaluated and compared. Our results show that the commercial Klarite® substrate is capable of detecting glucose down to 10^{-5} M, and nanocrystalline silver is able to detect R6G down to 10^{-10}M in the presence of an aggregation agent.

CHAPTER 4

GOLD NANOPARTICLES ASSEMBLED ON GRAPHENE-LIKE SHEETS FOR SURFACE ENHANCED RAMAN SPECTROSCOPY

4.1 Gold Nanoparticles on Graphene-like Sheet for SERS

4.1.1 Introduction

One of the functions of SERS technique is sensing molecules in trace amounts in the area of biochemical and chemical analytics. Molecular fingerprint specificity is combined with potential sensitivity of a single molecule in the Raman spectroscopy (SERS) enhanced on the surface. Therefore, chemists use this powerful technique in a wide range of applications, in particular natural dye identification, trace analysis of pesticides [33, 61], analysis of glucose [61, 63-65], biosensors, etc. Moreover, SERS can be applied to implement immunoassay labeling [66, 67], identify bacteria [68], nucleic acid-based detection [69], genetic diagnostics [10] and trace level detection of contaminants [70].

D-glucose plays significant factor in the equilibrium of metabolic activities in our body, because it is the source of energy and it maintains the proper function of the human body when taken or saccharide formation through the process of biosynthesis. When it enters in the cells, the glucose can be broken down through glycolysis to provide energy or polymerized an important constituent of the plant cell wall called cellulose and starch. In our body, the glucose can covalently join the lipids (glycolipids) and proteins (glycoproteins) and other biological molecules to form glycol-conjugates. These are essential building components of cell membranes [113]. Presently, electrochemical methods have been the most successful way to measure glucose indirectly, relying on the detection of hydrogen peroxide yielded by the glucose oxidation [114-117].

Electrochemical glucose biosensors basically check or monitor oxidative current produced by glucose oxidase (GOx). This accelerates free glucose to become gluconic acid and hydrogen peroxide. Hydrogen peroxide, which is produced by GOx, deprotonates to produce protons, oxygen and two electrons. The measured electrical signal is therefore directly proportionate to glucose concentration[118] as shown in Figure 4.1.

$$Glucose + O_2 \rightarrow gluconic\ acid + H_2O_2 \rightarrow 2H^+ + O_2 + 2e\text{-}$$
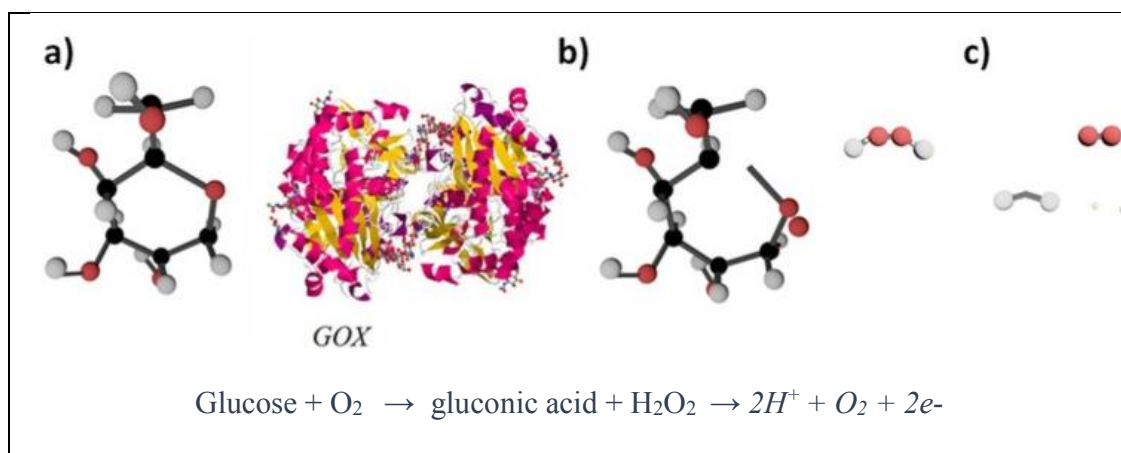
Figure 4.1 The fundamental working concepts for glucose biosensors. It involves three steps. First, glucose binds in the enzyme-binding pocket of glucose oxidase (GOX). Second, an applied potential hastens the oxidation of glucose to become Gluconic acid and hydrogen peroxide. Finally, the hydrogen peroxide separates to O_2, 2 H+, and 2 electrons. These electrons are measured using either an optical or an electrochemical method. Source:[118].

However, this indirect technique presents a challenge: the glucose oxidase that catalyzes the oxidation should be replenished. As a consequence, the lifetime of the sensor is short, or limited. Another downside of enzymatic glucose sensors is that they are unstable because of the inherent nature of the enzymes[64]. Furthermore, fluorescence spectroscopy is one of the indirect methods to detect glucose[64, 119]. This method is highly sensitive , it can detect glucose all the way down to the molecule level. Because of the sensitivity and the infinitesimal size of the fluorescent probes (dyes and quantum dots), sensors can be

bio-functionalized and put into a cell by diffusion without undergoing endocytosis[120]. A new direct glucose detection method has been developed recently. It includes both laser polarimetry and vibrational spectroscopies [117, 121].

Glucose in Raman cross-section of small normal type is 5.6×10^{-30} cm^2 /(molecule-sr) [109]. SERS can ensure lower level of detection and Raman signals of higher intensity. Optimization of sensitivity SERS ensures and facilitation of the process of molecule absorption are enhanced by SERS substrates via the application of chemical and electro-magnetic mechanisms [122, 123].

Various types of chemical compounds can be detected easier with the help of SERS substrates using the Raman resonance concept even if the quantities of the compounds are low. Both chemical analysis and scientific research benefit from using SERS substrates which are defined as vital. Until recently, a preferable substrate material for SERS has been graphene in case of using all kinds of biological species as it has appropriate compatibility and suitable chemical inertness [123, 124] .

Graphene is one- to few layered carbon atoms formed in honeycomb structure. Due to its unique two-dimensional sp^2-bonded structure [125], graphene has surfaced as a substance that has extraordinary mechanical, electronic, thermal and optical properties including higher electrical conductivity, larger surface area, and better chemical and thermal stability [116, 126-129]. Furthermore, graphene is known for its distinct and unique electrical activity as well as its astonishing role in nanoscale electronics. These fascinating properties refer to the inherent structural feature of graphene, which comprises a hexagonal carbon network sheet [130, 131]. Graphene has played an important role in

molecular sensing in various methods including electrical and optical procedures [132-134].

There are reasons why graphene is extremely sensitive to changes in its chemical environment [135, 136]: a) Its electron transport continues to exist ballistic up to 0.3 u at 300 K and has extremely high electron mobility when suspended at room temperature, b) Each carbon atom is a surface atom giving the most possibility of surface area per unit volume. c) Graphene has a very high electrical conductivity and has inherently low electrical noise. These properties stem from its unique single to few layer 2-dimensional structure. For these reasons, graphene is considered a perfect material for different sensing applications although high structural variability leads to poor reproducibility in its sensing properties [37].

Here, we use commercially developed multilayer graphene-like sheets with reproducible structure as substrates on which gold nanoparticles are chemically assembled by citrate reduction for glucose detection.

4.1.2 Experimental Details

4.1.2.1 Gold Nanoparticle Preparation. Citrate methods were used to get the gold nanoparticle ready following the same method as described in Turkevish [137] and Frns[138] in terms of the analysis of chemical reduction. The solution of aqueous Au (0.5M, 25ml) was then heated to 98°C. It was then stirred and a one percent aqueous sodium citrate solution (one ml) added to it. The obtained mixture was kept at 95°C. It was then continuously stirred during the next thirty minutes. As a result, the solution becomes dark red in color.
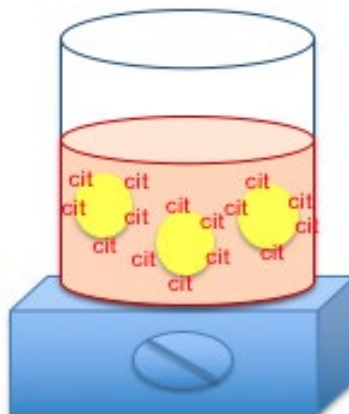
Figure 4.2 Schematic showing the simple set up for the bottom-up synthesis of gold nanoparticles based on the Turkevish and Frns method.

This section presents the synthesis of gold nanoparticles using the mechanism with all the stages included and all intermediates [139]. The first stage is referred to the citrate oxidation with the resulting dicarboxy acetone. It is followed with the second stage of auric salt reduction to aurous salt. The final stage is the process of disproportionation to gold (I) species:

$$(^-OCCH_2)_2C(OH)CO^- \longrightarrow$$

$$(^-OCCH_2)_2C{=}O \ + \ CO_2 \ + \ H^+ \ + 2\,e^- \tag{1}$$

$$AuCl_3 + 2e \quad \rightarrow \quad AuCl + 2C^{l-} \tag{2}$$

$$3AuCl \quad \rightarrow \quad 2Au^O + AuCl_3 \tag{3}$$
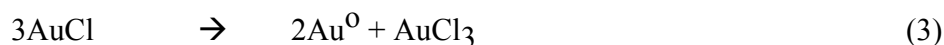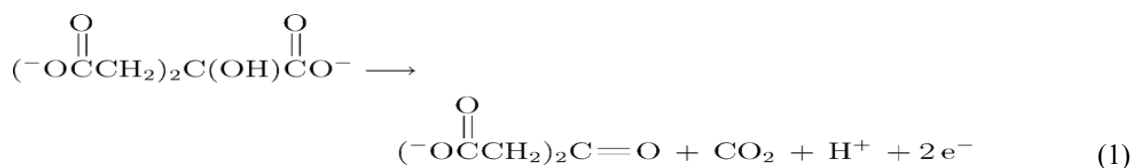
The stage of disproportionation implies having three molecules of aurous chloride for combinations. The process is facilitated with dicarboxy acetone that forms a complex and takes part as an organizer [137]. Figure 4.3 shows a visualized complex discussed in this part. It demonstrates a structure in the form of a chain with three Au^+ tethered by the molecules of dicarboxy acetone in the minimum quantity of two.
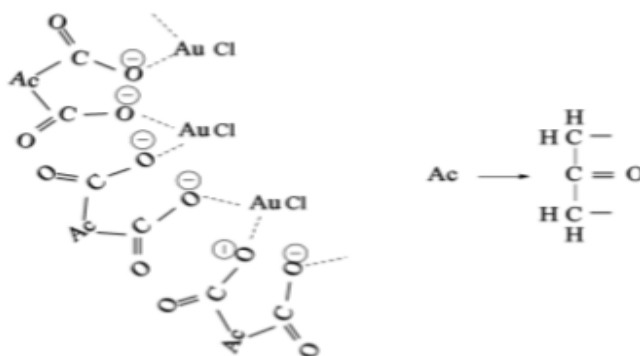
Figure 4.3 Diagram showing complex of aurous species and dicarboxy acetone
Source: [139].

In general, the reduction reaction stoichiometry can be demonstrated in the following way:

$$2\,AuCl_3 \;+\; 3\,(^-O\overset{O}{\overset{\|}{C}}CH_2)_2C(OH)\overset{O}{\overset{\|}{C}}O^- \longrightarrow$$

$$2\,Au^\circ \;+\; 3(^-O\overset{O}{\overset{\|}{C}}CH_2)_2C{=}O \;+\; 6\,Cl^- \;+\; 3\,H^+ \;+\; 3\,CO_2 \qquad (4)$$
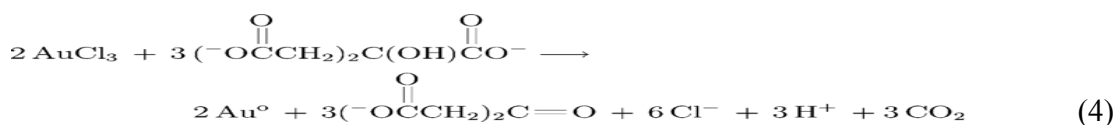
In general, the stoichiometry for the reduction of two molecules of auric chloride requires three molecules of citrate. It should be noted that under the conditions of high temperatures as a result of side reactions, dicarboxy acetone forms acetone and is removed [137].

$$2\,H_2O \;+\; (^-O\overset{O}{\overset{\|}{C}}CH_2)_2C{=}0 \longrightarrow (CH_3)_2C{=}O \;+\; 2\,CO_2 \;+\; 2\,(OH)^- \qquad (5)$$
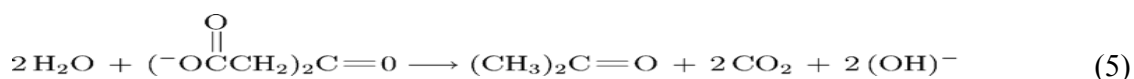
It is assumed that extra reduction of the auric chloride and consequent overall conversion are resulted from the dicarboxy acetone degradation and formed acetone. This reaction gets 4 as a stoichiometric ratio.

$$(CH_3)_2C{=}O + 4AuCl_3 \rightarrow 4AuCl + products \qquad (6)$$
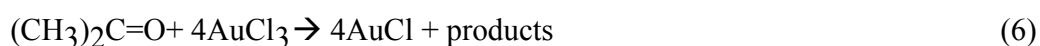
Thus, it is possible to implement reduction of approximately three moles of auric chloride by one mole of citrate in full. The made assumption is valid for <1.5 as ratios of

citrate to gold in its impact on the model. The ratios allow having large-sized particles; therefore, the mentioned system may have lower significance in preparation.

4.1.2.1.2. Substrate preparation. In the course of the experiment, a citrate method was used to prepare the gold nanoparticle solution using glucose stock solutions in the following concentrations: 1M, 10^{-3}M, 10^{-4}M, 10^{-5}M, 10^{-6}M, and 10^{-8}M, and a stock solution of gold nanoparticles at 0.04 M concentration. At the beginning, several drops of gold nanoparticles were deposited by drop coating on a graphene sheet. After they have dried, a glucose stock solution in different concentrations was dropped on several graphene sheets. When the gold nanoparticle solution was placed on the sheet, the drying was done at 35°C in the oven. After that, the Raman spectra of the graphene sheets were taken each separately.
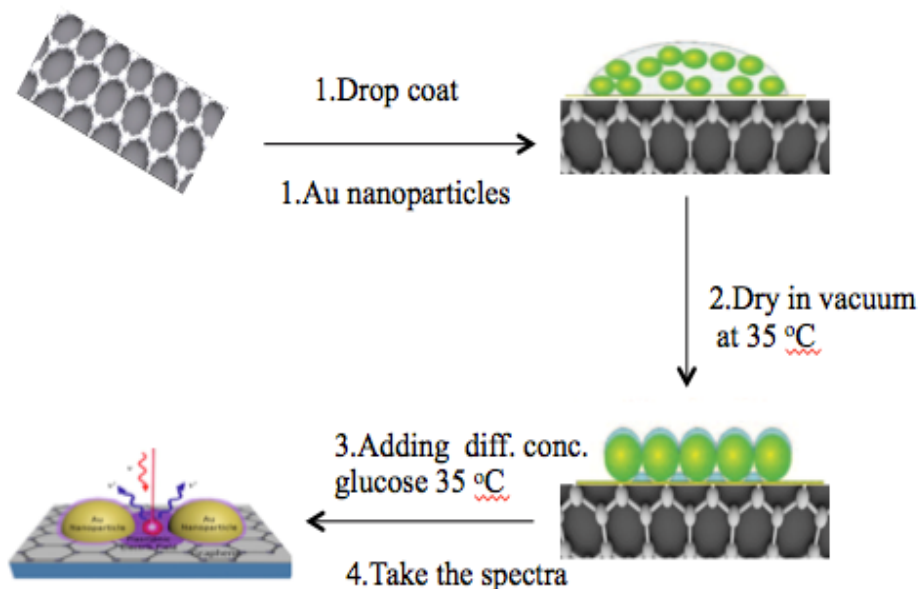
Figure 4.4 Diagram for SERS substrate preparation.

4.1.3 Results and Discussion

Scanning electron micro-scope (SEM) images were obtained with a VP-1530 Carl Zeiss LEO which was described in Chapter 2. Figure 4.5 exhibits the graphene-like sheet SEM images after gold was placed in various types of magnification. The figure shows that gold nanoparticles deposition on the graphene sheet can be defined as uniform. The percentage of gold nanoparticles is higher between the sheets than on top of the sheets. In addition, the percentage of gold nanoparticles on the surface was 4.6% and the particles were distributed on the surface in a non-uniform fashion.
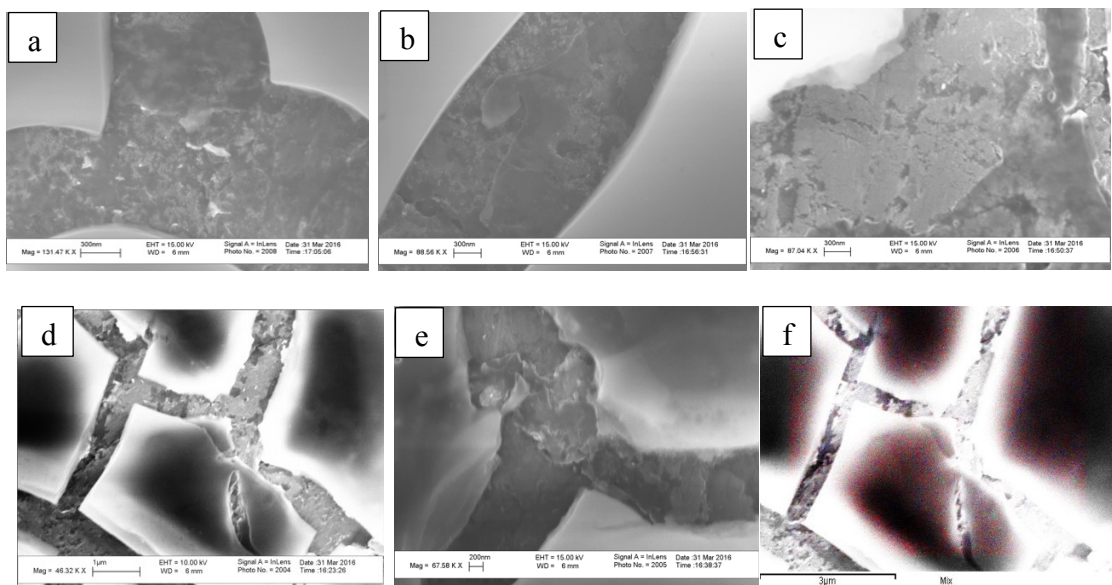
Figure 4.5 SEM images for pristine multilayer graphene sheet a, b and c) at 300nm, and at after gold nanoparticle deposition at d) 1μm of magnification e) at 200 nm of magnification f) 3μm of magnification to show the distribution of gold nanoparticles on graphene sheet
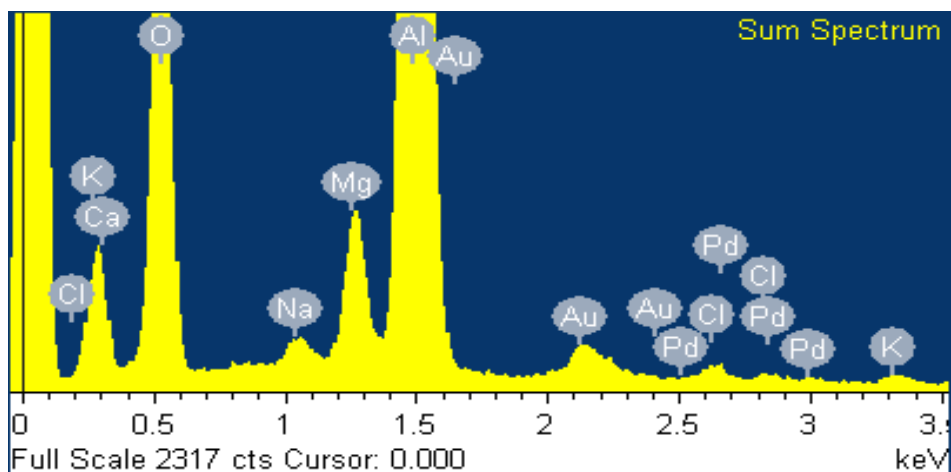
Figure 4.6 Shows EDS that gives the percent of the gold in the graphene multilayer sheets, which is equal to 4.6%.

A bright field in the graphene sheet may be due to the aluminum substrate or the addition of gold nanoparticles. This is because the gold nanoparticles are much lighter in color, and they were present during the experiment [140]. This is shown in Figure 4.5. Thus, gold nanoparticles display a brighter color contrast in comparison to both the substrate and graphene [141]. An increased intensity of gold nanoparticles was observed, which can be attributed to the use of a citrate solution, which ensured reduced space between the particles.
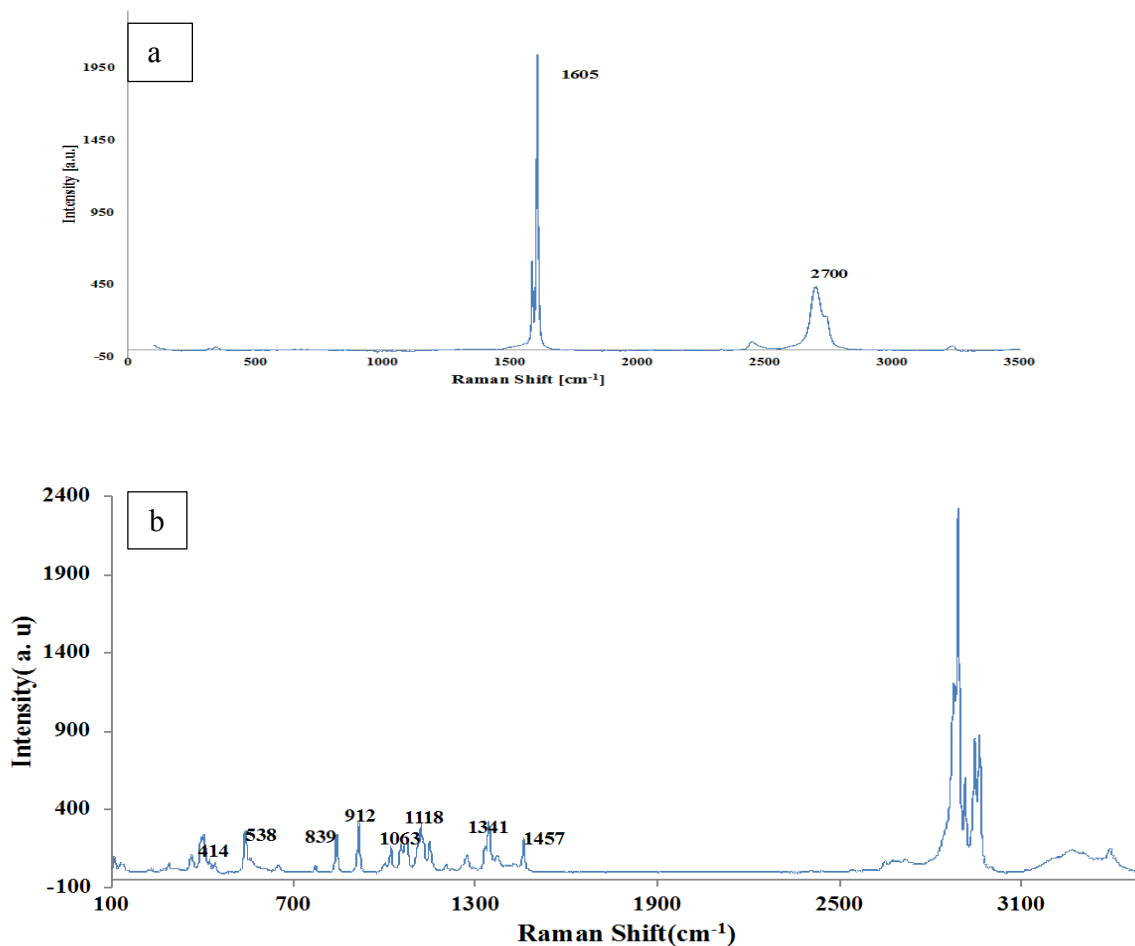
Figure 4.7 a) Spectra for pristine graphene sheet, λ_{ex}=532nm, P=10 mW, acquisition time = 45s,b) Normal Raman spectrum of crystalline glucose for comparison, λex=532 nm, P=10 mW, acquisition time = 45 s.

Figure 4.7a shows the conventional Raman spectrum of pristine multilayered graphene where the graphitic mode at 1,580cm^{-1} is extremely sharp, indicating highly-ordered carbon layers whereas the so-called G line at 2,720cm^{-1} is broadened with many features due to multilayering.

A Thermo Scientific DXR spectrometer of MicroRaman model is used for the crystalline glucose Raman spectrum that was received via laser radiation (532nm). The crystalline glucose signatures have vibrational modes at 919 (O-C1-H1 bend), 1340 (C-C-

H bend), 1270, 1164, 1116 (C-C + C-O stretch), 860cm^{-1} (C-C stretch), and 1070 (C1-OH

stretch) as shown in Figure 4.7 B [64].
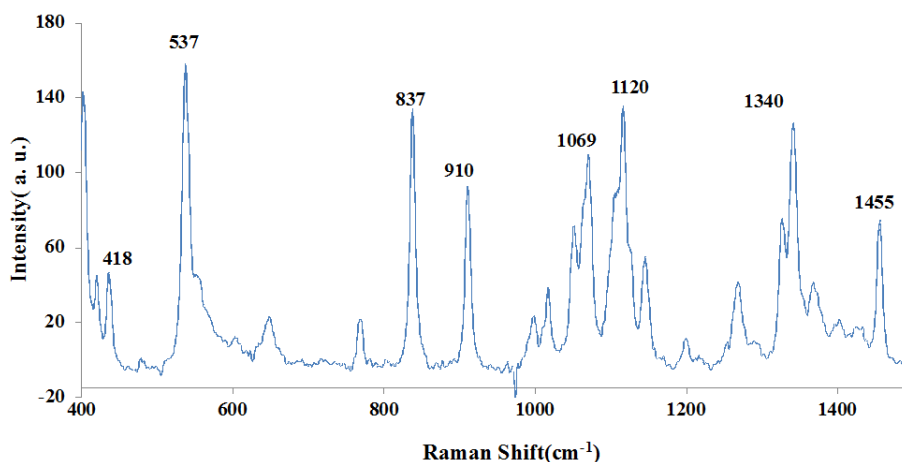
Figure 4.8 Normal Raman spectrum of 1M glucose ON Au/SERS, λex=532, P = 10 mW, acquisition time = 45 s, 50x.50 slit.

Figure 4.8 gives a clear illustration of the Raman signal in eight glucose modes for

1 M glucose placed on Au/graphene. Glucose Raman spectrum shows the following peaks:

413, 540, 842, 914, 1070, and 1120. In addition, the glucose fingerprints of 1344 and 1457

can be seen.

Detecting glucose was implemented at 15s. Increasing the time of exposure ensures

that the same compounds are not obtained, because of the role that the gold nanoparticles

play as catalysts. The gold nanoparticles cause glucose oxidation and provide oxygen to

various compounds, in particular gluconic acid [142] . Furthermore, when glucose is taken

at extremely low concentrations, there is the form of an open chain which makes it possible

for the aldehyde group to go through oxidation and provide gluconic acid [143] .

The results are different in the same substrate because the glucose prepared in the

open-chain form of solution ("D-" or "L-") is in the state of equilibrium with certain isomers

of cyclic nature. Each of them comprises a carbon ring closed with an atom of oxygen.

Such cyclic forms as D-glucopyranose in neutral water are referred to the typical and commonly applied glucose tautomers [143].
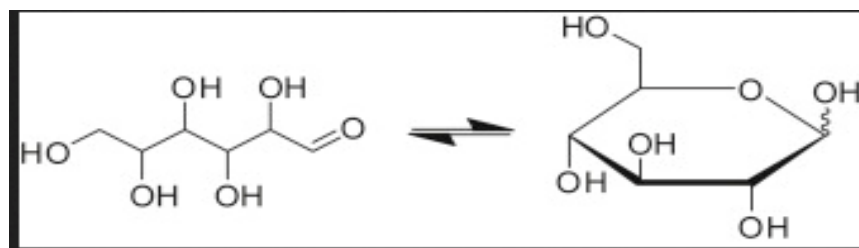
Figure 4.9 Linear and cyclic form of d-glucose[143].
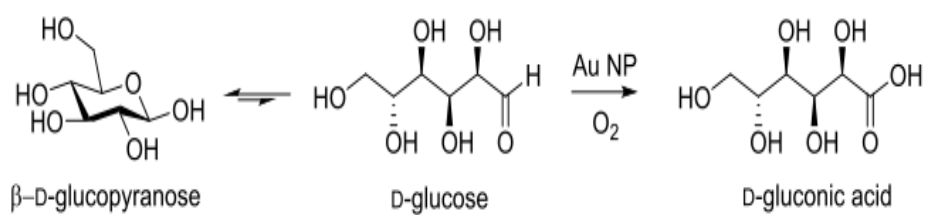
Figure 4.10 Possible tautomer of glucose and its oxidation to gluconic acid
Source: [143].
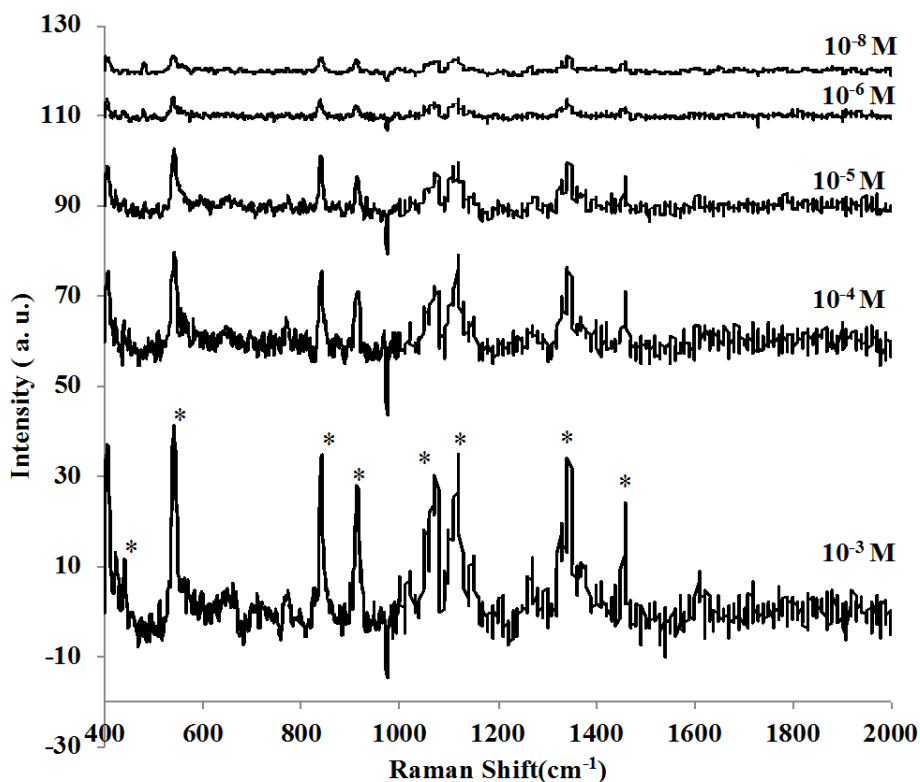
Figure 4.11 a) Normal Raman spectrum of different concentration of glucose on Au/Graphene, λex=532nm, P=10 mW, acquisition time = 45s. b) All spectra display peaks in the SERS spectrum 413, 540, 842, 914.,1070, 1120, 1344, and 1457 cm^{-1} corresponding with the Raman spectrum of crystalline glucose.

Figure 4.11 shows the fingerprint for glucose peaks. It appears that there is some shift in the glucose peaks around 10cm^{-1}. The literature shows that SERS spectral bands move up to 25cm^{-1} when compared to the normal Raman spectral bands of the same compound [144]. Most peaks in the SERS spectrum, especially at 1340 and1460cm^{-1}, match with the Raman spectrum of crystalline glucose.

The two lines in Figure 4.11 at 1340cm^{-1} and 1460cm^{-1} differ between glucose and galactose, which is a monosaccharide sugar and has a C-4 epimer of glucose, as can be seen in Figure 4.12 below. Figure 4.11 above shows the finger print for glucose, the significant two peaks that distinguished glucose on other suchaired appear in the spectra.
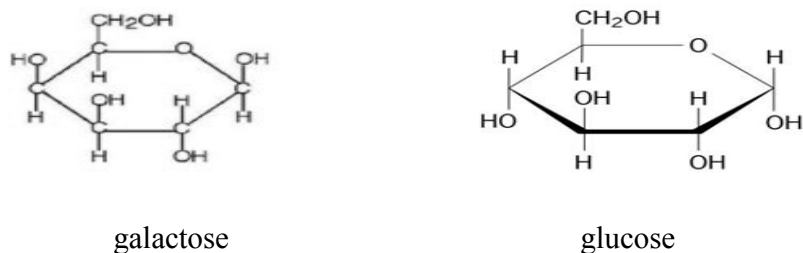
galactose   glucose

Figure 4.12 Molecular structure of glucose and galactose.

$y = 26768x + 6.7842$
$R^2 = 0.9019$
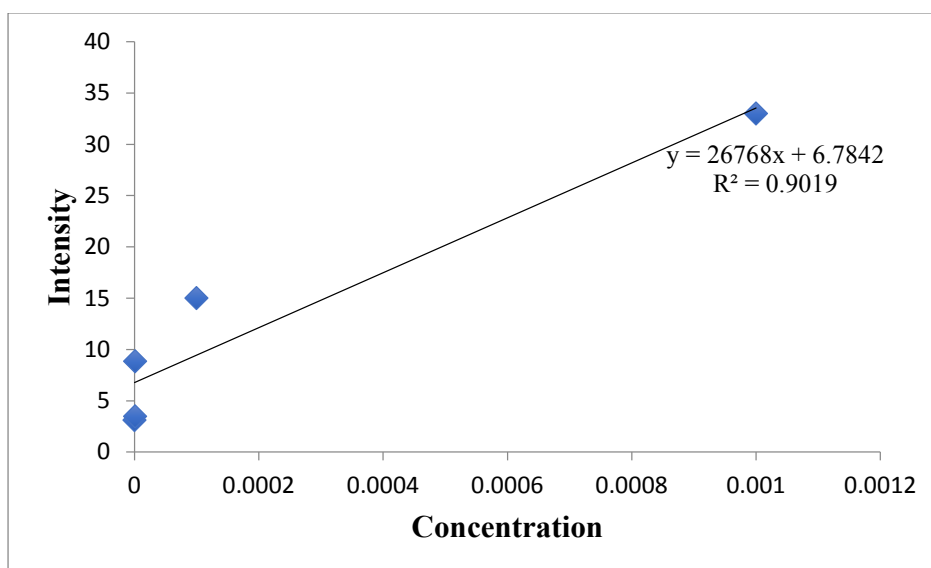
Figure 4.13 Intensity in arbitrary units of the glucose Raman peak at 1,340 cm versus the molar concentration of glucose on the SERS substrate.

Figure 4.13 shows how the glucose Raman intensity and its corresponding concentration at 1340cm^{-1} are related. There is an increase in the peaks if the concentration of glucose goes higher. We managed to determine a good SERS linear response from 10^{-3}M to10^{-8}M. In accordance with the linear fit calibration that results in $R^2 = 0.90$, the most effective enhancement occurs at the Raman peak of 1340cm^{-1}.

Optimization of the LSPR excitation wavelength led to an optimized signal and more accurate results. The variation in spectra was obtained by getting the difference in the concentration levels. According to literature, SERS bands are more likely to shift to 25cm^{-1} in comparison with the normal Raman band [145]. This change was observed in the experiment. The use of citrate-reduced gold nanoparticles enhanced the stabilization of the graphene sheet layers, which is best examined by SERS. This is because the EM field between the gold nanoparticles decreases with increased stability, thus leading to an increased SERS signal [146]. The aggregation process of gold nanoparticles was also ensured when the sodium citrate was added. A citrate is useful in activating ions, which in turn ensured better results. Consequently, the observed results were enhanced by using citrate as an aggregation agent and to reduce the distance between Au nanoparticles [147].
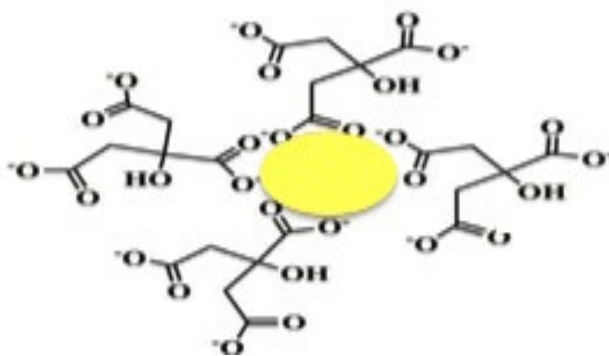
Figure 4.14 Proposed model of interaction and orientation of citrate with gold nanoparticles.
Source:[147].

From the results, a significant advancement towards a SERS-based glucose, which will be implantable and continuous, is evidenced. This is because the detection of glucose through a graphene sheet is easier and yields better results [148]. Although there are still more improvements that can be made from the experiment, the fact that glucose detection through the simple experiment was made possible is outstanding [149]. For future

experiments, gold nanoparticles can be used along with silver so that more consistent results can be obtained [150] .

4.2 Using Partition Layer to Improve the Efficiency of Graphene-like Sheet Substrate for Glucose Detection by SERS

4.2.1 Introduction

The affinity of substrates, such as glucose, for the nanoparticles where SERS is to be implemented is very low [54]. It necessitates the need for a partition layer that connects the nanoparticles with the specific probe. Characteristically, the layer should be biocompatible with excellent hydrophilic and hydrophobic properties [151] . The basic mechanism is enhanced substrate to SERS detection as well as reversible attachment to the metal surfaces. Partition films are important since they promote the interaction between the substrates, such as metallic surface, and the glucose [152]. For example, Tri- ethylene glycol-terminated alkane and decanthiol DT are some of the perfect partition layers, as they exhibit appropriate hydrophilic and hydrophobic properties [153]. Besides, they are incompatible in aqueous conditions.

The affinity of glucose to bare metal surfaces is defined as low. Consequently, it is required to ensure facilitation of the interaction between the partition layer and glucose molecules to increase substrate sensitivity . Moreover, it is also needed to ensure that the partition layer can reversibly bind glucose. The preference was given to TEG(Triethylene glycol mono-11-mercaptoundecyl ether monolayer) as a glucose partition layer because it is biocompatible, and it has excellent hydrophobic and hydrophilic properties. The progress is made towards the long-term objective of implantable glucose sensor fabrication. The

used mixed compound with its hydrophilic and hydrophilic characteristics is chosen as a perfect option for detecting glucose.

The present work presents the use of partition layer TEG to facilitate the interaction between glucose and nanoparticles.

4.2.2 Experimental Details

4.2.2.1 Substrate preparation. Using glucose stock solutions and a stock solution of gold nanoparticles at 0.04 M concentration. First, several drops of gold nanoparticles were deposited by drop coating on a graphene sheet. Then, some drops of Triethylene glycol mono-11-mercaptoundecyl ether monolayer were dropped and left in the vacuum for 24h. After they have dried, a glucose stock solution in different concentrations was dropped on several graphene-like sheets. When the gold nanoparticle solution was placed on the sheet with the partition layer, the drying was done at 35ºC in the oven. After that, the Raman spectra of the graphene sheets were taken each separately.

Figure 4.15 schematically explains the simple process for the preparation of TEG/AuNPs/Graphene-like sheet substrate fabricated by using a drop coating method. The Au nanoparticles were synthesized by chemical reduction methods described by Turkevich[137] and Frens[138] .
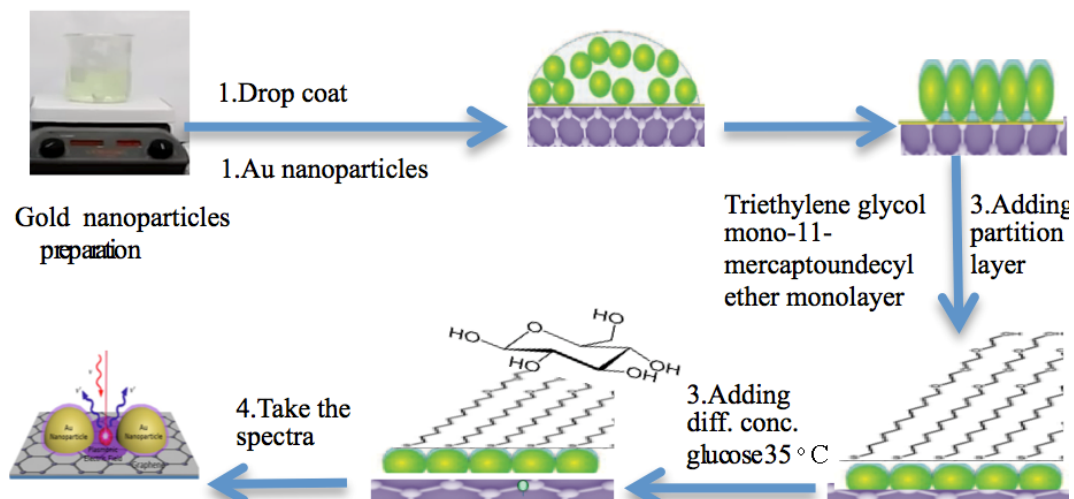
Figure 4.15 Diagram showing graphene-like SERS substrate preparation.

4.2.3 Results and Discussion

Cross-sectional and top view SEM images in Figures 4.16 a-c show essentially total coverage of the partition layer on AuNPs/graphene-like sheet. as can be seen from cross-sectional and top view images.
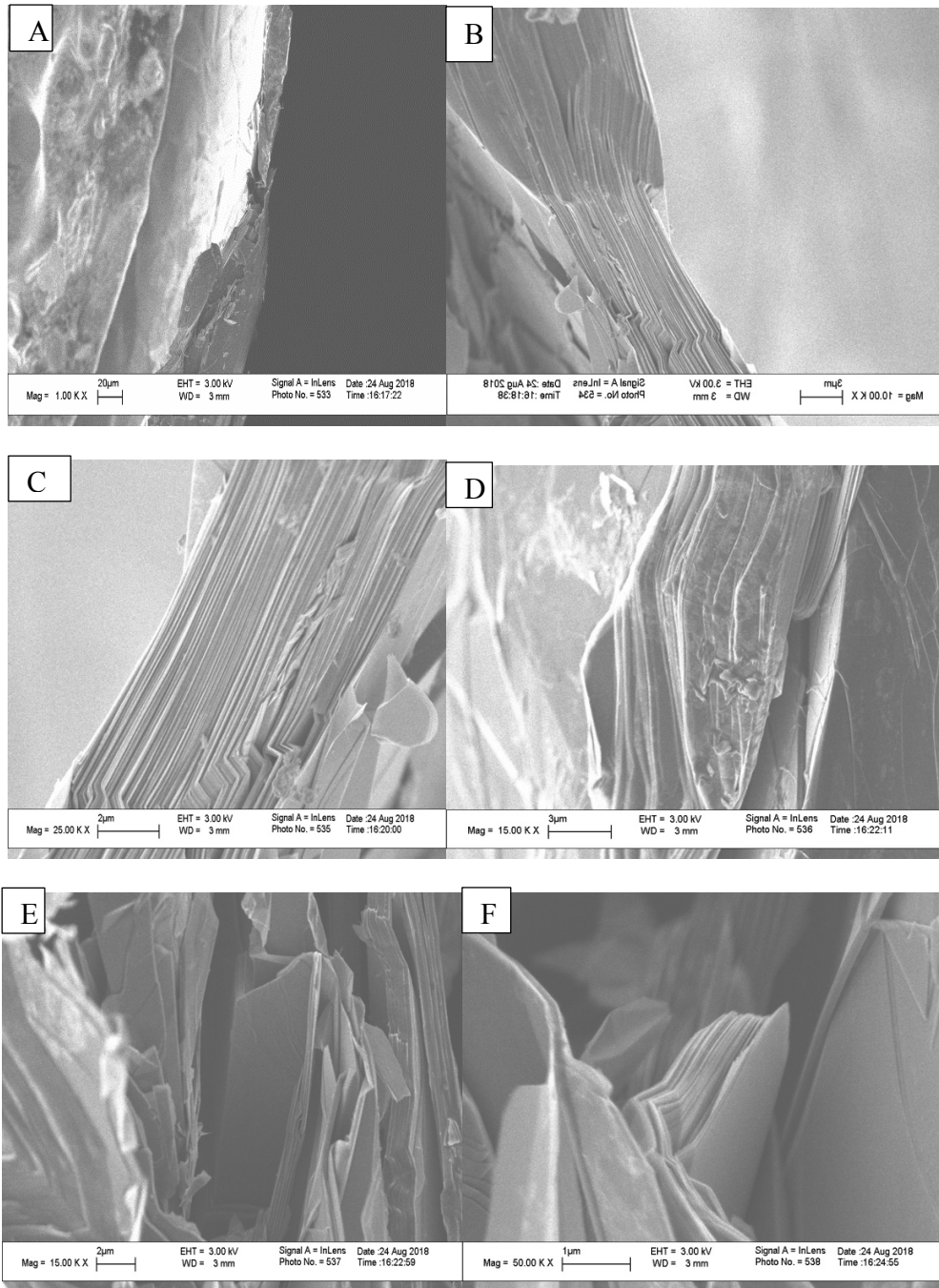
Figure 4.16a Cross-sectional SEM images showing multi-layer pristine graphene-like sheet at different magnifications.
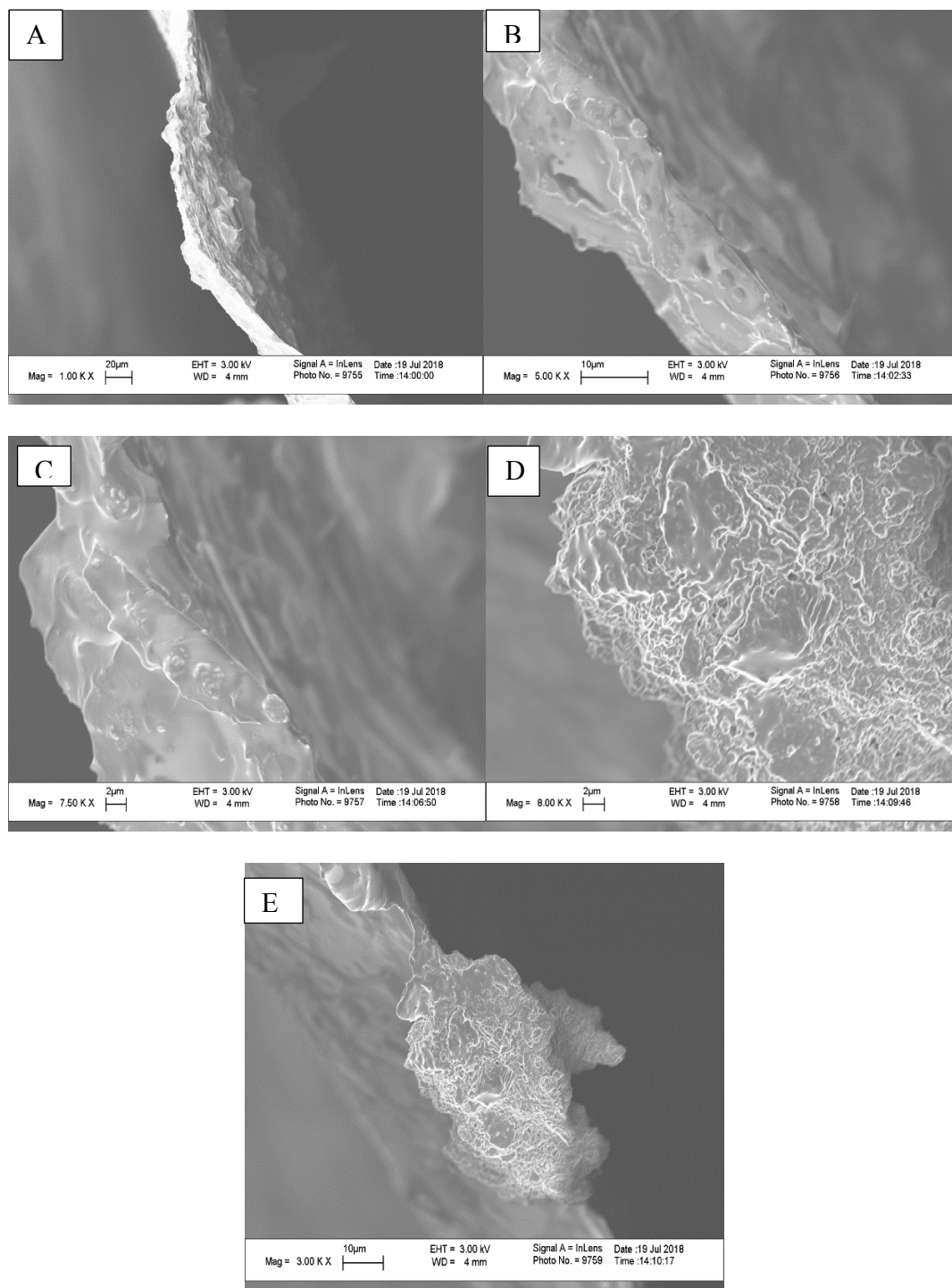
Figure 4.16b (A, B, C,D, E) Shows cross-sectional SEM images depicting multi-layers of pristine graphene like sheet at 1K, 5K, 7.5K, 8 K and 3K magnifications after partition layer deposition.
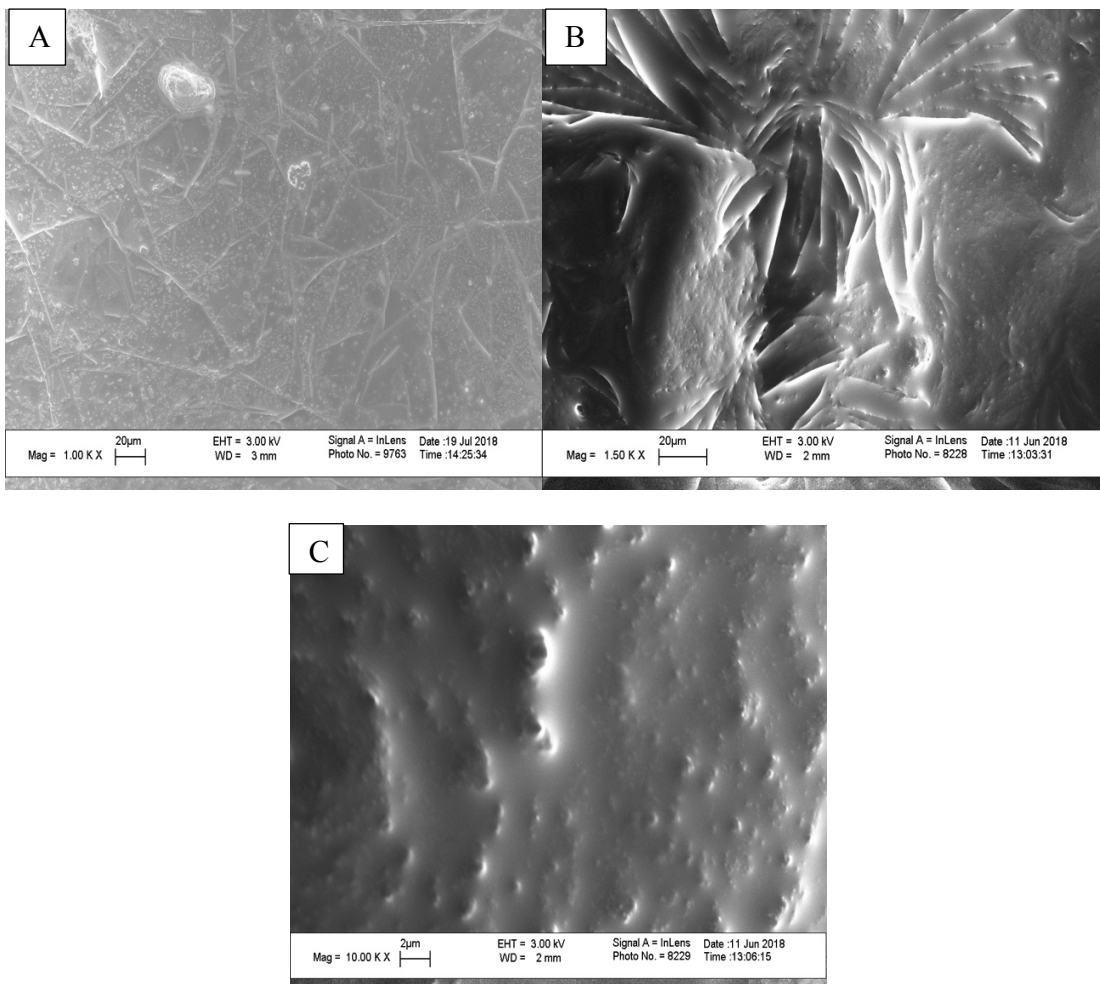
Figure 4.16c Top view SEM images of graphene-like sheet after partition layer deposition at magnifications of 1K, 20K and 2K.

Figure 4.17 shows TEG terminated with thiol, with molecular weight of 336.53 g/mole on average comprises the group of hydroxy closer to the end thiol group. TEG is covalently attached to the Au NPs via the thiol group.
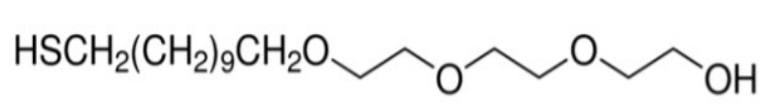
Figure 4.17 Molecular structure of the triethylene glycol mono-11-mercaptoundecyl ether.

Figure 4.18 presents Raman spectrum for Triethylene glycol mono-11-mercaptoundecyl ether using 780 laser for 30s on Au nanoparticles /graphene like sheet. TEG-AuNPs/ graphene like sheet is shown better enhancement compare by the previous substrate for some significant reasons. First, TEG Ligand is mandatory to bind the nanoparticles surface by either chemisorption, hydrophobic interactions or electrostatic attraction. The bond between the gold surfaces and thiols (-SH) is (Au-S,~ 50 Kcal mol^{-1}) which is stable and strong bond[154] . Furthermore, AuNPs are coated with citrate, that increase the stabilization and prevent the aggregating between the nanoparticles , as can be seen in Figure 4.19.
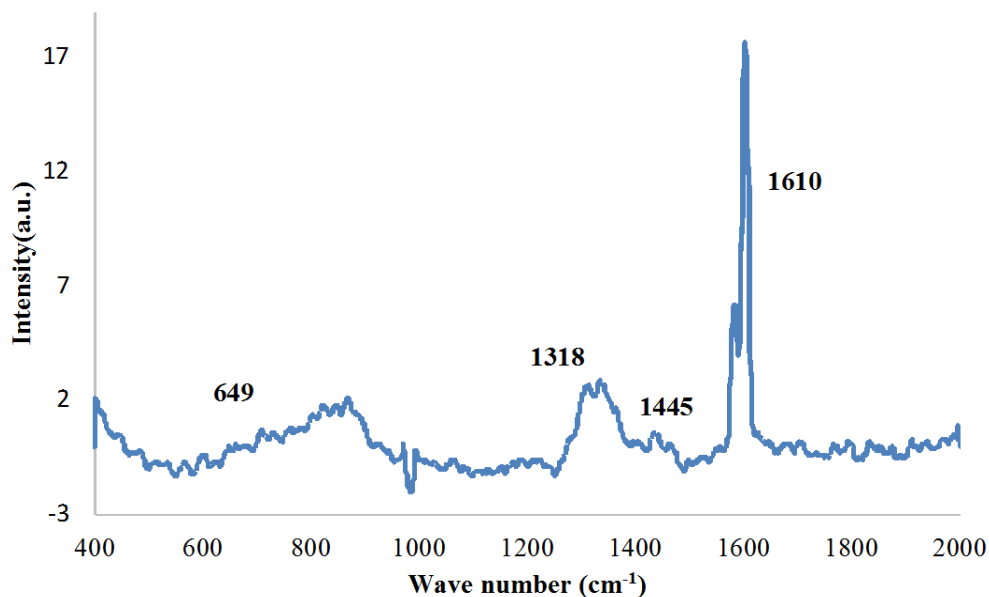
Figure 4.18 Raman spectrum for Triethylene glycol mono-11-mercaptoundecyl ether on Ag nanoparticles/graphite sheet using 780 laser for 30s.
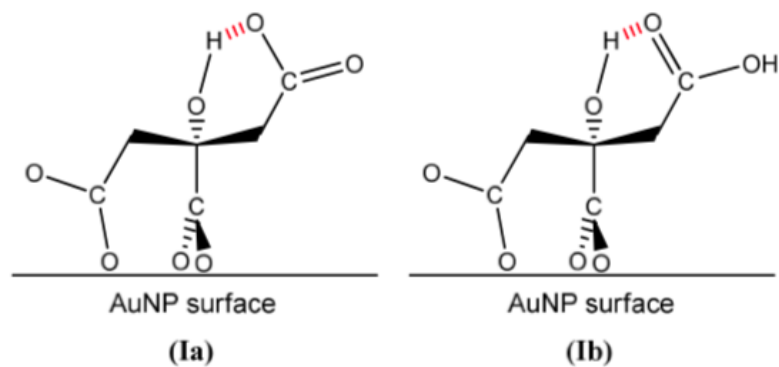
Figure 4.19 Possible interactions between the hydroxyl group and the carboxylic acid group of citrates adsorbed on the surface of AuNPs.
Source:(56)

The glucose peak fingerprint is shown in Figure 4.20. That is a sign of the available glucose peak shift of approximately 10cm^{-1}. According to the literature, the movement of the SERS spectral bands can be up to 25 cm^{-1} in comparison with the typical same-compound Raman spectral bands [144]. The SERS spectrum has every peak matched with the crystalline glucose Raman spectrum with the following peaks: 402, 521, 835, 900, 1063, 1118, 1341 and 1449 cm^{-1} correspondence with the crystalline glucose peaks.
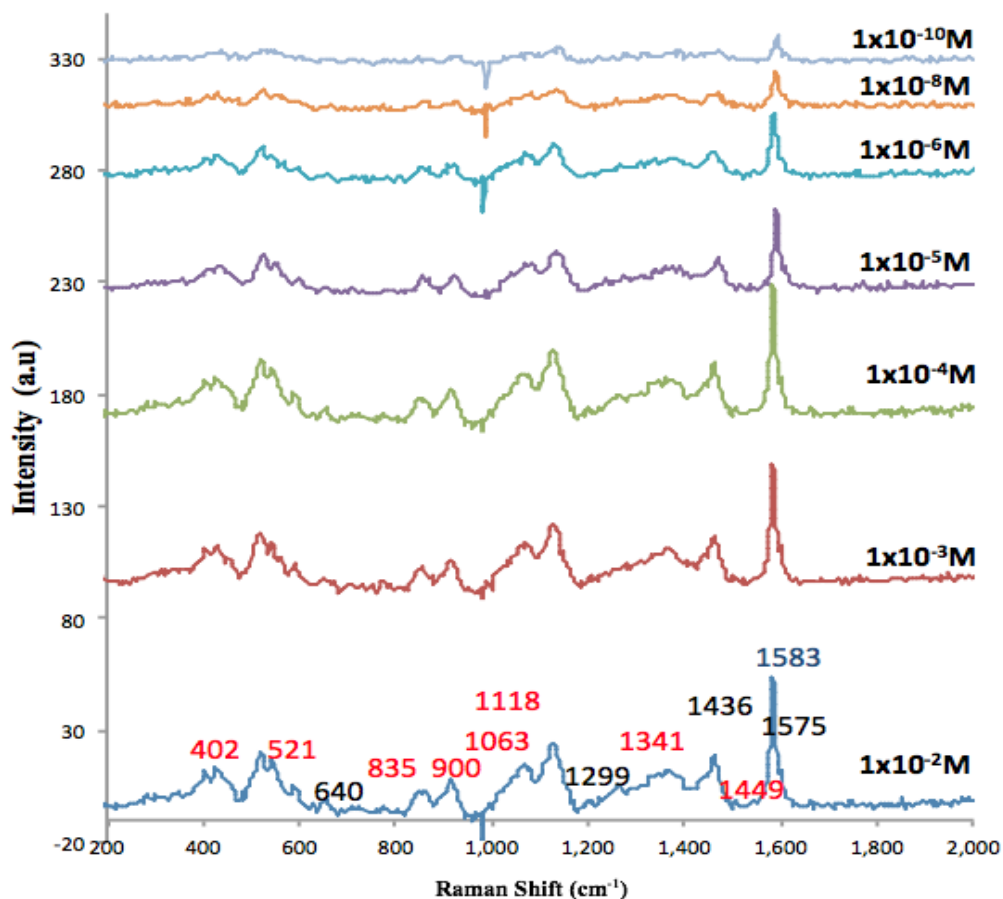
Figure 4.20 SERS for different concentrations of Glucose on Au nanoparticles /Graphene with partition layer using λ_{ex}=532nm, P=10 mW, acquisition time =15s, average=3 scans. All the peaks shown in red in the SERS spectrum at 402, 521, 835, 900, 1063, 1118, 1341 and 1449cm^{-1} correspond to the Raman spectrum of crystalline Glucose.

Figure 4.21 demonstrates a good linear relationship between the measured SERS intensity and glucose concentrations at 1340cm^{-1} in the range of 10^{-2}M to 10^{-10}M. In accordance with the linear fit calibration that results in $R^2 = 0.81$, the most effective enhancement occurs at the Raman peaks of 1340cm^{-1}.
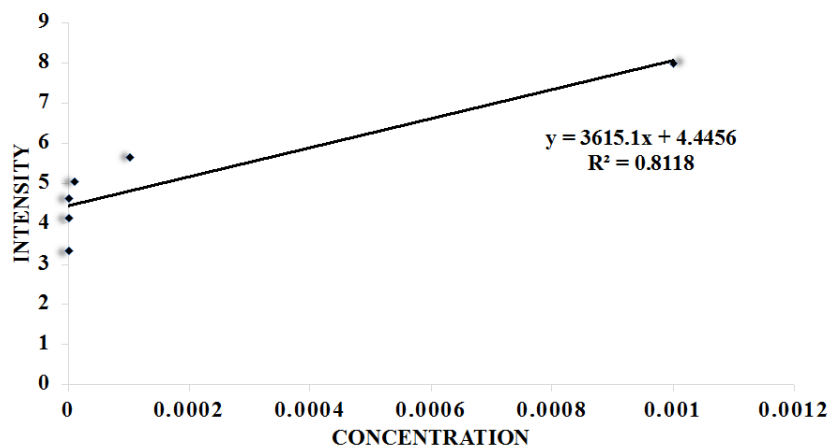
Figure 4.21 Intensity in arbitrary units of the glucose Raman peak at 1,340 cm^{-1} versus the molar concentration of glucose on the SERS substrate.

One of the features of this substrate is long-term stability, which ensured SERS activity during a three months period with no noticeable changes in the substrate morphology as exhibited in Figure 4.22.
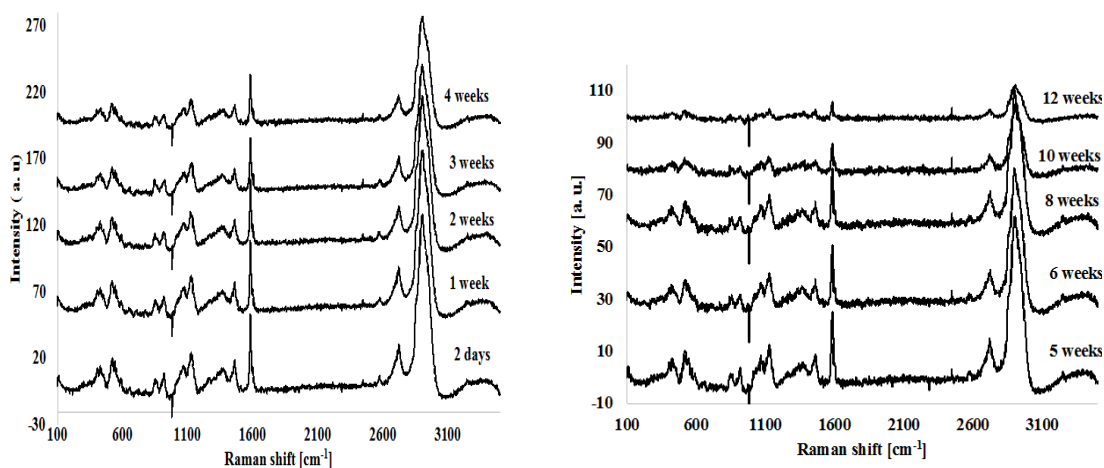
Figure 4.22 SERS spectra obtained from 1×10^{-1}M Glucose adsorbed on TEG-AuNPs using λex=532nm,P=10 mW, acquisition time =15 s, average=3 scans. All the peaks shown in the SERS spectrum at 402, 512, 835,900,1063 ,1299, 1336, and 1449 cm^{-1} correspond to the Raman spectrum of crystalline Glucose.

As for the aspect of sensitivity, the efficiency of TEG-AuNPs/graphene-like sheet was higher than Au NPs/graphene like sheet. The current results from glucose detection shows that the detection limit is around 10^{-10}M with the enhancement factor 5.5×10^{11}. Therefore, our results illustrate that SERS is capable of detecting, the probe with high enhancement factor.

4.3 Using Partition Layer to Improve The Efficiency for Modified-graphene Like Sheet Substrate for Glucose Detection

4.3.1 Experimental Details

4.3.1.1 Substrate preparation. Figure 4.23 schematically explains the simple process for the synthesis of TEG/AuNPs/ modified-Graphene like sheet. The substrate was exposed to the plasma treatment using of 60W for one hour (60mins). The Au nanoparticles was also synthesized by chemical reduction methods as described by Turkevich [137] and Frens [138].
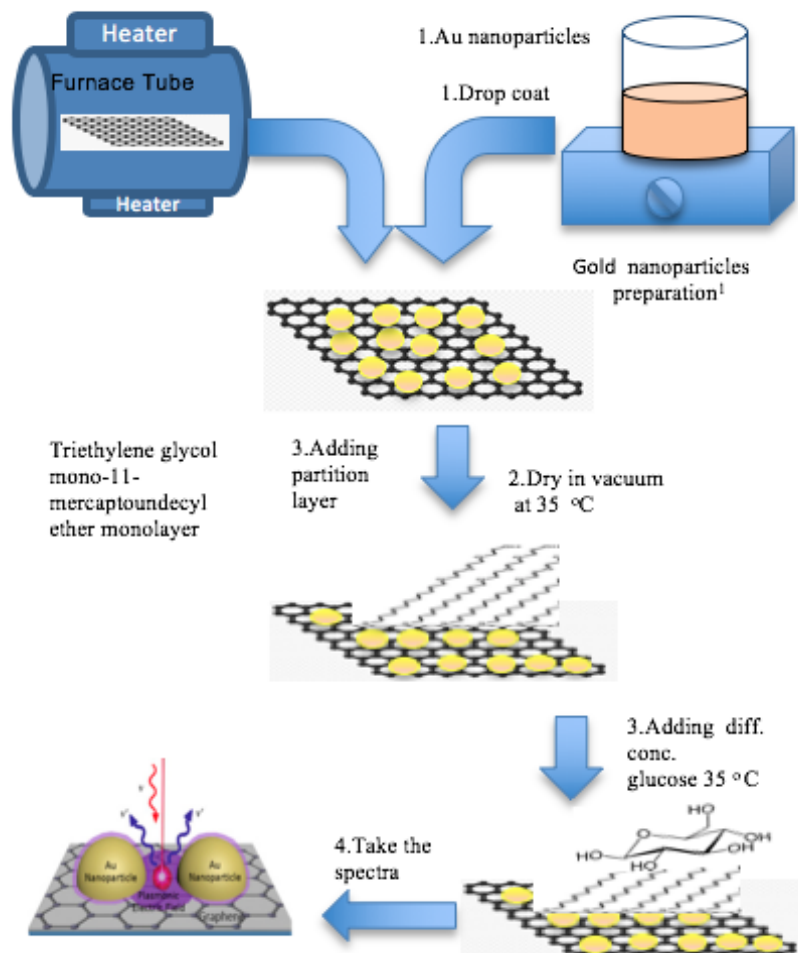
Figure 4.23 Diagram of SERS substrate preparation.

4.3.2 Results and Discussion

Investigation of the inherent physical characteristics of graphene requires Raman spectroscopy as one of the main tools [155]. This part analyzes how the pristine graphene of Raman spectra acts prior to and after plasma treatment. The characteristics of the Raman spectrum for pristine sample are the following: 2D band (~2700cm^{-1}) and G band (~1580cm^{-1}) [156]. The G band intensity is longer than that of the 2D band; that is an indication of the multilayer nature of graphene as can be seen in Figure 4.24).

Nitrogen plasma treatment is followed with the appearance of D band and D′ band (1620cm^{-1}). The increase in the D peak (approximately 1350cm^{-1}) several times is evident of the deficiencies made by the plasma treatment [157-159]. However, there is also D′ or D^0 peak (approximately 1617cm^{-1}) correspondence to the deficiencies in the graphene crystalline lattice shown by pyrrolic -N(sp^3 structure) and graphitic relation (N C–N bonding) [160]. Increase the number of defects after the plasma treatment can be seen in SEM images in Figure 4.25.
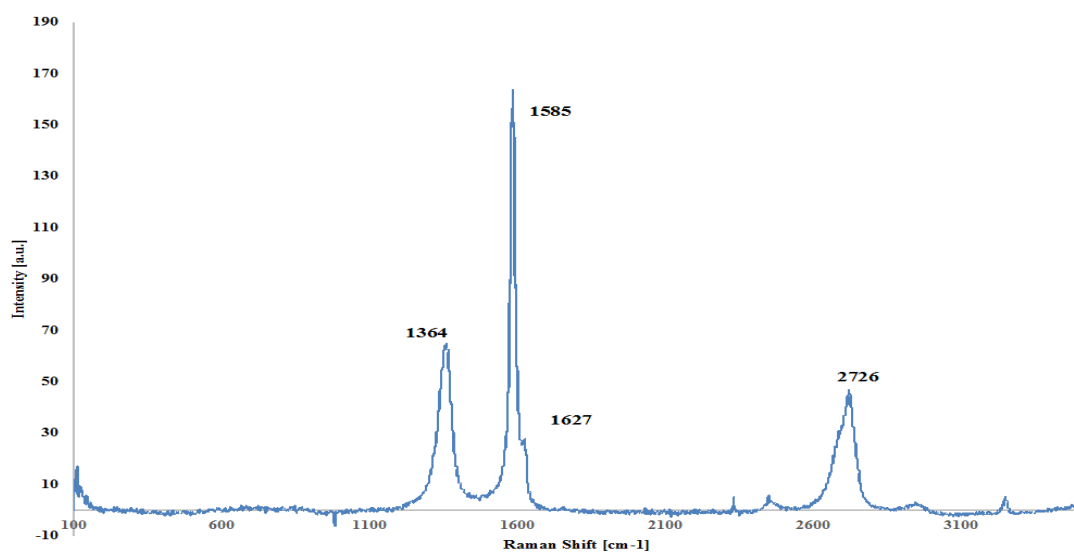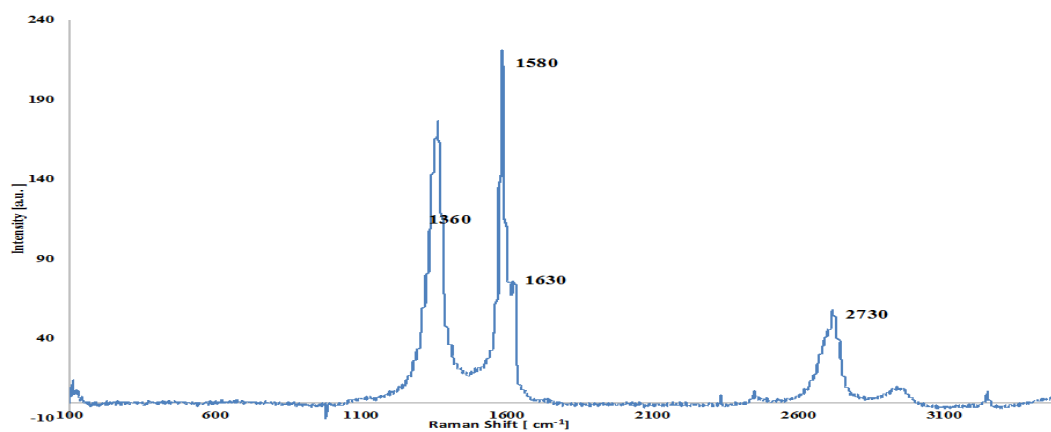
Figure 4.24 Normal Raman spectrum for modified graphene like sheet after plasma treatment λex=532nm, P=10mW, acquisition time = 45s.
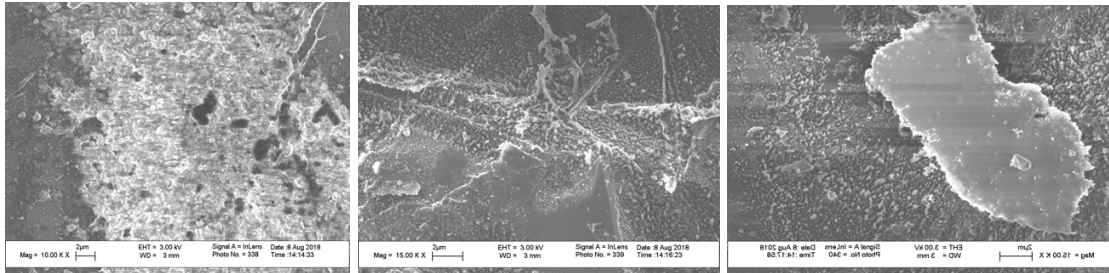
Figure 4.25 SEM image for graphene like sheet after plasma treatment at 2μm.

Increase in the number of defects after the plasma treatment can be seen in SEM images in Figure 4.25. Figure 4.16 shows the graphene-like sheet prior to plasma treatment, it is possible to observe several cracks in graphene, and the number of cracks significantly grows as a result of plasma treatment [161].

Figure 4.26 presents Raman spectra of glucose on TEG-AuNps-modified graphene-like sheet. Raman signal can be enhanced with the nitrogen doping in graphene. When the quantity of hydrophilic polar sites increases, it leads to the increased number of surface areas which the gold nanoparticles can access. The local electronic structures can be under the control of pyrrolic and pyridinic nitrogen atoms, and that enhances the bonds between the Au nanoparticles and N atoms.
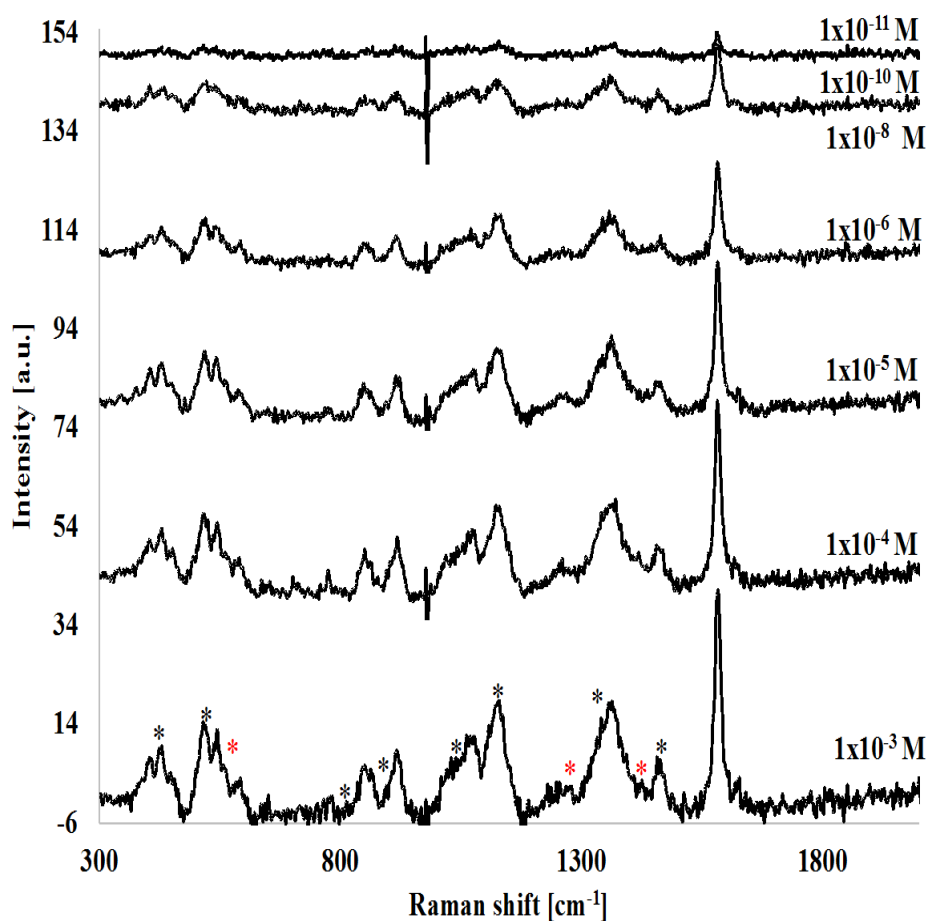
Figure 4.26 Normal Raman spectrum with various levels of Glucose concentration on modified-Graphene / Au nanoparticle with TEG partition layer , P=10mW λex=532nm; acquisition time 15 s for $1x10^{-1}$M; acquisition time 20s for $1x10^{-3}$ M; acquisition time 30s for $1x10^{-4}$M; acquisition time 40 s for $1x10^{-5}$M; acquisition time 45 s for $1x10^{-6}$M; acquisition time 60 s for $1x10^{-8}$M; acquisition time 90s for $1x10^{-10}$M; acquisition time 120s for $1x10^{-11}$M. SERS spectrum has black lines at 430, 545, 855, 922, 1070, 1130, 1353 and 1461cm^{-1} in accordance with the crystalline glucose Raman spectrum.
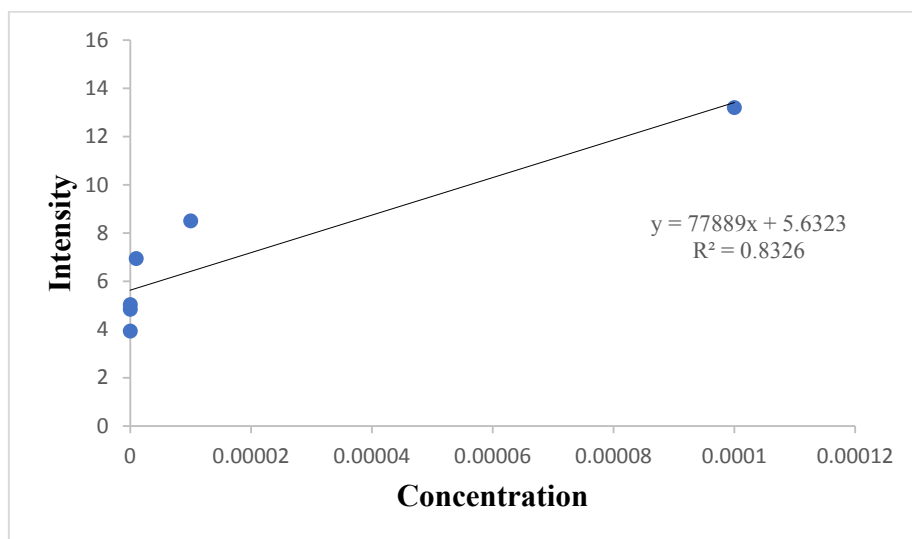
Figure 4.27 Intensity in arbitrary units of the glucose Raman peak at 1,340 cm^{-1} versus the molar concentration of glucose on the SERS substrate.

Figure 4.30 demonstrates the relation between the intensity of glucose Raman peak and relevant concentration at 1340cm^{-1}. We identified an adequate SERS linear response at the range of 10^{-3}M to 10^{-11}M. The linear fit calibration demonstrates $R^2 = 0.83$, and the enhancement of the highest efficiency takes place at Raman peaks (1340 cm^{-1}).

Conclusions

The results discussed demonstrate that SERS is capable of detecting probe molecules with high enhancement factors. The modified graphene-like sheet with gold nanoparticles exhibit the best result so far, it gives excellent enhancement for glucose detection up to 10^{-11} M, due to use of the partition layer discussed here on this substrate.

Metal nanostructures provide extremely high EFs for Raman scattering, making single molecule detection possible. The Table following shows the enhancement factors for the substrates studied.

Table 4.1 Enhancement Factor and Limit of Detection for Graphene like Sheet Substrates

Substrate	Limit of detection	Enhancement Factor
Glucose/ AuNP Graphene like sheet	1×10^{-8}	2.4×10^{9}
Glucose/ TEG/AuNP Graphene like sheet	1×10^{-10}	5.5×10^{11}
Glucose/ TEG/AuNP Modified Graphene like sheet	1×10^{-11}	6.4×10^{12}

CHAPTER 5

PART I(SILVER NANOPARTICLES ON GRAPHITE MICROFIBER SHEET AS SERE SUBSTRATE)

5.1 (Triethylene Glycol-Stabilized Silver Nanoparticles On Graphite Microfiber Sheet For SERS)

5.1.1 Introduction

In this chapter we will be focused on the efficiency of Ag NPs functionalized with TEG on graphite fibers in SERS of glucose and R6G. The stability of the partition layers will be studied and in the second part of this chapter the use of Au nanoparticles on graphite fibers with TEG for SERS will be studied. The goal will be to compare the two types of nanoparticles.

5.1.2 Experimental Details

5.1.2.1 Substrate preparation using silver nanoparticles to detect R6G.

First step: Using R6G stock solutions in the following concentrations: 10^{-2} M, 10^{-3} M, 10^{-4}M, 10^{-5}M, 10^{-6}M, 10^{-8}M, 10^{-12} M and10^{-16}M, and commercial silver nanoparticles that are prepared via citrate reduction. At the beginning, several drops of silver nanoparticles were deposited by drop coating on a graphite fiber sheet. Then, a few drops of triethylene glycol mono-11-mercaptoundecyl ether monolayer were dropped and left in the vacuum for 24 h. After the drops have dried out, a R6G stock solution in different concentrations is dropped on several graphite sheets. When the silver nanoparticle solution was placed on the sheet with the partition layer, the drying was done at 35° C in the oven. After the drying was done, the Raman spectra of the graphene sheets were taken each separately.

5.1.2.2 Substrate preparation using silver nanoparticles to detect glucose. The silver nanoparticles were used to prepare the substrate with a partition layer as described in the previous step in order to detect glucose at different concentration.

5.1.2.3 Substrate preparation. Herein, the gold nanoparticles were used to prepare the substrate instead of silver nanoparticles as described in the previous step to detect glucose at different concentrations as can be seen in Figure.
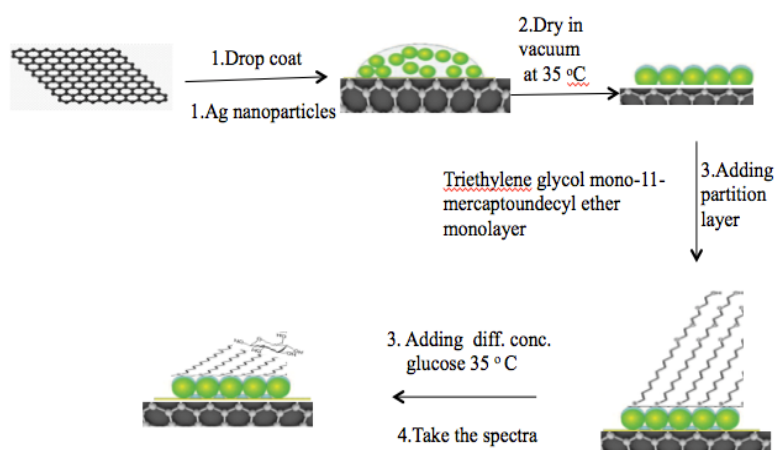
Figure 5.1 Diagram of SERS substrate preparation

5.1.3 Results and Discussion

Figure 5.2 demonstrates the graphite fibers sheet SEM images after gold was placed in various types of magnification. Figure 5.3 show that silver nanoparticles deposition on the graphite sheet can be defined as uniform.
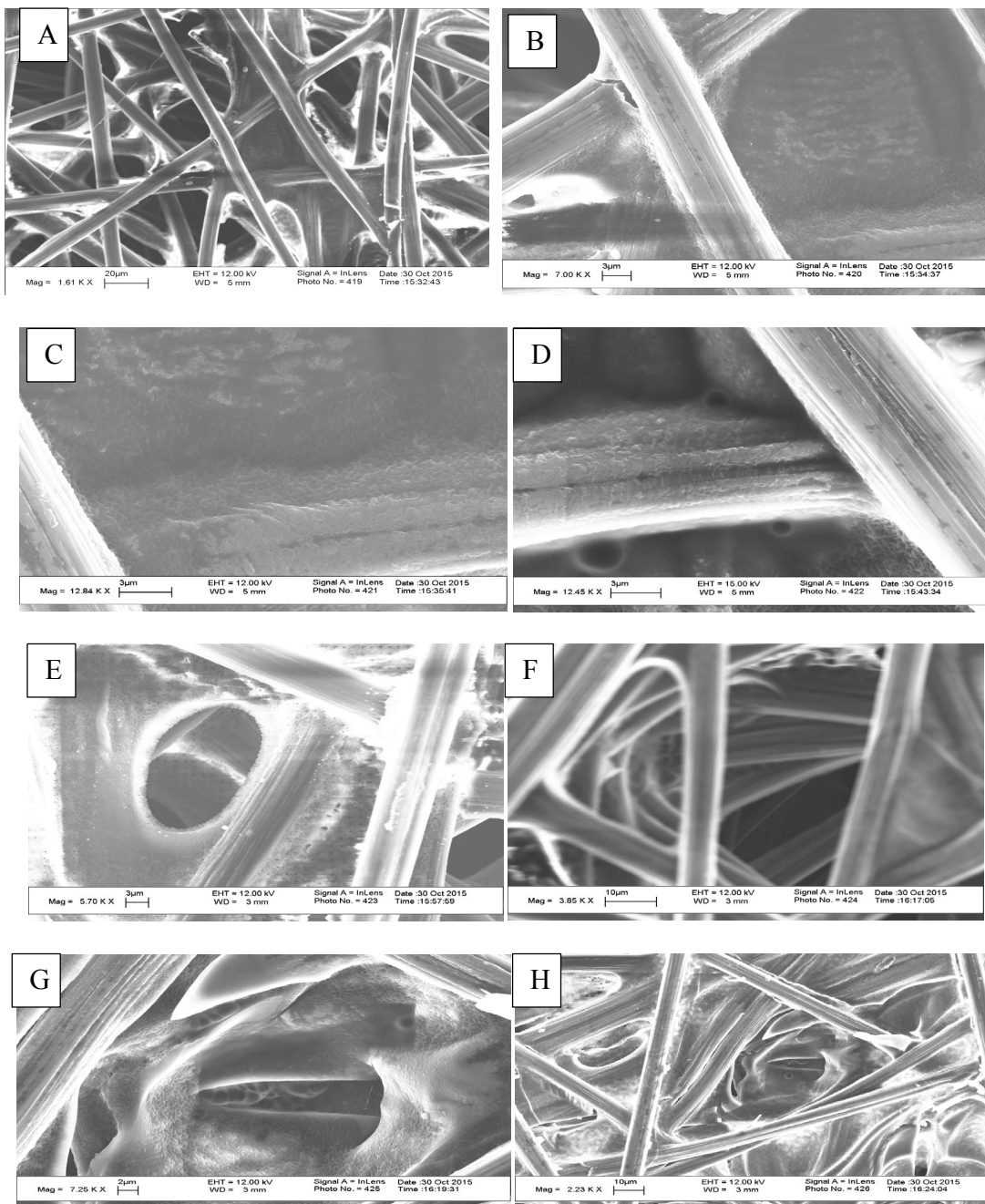
Figure 5.2 SEM images for pristine graphite nanofiber sheet at different magnifications: A) 20μm of magnification, B, C, D, E) 3μm of magnification G) 2μm of magnification and H)10μm to show the morphology of graphite fibers sheet.
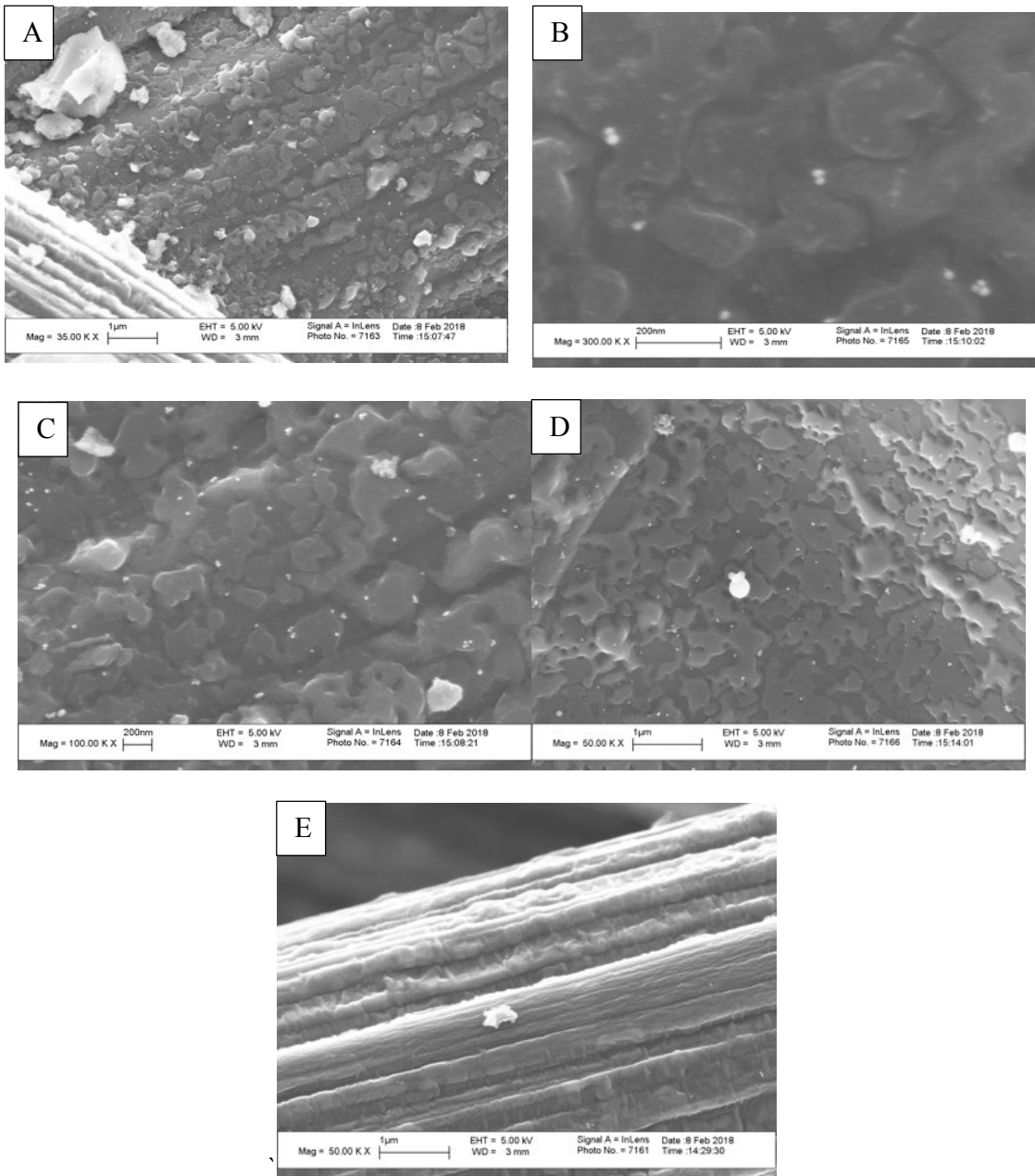
Figure 5.3 SEM images for graphite fibers sheet after silver nanoparticle deposition at
A, D, E) 1μm of magnification, and B, C) 200nm of magnification to show the distribution
of silver nanoparticles on graphite fibers sheet.
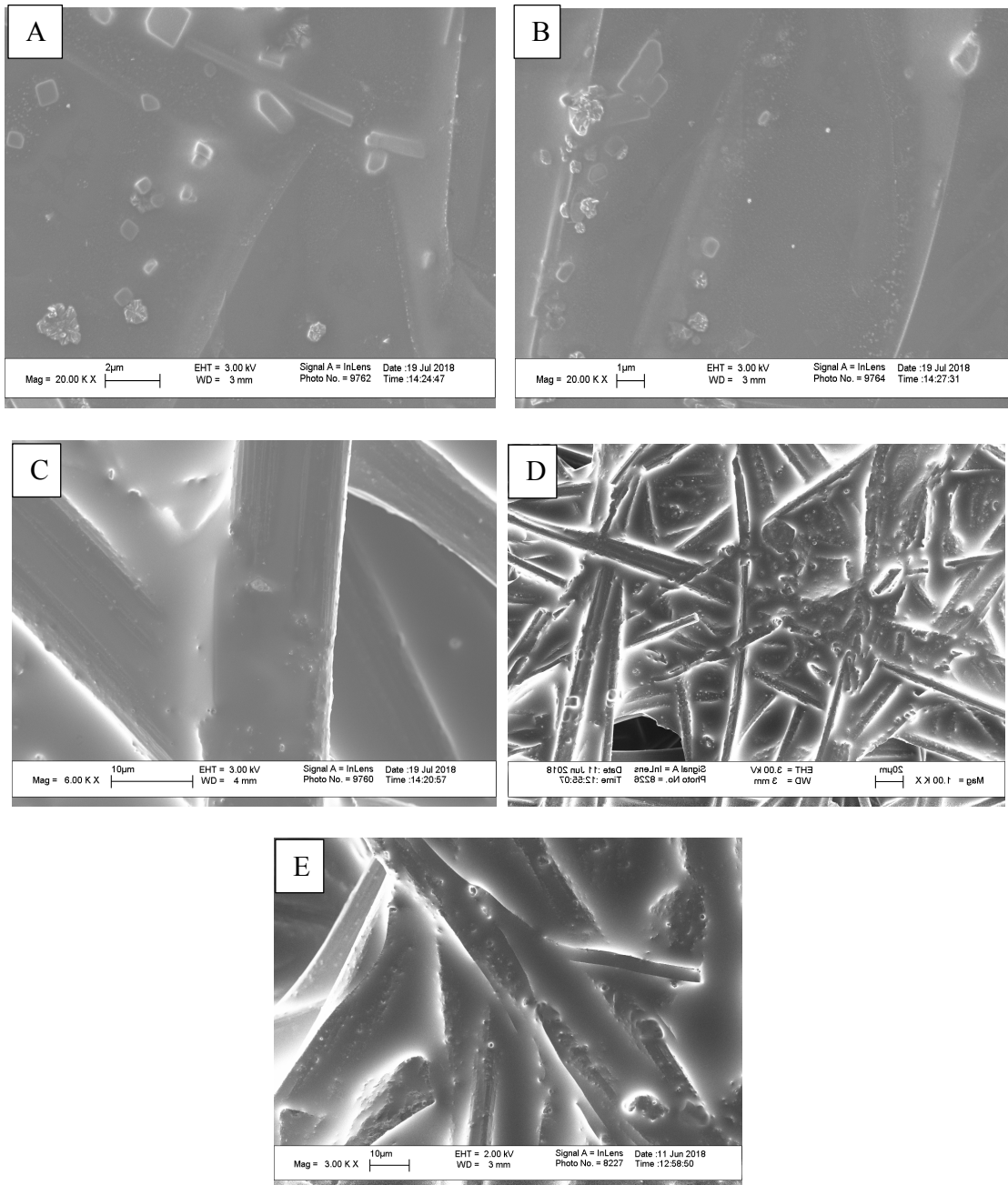
Figure 5.4 SEM images for graphite sheet after silver nanoparticle and partition layer deposition at A) 2μm of magnification B) at 1μm of magnification C, E) 10μm of magnification, D) at 20μm of magnification to show the distribution of partition layer on graphite fibers sheet.

The first stage, including partitioning of R6G, was done into triethylene glycol mono-11-mercaptoundecyl ether monolayer with absorption over graphite sheet on a silver nanoparticles film; it was pre-concentrated in the frames of the electromagnetic field enhancement zone.

Figure 5.5 demonstrates the Raman spectra related to Triethylene glycol mono-11-mercaptoundecyl ether provided that 780 laser for 30s is used for Ag nanoparticles/graphite sheet. There is a significant difference with the SERS response development for TEG-Ag/graphite sheet. Initially, the TEG-AgNPs /graphene like sheet demonstrated a negligible SERS signal, which was increased greatly when the partition layer was added for connections between the OH group and R6G, or glucose as well as the SH group and nanoparticles. TEG Ligand is mandatory to bind the nanoparticles surface by either chemisorption, hydrophobic interactions or electrostatic attraction. The bond dissociation energy associated with Ag−S is 216.7 ± 14.6 kJ mol^{-1} which is a stable and strong bond [162].
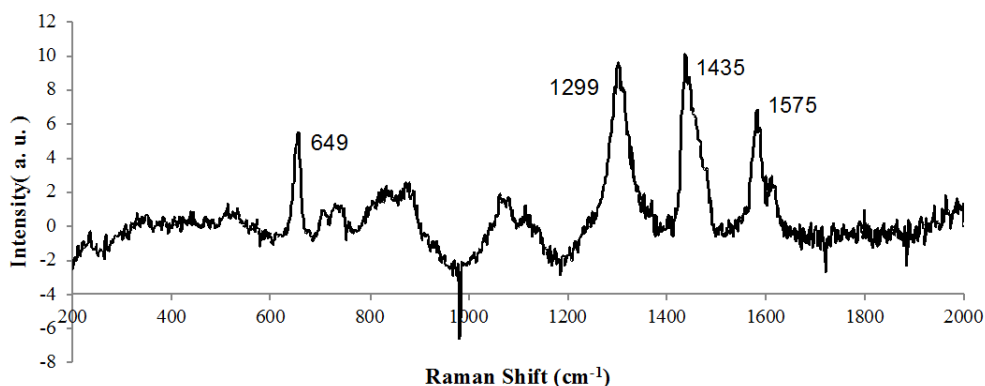
Figure 5.5 Raman spectra for triethylene glycol mono-11-mercaptoundecyl ether on Ag nanoparticles/graphite sheet using 780 laser for 30s.
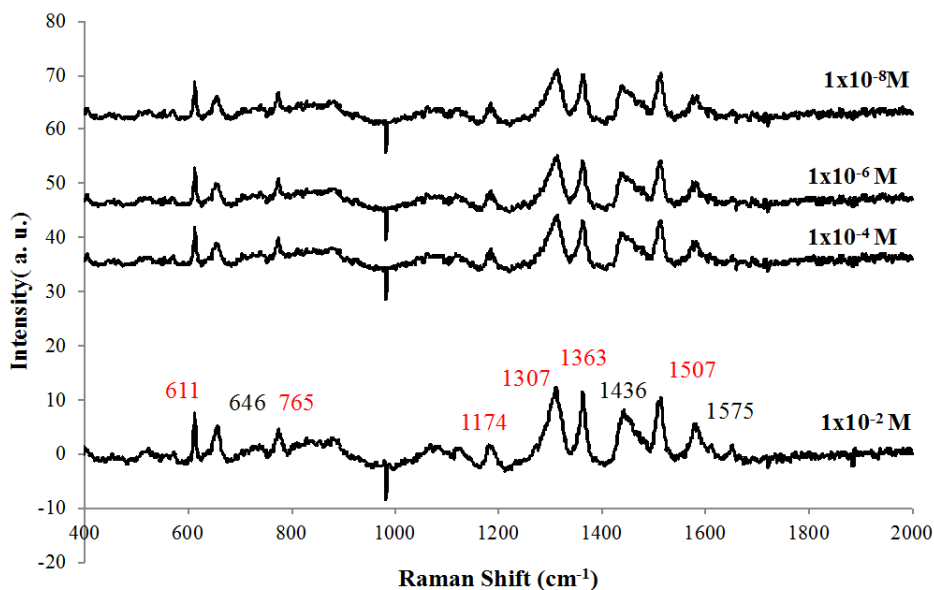
Figure 5.6 a) SERS for different concentrations of R6G on Ag nanoparticles /Graphite with partition layer using λ_{ex}=782nm, P=10mW, acquisition time =15s, average=3 scans. All the peaks shown in red in the SERS spectrum at 611, 765, 1174, 1307, 1363 and 1507cm^{-1} correspond to the Raman spectrum of crystalline R6G.
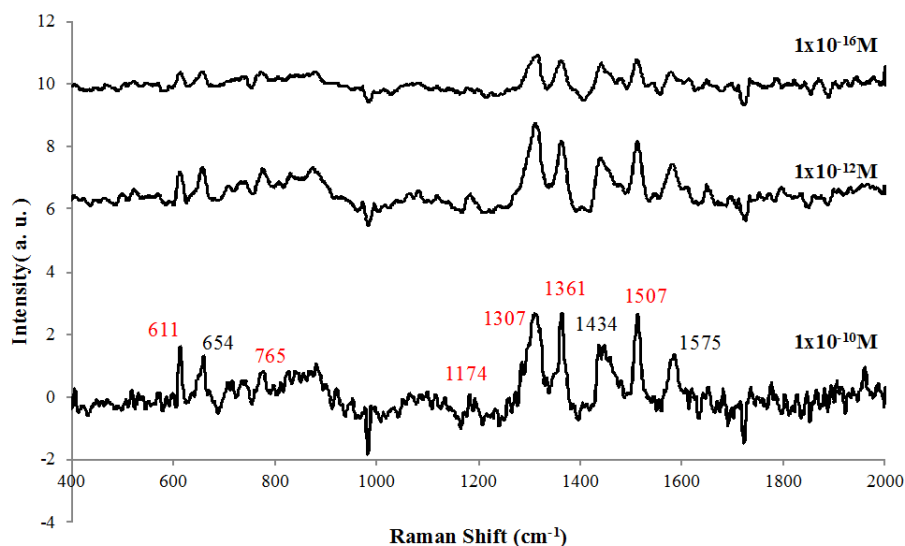
Figure 5.6 b) Normal Raman spectrum of different concentrations of R6G on Ag nanoparticles /Graphite with partition layer, λ_{ex}=782nm, P=10mW, acquisition time for 1x10^{-10}M =60s, acquisition time for 1x10^{-12} M =90s and acquisition time for 1x10^{-16} M=120 s. All the numbers in red in the SERS spectrum at 611, 765, 1174, 1307,1363 and 1507 cm^{-1} correspond to the Raman spectrum of crystalline R6G.

84

According to the results obtained, the substrates can ensure the enhancement of SERS factors up to 2.3×10^{14} (10^{-16}M as a detection limit) in R6G aqueous solutions.

The second stage includes the affinity of glucose to bare metal surfaces, which is very low. Consequently, it is necessary to ensure the partition of the glucose TEG to the surface for SERS detection. It is also required to ensure facilitation of the interaction between the surface triethylene glycol mono-11-mercaptoundecyl ether monolayer and the probed glucose molecules in order to increase the number of the glucose. Moreover, we also need to ensure that the partition layer can reversibly bind glucose; thus, the reflection of the glucose level fluctuations should be accurate.

The increase in the intensity of the interaction between the surface and glucose can be attained with the help of a TEG partition layer, which also enables the researchers to implement the reversible glucose binding. Partitioning of glucose was done with TEG via adsorption on a film made of silver nanoparticles over graphite fibers sheet; besides, it was pre-concentrated in the limits of the electromagnetic field enhancement zone.

The preference was given to TEG as a glucose partition layer because it is biocompatible, and it has excellent hydrophilic and hydrophobic properties. Significant progress is being made towards the long-term objective of glucose sensor fabrication. The used mixed compound with its hydrophilic and hydrophilic characteristics is chosen as a perfect option for detecting glucose.

Previous research has demonstrated that it is effective to use decanthiol DT[121] as well as tri-(Ethelene glycol)-terminated alkane) (EG3) [64] as partition layers. This assumption was stems from other investigations that have specified the hydrophobic

features of DT and its incompatibility with the aqueous environment. As for EG3, it does not allow appropriate synthesis; thus, it is available only in limited quantities.

Figure 5.7 demonstrates analysis of different glucose concentration in Raman spectra on TEG-Ag nanoparticles/graphite sheet. It also presents the peak fingerprint of glucose, which identifies the peak shift of glucose equal to about 10cm^{-1}. The research of the sources certifies that in contrast to the Raman spectral bands of a same-compound typical kind, the SERS spectral bands can move up to 25cm^{-1} [144]. There is an exact matching of peaks in SERS spectrum with the Raman spectrum crystalline glucose at such peaks as 425, 538, 839, 910, 1069, 1124, 1343, and 1456cm^{-1}.

The glucose spectra are characterized with a high level of strength and stability of the bond. Moreover, the citrate-reduced silver nanoparticles (AgNPs) have the citrate coating to reduce the static repulsion and increase the stabilization for nanoparticles [163].

Figure 5.7 shows Raman spectra on TEG - Au nanoparticles/graphite sheet for glucose.
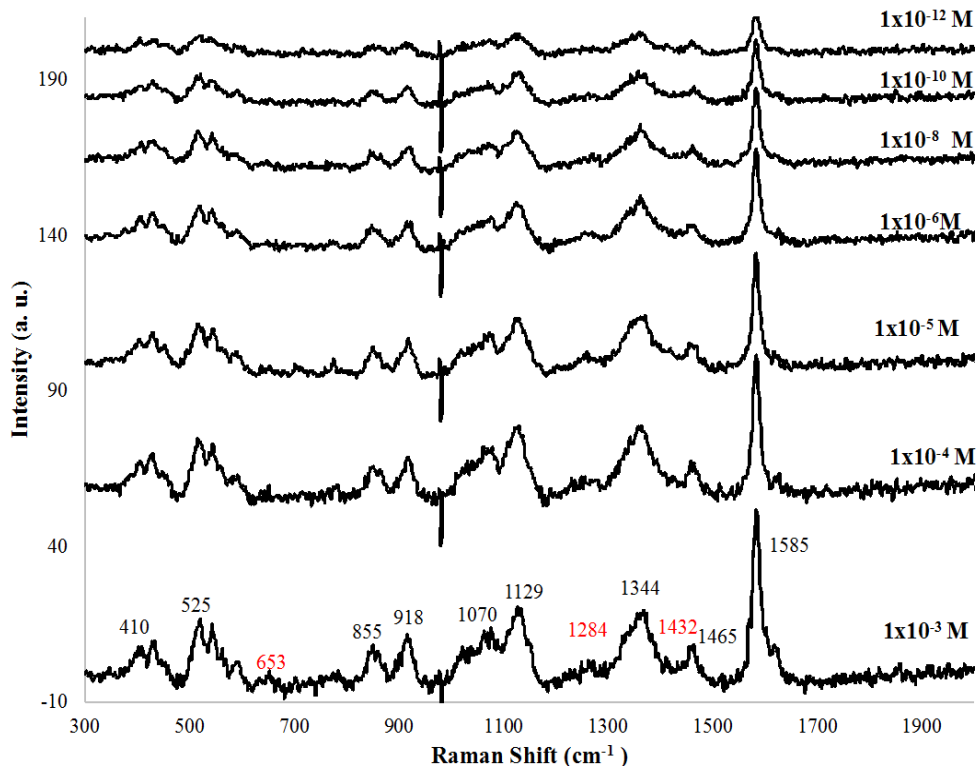
Figure 5.7 SERS for different concentrations of Glucose on Ag nanoparticles /Graphite with partition layer using λ_{ex}=532nm, P=10mW, acquisition time =15s, average=3 scans. All the peaks shown in red in the SERS spectrum at 427, 509,834, 907, 1064,1110,1356, and 1449cm^{-1} correspond to the Raman spectrum of glucose.

The stability of nanoparticles can be increased under the effect of the following three factors: first, it is the citrate needed to ensure that gold and silver nanoparticles get attached to gold or silver with the help of carboxylic or hydroxy group. Secondly, TEG ligand or the partition layer impacts the stability and spectra via the connections between nanoparticles and SH group as well as glucose and the OH group. Binding of the surfaces that nanoparticles have can be done with obligatory TEG Ligand by electrostatic attraction, hydrophobic interactions, or chemisorption. Thirdly, the nanoparticles' stability can be increased with glucose as a capping agent. Previous research results indicate that the

surface concentration and conformation of thiol-terminated poly(ethylene glucol) PEG on gold nanoparticles are studied before and after coadsorption of alkane-thiols. The results of the TGA or thermo-gravimetric analysis specify that alkane-thiol ligands will competitively adsorb on gold nanoparticles surface, and that the extent of PEG-thiol replacement depends on the specific length of the alkane-thiol molecule [164].
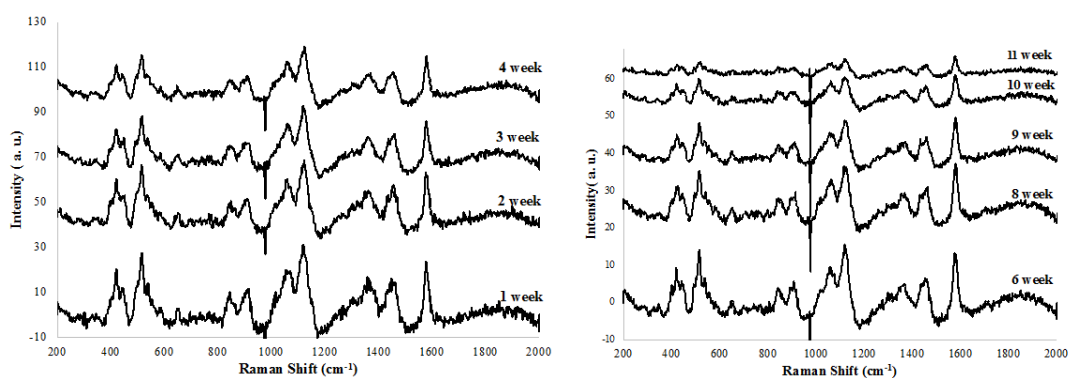
Figure 5.8 SERRS spectra obtained from 1×10^{-1}M Glucose adsorbed on TEG-AgNPs/ graphite sheet using λ_{ex}=532nm, P=10mW, acquisition time =15s, average=3 scans. All the peaks shown in the SERS spectrum at 427, 509, 834, 907, 1064, 1110, 1356, and 1449 cm^{-1} correspond to the Raman spectrum of crystalline glucose.

PART II(GOLD NANOPARTICLES ON GRAPHITE MICROFIBER SHEET AS SERS SUBSTATE)

5.2 Use of Partition Layer to improve Raman Enhancement on Graphite Nano-fiber Sheets with Gold Nanoparticles.

Figure 5.9 shows the graphite sheet SEM images after gold was placed in various types of magnification. Figures(5.9-5.10) show that gold nanoparticles deposition on the graphite sheet can be defined as uniform. The size of gold nanoparticles is large when compared to silver nanoparticles, as shown in SEM images. In addition, the gold nanoparticles are on the fiber surface and the particles were distributed on the surface in a non-uniform method.
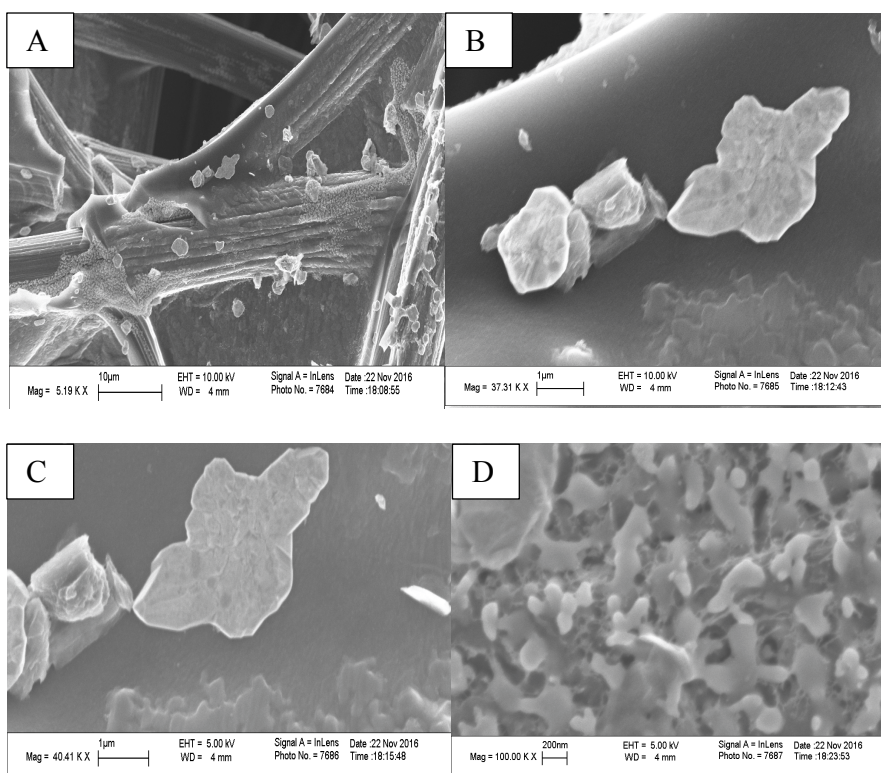
Figure 5.9 SEM images for graphite fiber sheet after gold nanoparticle deposition at A)10μm of magnification B) at 1μm of magnification C) at 1μm of magnification D) 200nm of magnification to show the distribution and the size of gold nanoparticles on graphite fiber sheet
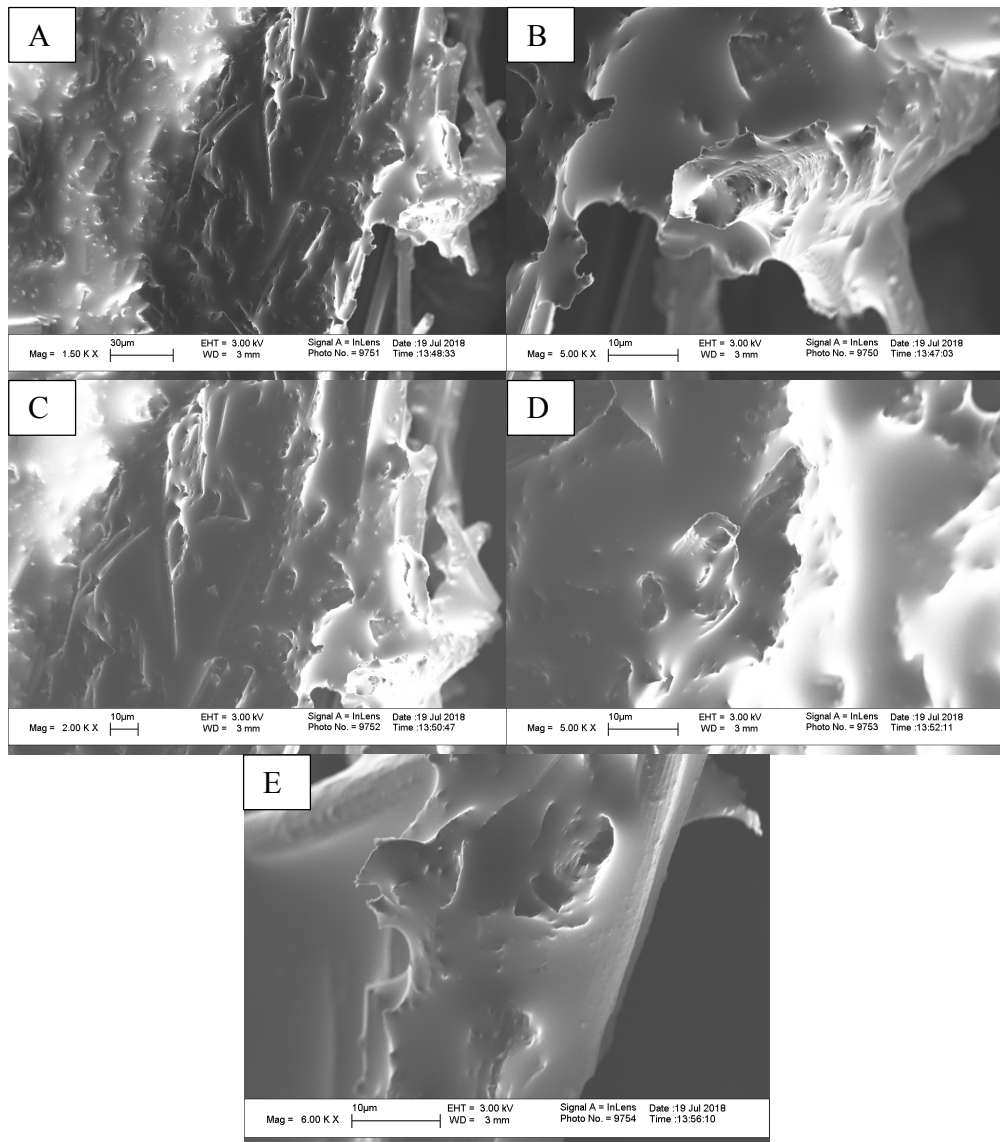
Figure 5.10 SEM images for graphite fiber sheet after partition layer deposition at A) 30μm of magnification B, C, D, and E) at 10μm of magnification to show the distribution of partition layer on graphite fiber sheet.
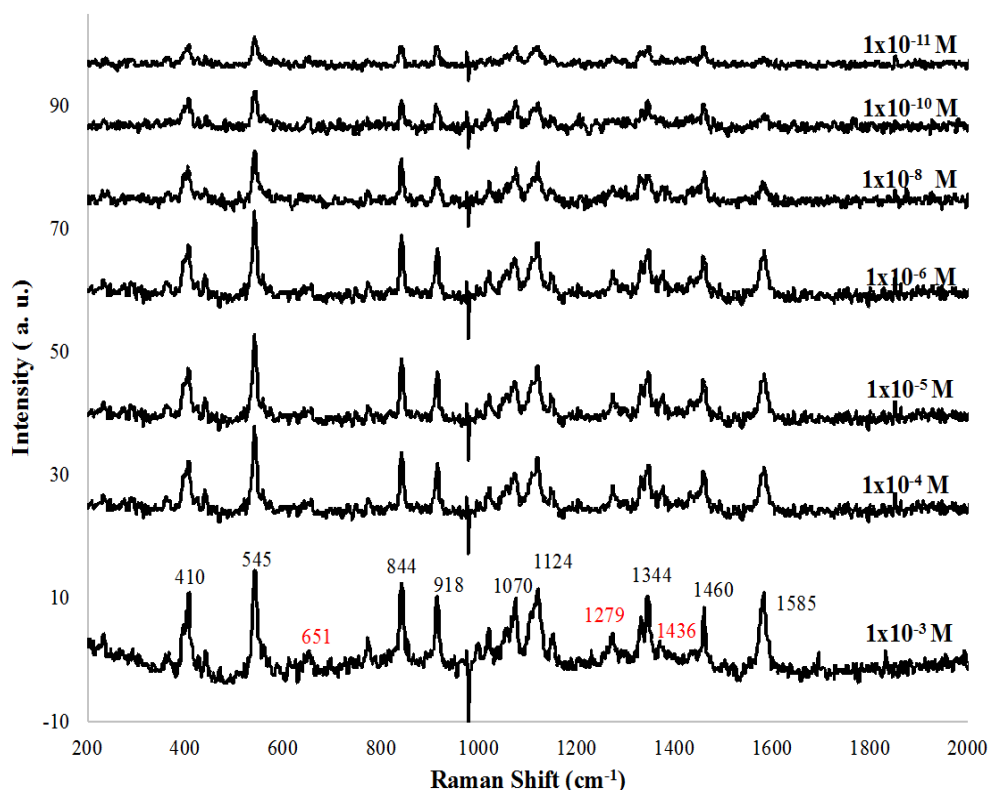
Figure 5.11 SERS for different concentrations of Glucose on Ag nanoparticles /Graphite with partition layer using λ_{ex}=532nm for 60s with P=10mW, acquisition time =15s, average=3 scans. All the peaks shown in red in the SERS spectrum 410, 545, 844, 918, 1064,1124, 1344, and 1460cm^{-1} correspond to the Raman spectrum of crystalline glucose.

The sensitivity perspective shows higher efficiency of TEG-AgNPs-graphite sheet in comparison to TEG-Au NPs-graphite sheet. the lowest detection limit of glucose is 10^{-12} M on TEG -Ag NPs-graphite sheet with enhancement factor equal to 2.83×10^{13} while the lowest detection limit of glucose on TEG-AuNPs -graphite sheet is 10^{-11} with enhancement factor equal to 2.43×10^{12}. These different results for the graphite sheet may refer to nanoparticles size , where the gold nanoparticles average size is 10 - 45 nm, while silver nanoparticles size is 20 nm

The thiol group helps to form a stable modification on the gold or silver surface of SERS-active substrates. A partition layer is used to report and amplify the detection signal, and the

specific functional group on each thioalkane-based molecule contributes to the detection specificity.

Conclusion

In the present work, a TEG polymer at room temperature has been numerically modeled, based on the density-functional theory. All thermochemical values, including energies, geometries, and vibrational frequencies of ligand were investigated. Calculations were carried out with Spartan software, using the functional Hartee-Fock basis set $6\text{-}311 + G*$.

Figure 5.12 is showing the minimum energy structure for the polymer under study.
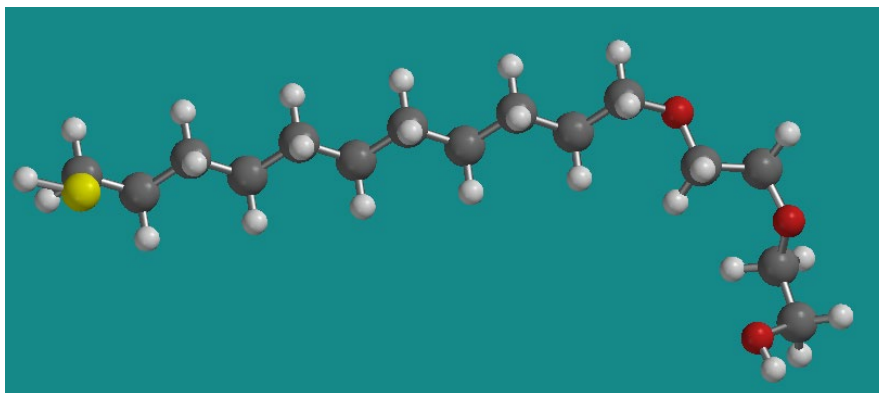
Figure 5.12 Minimum energy structure of TEG.

The IR absorption spectra displayed in Figure 5.13 . The most intense bands in the fingerprint region for TEG are located at 1299,14000.
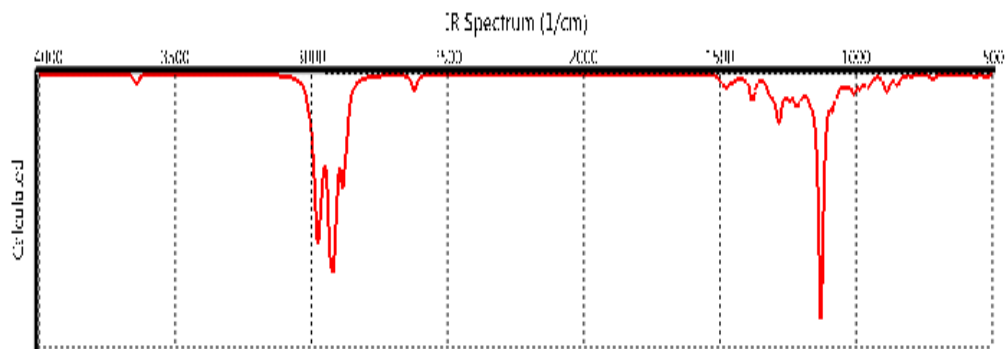
Figure 5.13 IR spectrum using DFT for TEG polymer.

The following Table 5.1 exhibits the thermodynamic properties of TEG polymer using geometry optimization .method REDF2 using BASIS SET: 6-31G(D).

Table 5.1 Thermochemical Values at 298 K for TEG. Energies in kJ/mol and Entropies in J/mol/K.

Method	Thermochemical Value				
	H^o	S^o (J/mol)	G^o	ZPE(kJ/mol)	
Hartee-Fock 6-311G*	-1213.59	549.99	-1213.659	1214.83	
REDF2 6-31G(D)	1213.59	595.05	-1213.659	1214.87	

As can be seen in the Table 5.1, there are slight differences between the results obtained using Hartree-Fock and REDF2 methods.

Raman spectra have been obtained for the (TEG) polymer using the same methods as can be seen in the following Figure 5.13.
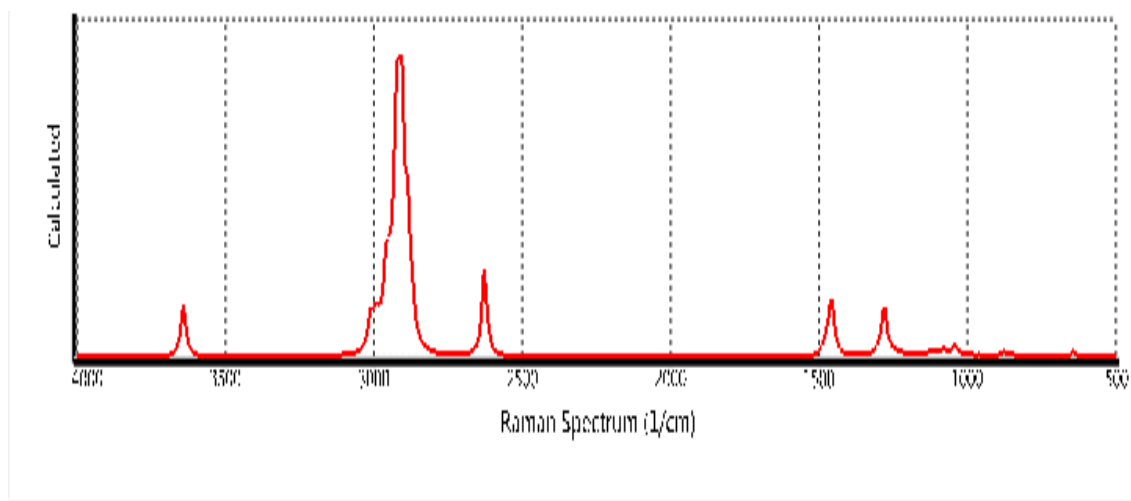
Figure 5.14 Calculated vibrational spectrum of TEG.

As shown in Figure 5.14, the 1169 to 1185cm^{-1} spectral range corresponds to the CH-rocking and -C-O-C stretching vibrational frequency of TEG. The two peaks at 1360 and 1467 cm^{-1} refer to -CH$_3$ and -CH$_2$ deformations and asymmetrical CH$_3$ deformations, respectively. Another feature in the Raman spectra is the appearance of the 650cm^{-1} line, attributed to the S-C stretching vibration.

The results discussed illustrate the ability of SERS to identify the probe molecules with high enhancement. Our results show that the previous substrate detects 10^{-16}M of R6G which is near single molecule detection. The substrate used exhibited an enhancement factor for SERS of 2.3×10^{14} due to the partition layer. One of the features of substrates was long-term stability, which showed SERS activity during a three-month period with no noticeable changes in substrate morphology. Graphite substrates demonstrate SERS performance that was several orders of magnitude higher than that of nanocrystalline silver on quartz presented in Chapter 3. The results for glucose detection show that the limit is around 10^{-12}M with the enhancement factor 2.83×10^{13}. Therefore, our results demonstrate

that SERS is capable of detecting analytes with high enhancement factor using the substrates prepared here.

CHAPTER 6

CONDUCTING POLYMER POLYPYRROLE ON MODIFIED GRAPHITE MICROFIBERS FOR SERS DETECTION OF GLUCOSE

6.1 Introduction

Despite the reliance of most SERS applications with high level of performance on coinage metal (gold, silver and copper) platforms [27, 165, 166] of micro or nanostructure [27, 165, 166], it is a matter of importance to apply the benefits of on SERS platforms that are free of metal. This was done at a large scale thanks to methods that are both cost- and time-effective. Consequently, the use of ZnO[167], Cu_2O[168], TiO_2 [169], CuTe[168], and other inorganic semiconductors is an object of interest in spite of certain restrictions, in particular synthetic accessibility and low level of performance. Furthermore, there are outstanding advantages of the organic films with the basis of small molecular semi-conductors of π-conjugation over their counterparts of macromolecular and inorganic types. Those advantages include effective control of film fabrication and facile synthesis, versatility in structure, and fine-tuning of optoelectronic characteristics [170-174].

Demand for durable, stable, and resilient semiconductors has driven research in development of organic semiconductors. This need is directed to the formation of organic thin-film semiconductors that require precise molecular designs [175] . Semiconductors are used for making vital parts of electronics, including resistors and memory chips [176]. Polypyrolle is a conductive organic polymer used for developing organic semiconductor applications due to its interesting electrical and electronic properties [177] [178].

Polypyrrole constitutes one of a series of heterocyclic polymers that exhibit both electrical conductivity and interesting electronic properties [179] . The polymer exhibits

relatively high electrical conductivity, as well as increased stability in various oxidized states [179]. Consequently, the polymer offers numerous benefits when compared to other polymers. These benefits include reduced cost in processing, increased water solubility, and an easier oxidation reaction [180].

In this chapter, we will discuss results of glucose detection by SERS using π-conjugated conducting polymers, such as polypyrrole (PPY), after gold nanoparticle deposition by drop-coating on graphite microfiber sheets. These results are related to those obtained for glucose detection using graphene-like sheets considered in Chapter 5. A uniform layer of polypyrrole on graphite microfiber sheets is prepared via electrochemical deposition under cyclic voltammetry conditions.

6.2 Experimental Details

6.2.1 Electrochemical Deposition of PPY

A three-electrode system was set up for polymerization and a graphite fibers sheet of size 1.5x 2cm^2 was used as a working electrode. An electrolyte solution containing 0.1M pyrrole and 0.5M H$_2$SO$_4$ was used for electro-deposition of PPy. Polymerization was carried out at deposition current densities of 15 mAcm^2 with the same deposition time of 400s. The PPy/graphite fiber sheets were used as SERS substrate as shown in Figure 6.1.

6.3.2 Substrate Preparation using Gold Nanoparticles to Detect Glucose

First Step: Using glucose stock solutions in the following concentrations: 10^{-2}M, 10^{-3}M, 10^{-4}M, 10^{-5}M, 10^{-6}M, 10^{-8}M and 10^{-10} M, and gold nanoparticles that are prepared via citrate reduction as described in Chapter 3. At the beginning, several drops of nanoparticles were deposited by drop coating on polypyrrole modified graphite fiber sheet which was

prepared in the previous step. After gold nanoparticles have dried, a glucose stock solution at different concentrations was dropped on several polypyrrole modified-graphite fibers sheets. When the glucose solution was placed on the sheet, the drying was done in an oven at 35º C. After that, the Raman spectra of the graphite sheets were each taken separately.
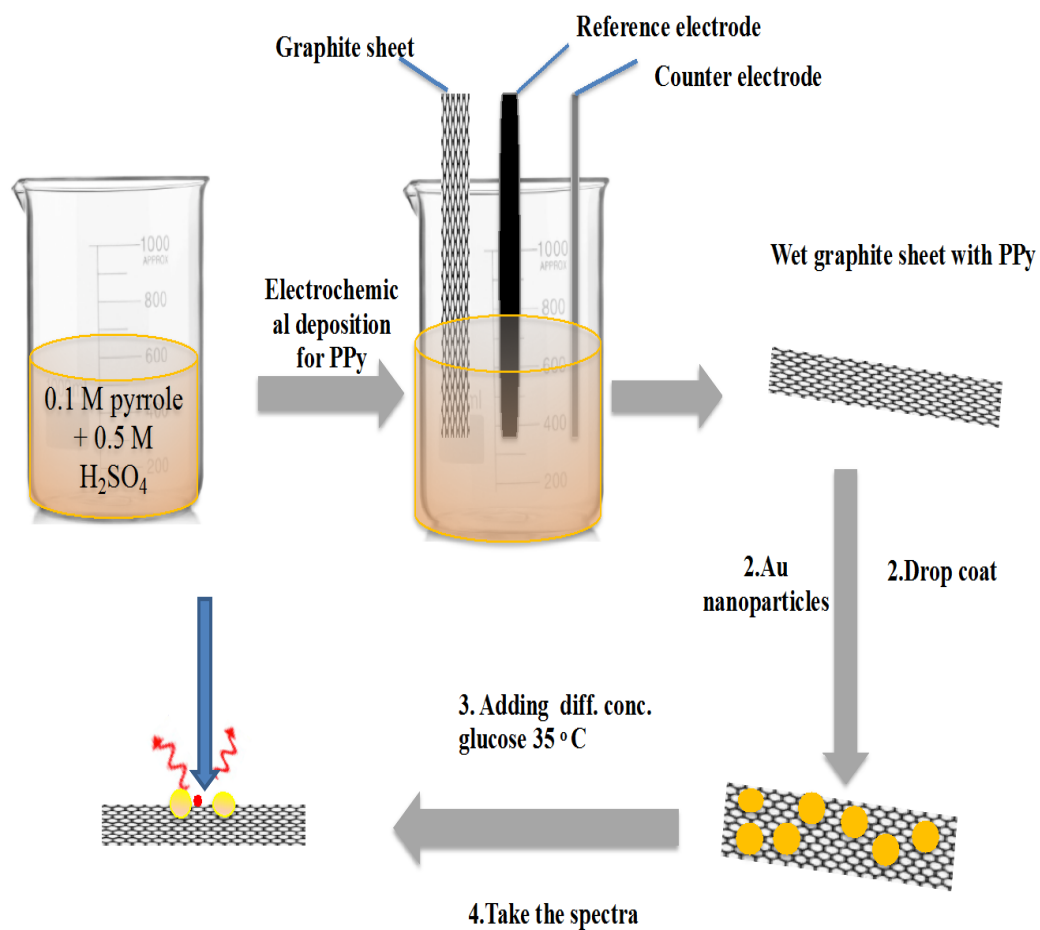
Figure 6.1 Diagram showing preparation of graphite microfiber substrate for SERS. Here the reference electrode is Ag/AgCl and the reference electrode is Pt.

6.3 Results and Discussion

Figure 6.2 displays the graphite sheet SEM images after PPy deposition at different magnifications.
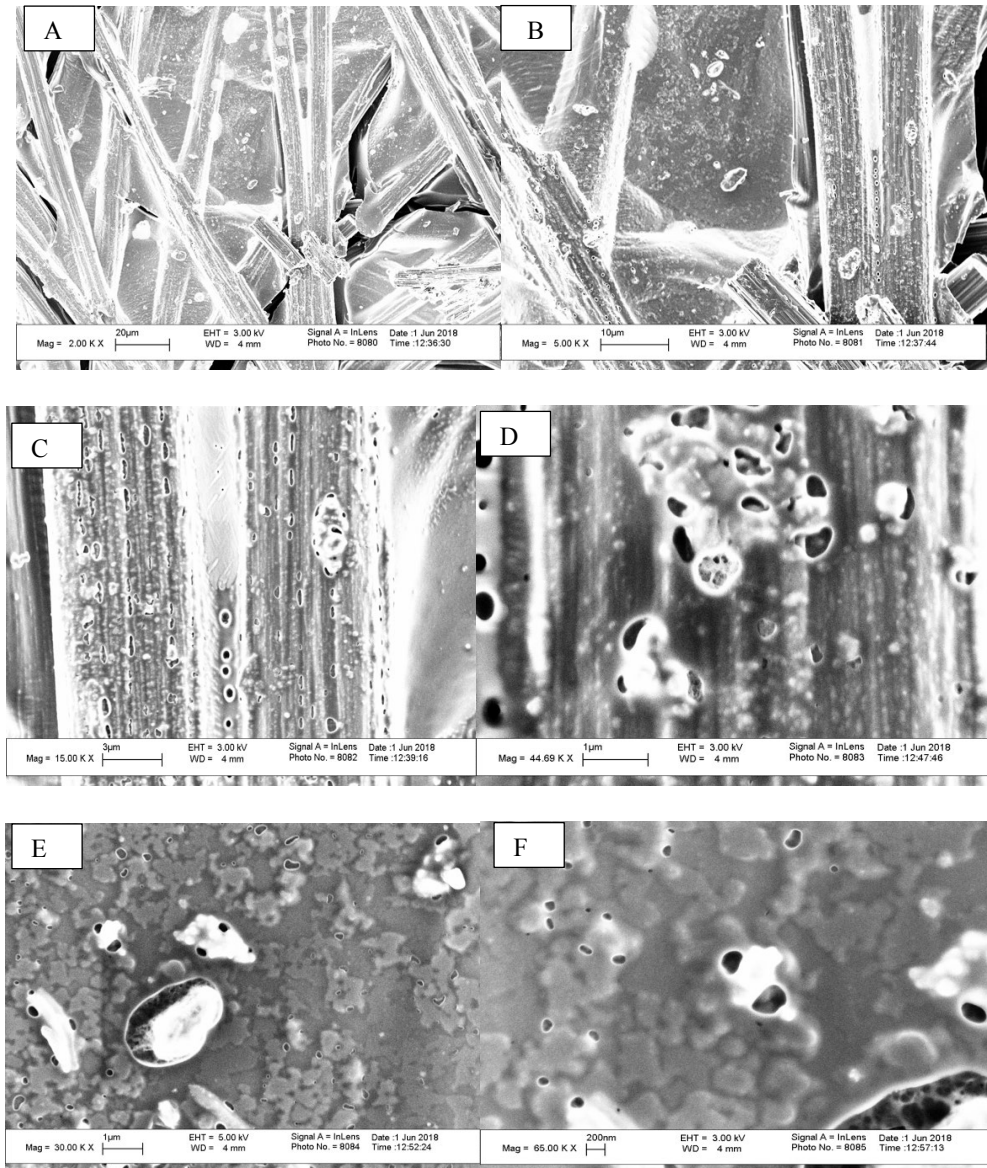
Figure 6.2 SEM images for graphite microfiber sheet after electrochemical deposition of polypyrrole at different magnification levels shown under the images.

The study of polyaniline, polypyrrole and other conducting polymers has been done extensively in terms of possible applications [181]. Synthesis of PPy (polypyrrole) differs

from other conducting polymers since it can be easily done in aqueous media. In comparison with the adhesion of polypyrrole to metal substrates, adhesion is stronger when it is deposited on a carbon electrode.

The pyrrole monomer undergoes electro-oxidation at the anode and deposition on the micro-carbon fiber working electrode. Figure 6.3 shows the cyclic voltammogram which opens up without peaks indicating side reactions.
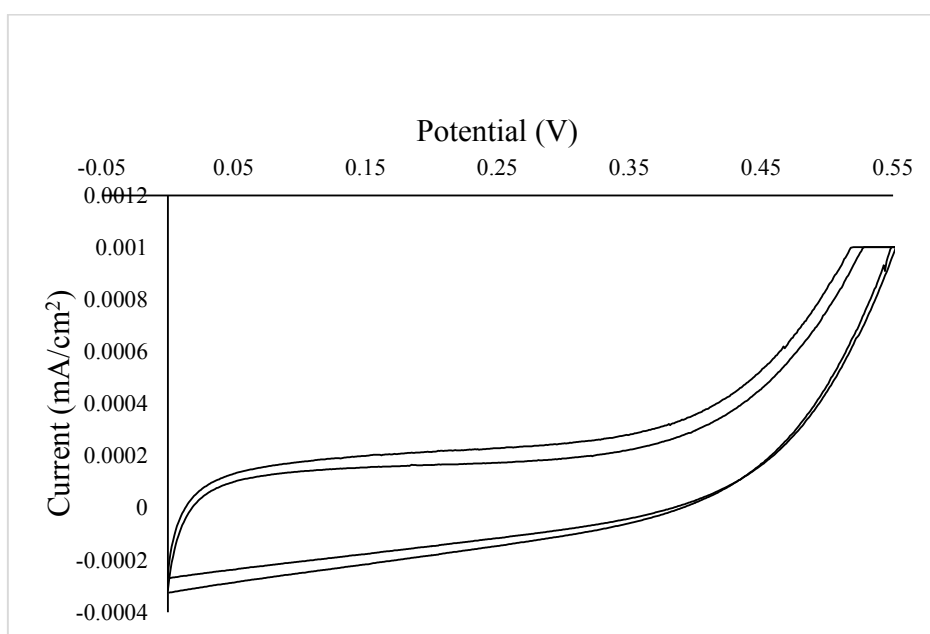
Figure 6.3 Cyclic voltammograms taken during the electro-polymerization of pyrrole (0.1 M) in the presence of 0.5M H_2SO_4 onto graphite fibers. Scan rate: 100 mV/s Number of scans: 4, 400s.

Figure 6.4 demonstrates the Raman spectrum of PPy film / graphite. Bipolaron or di-cations are formed as indicated by lines at 943, 1085, and 1261cm^{-1}, while radical polaron (cation) structure is related to the Raman line at 985cm^{-1} [182] [21].

Pyrrole ring torsion is associated with Raman lines at 616cm^{-1}, C–H wagging at 712cm^{-1}, inter-ring and C–C in-ring stretching at 1320cm^{-1}, and C=C stretching modes of two oxidized structures can be assigned to Raman bands at 1590cm^{-1} [182] [183].
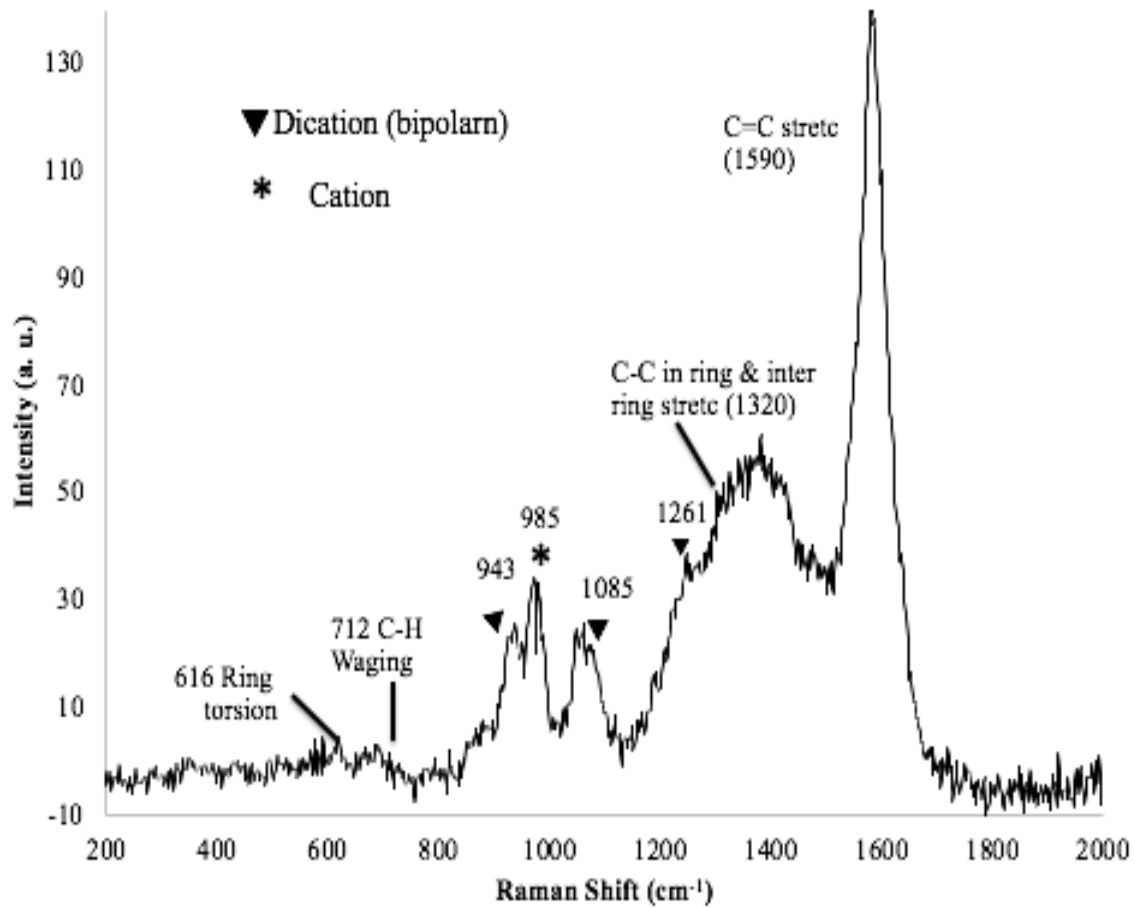
Figure 6.4 Raman spectra of pyrrole polymerization on graphitic microfiber sheet. All observed lines are assigned, confirming that the pyrrole was polymerized and is present in its conductive form in the coating.

Figure 6.5 shows the formation of polaron and bipolaron that occur in polypyrrole chains

through electrochemical reaction. the pyrrole was polymerized, and it is clear that it

presents in its conductive form in the composite
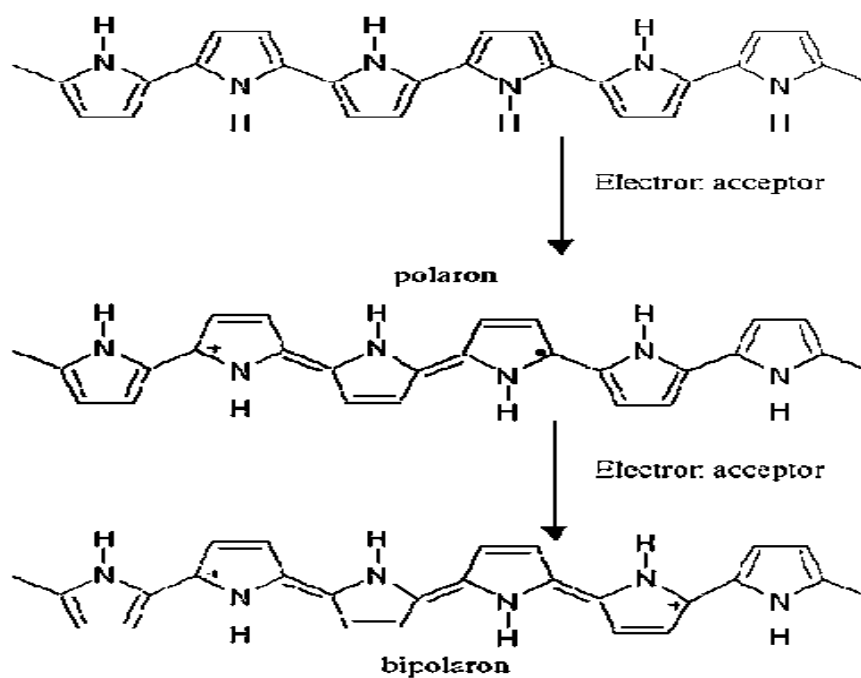
Figure 6.5 Formation of polaron-bipolaron in a polypyrrole chain.
Source: [181].

Figure 6.5 shows further corroboration for the formation of doped PPy with the FTIR (Fourier Transform Infrared) spectrum (see Chapter 2 for instrument description). The FTIR line at 2167cm^{-1} is assigned to C–N stretching mode, the N–H pyrrole ring deformation is assigned to lines at 1670cm^{-1} and 1350cm^{-1}. The Raman lines at 1217cm^{-1} and at 917cm^{-1} are assigned to stretching mode lines in doped PPy indicating the pyrrole monomer is polymerized. The line at 813cm^{-1} is assigned to a C–H deformation vibration [184].
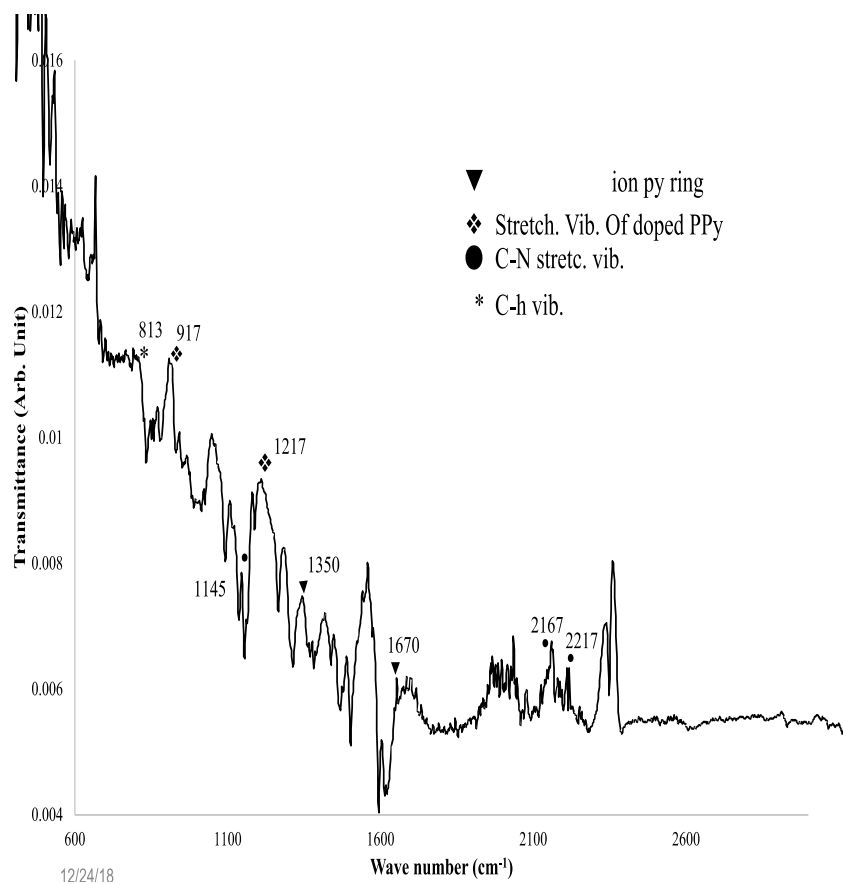
Figure 6.6 FTIR spectrum of PPy film which exhibits all the lines of doped PPy.

Figure 6.6 shows SERS Raman analysis of different glucose concentration in on gold Nanoparticles / Ppy modified-Graphite fibers sheet. It also presents the peak fingerprint of glucose, which identifies glucose peaks with a shift of about $10cm^{-1}$. According to the literature, the movement of the SERS spectral bands can be up to $25cm^{-1}$ in comparison with the typical same-compound Raman spectral bands [144]. There is an exact matching of peaks in SERS spectrum with the Raman spectrum from crystalline glucose with peaks as 425, 538, 839, 910, 1069, 1124, 1343 and $1456cm^{-1}$.

It is characterized with high level of intensity and stability of the Raman bands. Moreover, the citrate reduced gold nanoparticles (AuNP) have the ability to reduce the

static repulsion and stabilize the nanoparticles as previous shown in Chapter 4 [163]. This substrate is able to detect 10^{-3}M of glucose without using nanoparticles owing to significant properties for polypyrrole.
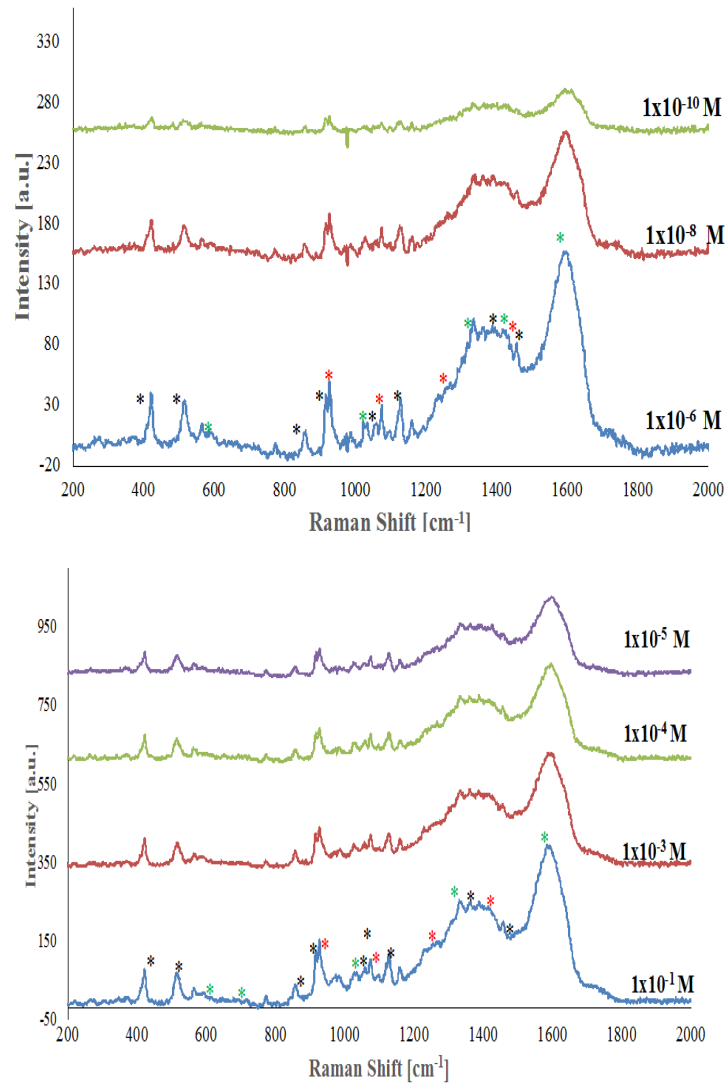
Figure 6.7 SERS for different concentrations of glucose on Au /PPY modified-graphite microfiber using λ_{ex}=532nm, P=10mW, acquisition time =15s, average=3 scans. All the peaks shown in black asterisks in the SERS spectra at 402, 521, 835, 900, 1063, 1118, 1341 and 1449cm^{-1} correspond to that of crystalline glucose.

Conclusion

This chapter presents the results of SERS on PPy (polypyrolle) electrochemically fabricated by cyclic voltammetry on Toray® graphite microfiber sheets. This substrate is able to detect glucose over broad concentration ranges from 0.1 to 10^{-10}M with enhancement factor equal to 2.64 x 10^{12}; therefore, it is very promising platform for glucose detection at low concentrations.

CHAPTER 7

SUMMARY, CONCLUSIONS AND SUGGESTED FUTURE WORK

7.1 Summary

The work discussed in this thesis is focused on novel approaches to detect primarily glucose using SERS by identifying and developing new nanostructured SERS substrates. It is organized as follows:

Chapter 1 gives the characteristics of Raman spectroscopy in general and surface enhanced Raman spectroscopy in particular. It introduces the fundamental mechanisms of both conventional and surface enhanced Raman scattering, and it presents the characteristic features typical of the hot spot model for SERS. Furthermore, it gives an insight into the previous relevant studies in the literature.

Chapter 2 deals with details about experimental techniques used in this dissertation. It gives explanations of the instrumentation used for Raman spectroscopy used as well as that of the lasers used for SERS. Details of the surface enhancement factor and approaches to SERS theoretical modeling are also discussed. In addition, other techniques used in this dissertation, such as cyclic voltammetry and scanning electron microscopy, are discussed.

Chapter 3 discusses results of SERS of glucose silver on spin-coated gold and silver nanoparticles, aggregated using calcium chloride. In addition, data of glucose placed on commercial nano-etched gold on silicon, referred to as Klarite®, is presented and discussed. Our results demonstrate that SERS is capable of detecting the probe analytes with high enhancement factor

Chapter 4 covers the results of SERS and subsequent discussion of glucose on drop-coated and chemically produced gold on graphene. The latter is used on the basis of conclusions made on the role of graphene enhancement as a result of the previous studies. The effectiveness of the glucose sensing with the use of graphene-like sheet substrate is improved with the help of TEG partition layer. Glucose detection is done with the use of CVD treatment with TEG for graphene for the improvement of the graphene-like sheet substrate efficiency. The results show that these substrates are capable of providing SERS enhancement factors up to 10^{10} with a detection limit to 10^{-8} M in aqueous solutions of glucose. The SERS performance on graphene substrates are many orders of magnitude higher compared with results on gold coated chemically etched Klarite® silicon substrates

Chapter 5 presents the results of SERS and subsequent discussion of glucose on drop-coated chemically produced silver on Toray® graphite microfiber sheets in two variants: with the available partition layers and without them. The results of SERS and analysis of the role of glucose on dropped-coated chemically produced gold on graphite microfiber sheets (Toray ®) with the use of partition layers are applied for the comparison with the relevant efficiency of using the same conditions and the same substrate with Ag nanoparticles. Theoretical modeling is used to support the functions of the partition layers. The discussed outputs illustrate the ability of SERS to identify the probe molecules that have a high factor of enhancement. R6G demonstrated detection of a near-single 10^{-16}M molecule. The obtained substrate demonstrated the enhancement factor of the SERS high activity on the order of 7.63×10^{12} due to the R6G partition layer

Chapter 6 presents the results of SERS on PP (polypyrolle) fabricated electrochemically by cyclic voltammetry on Toray® graphite microfiber sheets .

Chapter 7 summarizes the most important findings of the research and explains biomedical value of the work. Finally, the chapter gives guidelines and recommendations for future research.

7.2 Future Work

It is a matter of crucial importance to conduct further research. The results from graphene sheet and graphite sheet encourage using this substrate to detect other material in different fields. The following are some topics for future work related to this dissertation:

- Use SERS substrate developed to detect glucose oxidase an enzyme employed in biofuel cells and electrochemical glucose sensors

- Use theoretical modeling to understand the interaction between the partition layer, and metal nanoparticles and glucose

- Use theoretical modeling to understand the interaction between pyrrole, and metal nanoparticles and glucose.

REFERENCES

1.   Fleischmann, M., P.J. Hendra, and A.J. McQuillan, Raman Spectra of Pyridine Adsorbed at a Silver Electrode. Chemical Physics Letters, 1974. **26**(2):p. 163-166.

2.   Jeanmaire, D.L. and R.P. Van Duyne, Surface Raman spectroelectrochemistry: Part I. Heterocyclic, Aromatic, And Aliphatic Amines Adsorbed On The Anodized Silver Electrode. Journal of Electroanalytical Chemistry and Interfacial Electrochemistry, 1977. **84**(1): p. 1-20.

3.   Albrecht, M.G. and J.A. Creighton, Anomalously Intense Raman Spectra of Pyridine at a Silver Electrode. Journal of the American Chemical Society, 1977. **99**(15):p 5215-5217.

4.   Moskovits, M., Surface Roughness and The Enhanced Intensity of Raman Scattering By Molecules Adsorbed On Metals. The Journal of Chemical Physics, 1978. **69**(9): p. 4159-4161.

5.   Creighton, J.A., C.G. Blatchford, and M.G. Albrecht, Plasma Resonance Enhancement of Raman Scattering by Pyridine Adsorbed on Silver or Gold Sol Particles of Size comparable to the Excitation Wavelength. Journal of the Chemical Society, Faraday Transactions 2: Molecular and Chemical Physics, 1979. **75**: p. 790-798.

6.   Le Ru, E., E. C., Blackie, E., Meyer, M., & Etchegoin, P. G. Surface enhanced Raman scattering enhancement factors: a comprehensive study. The Journal of Physical Chemistry C, 2007. **111**(37): p. 13794-13803.

7.   Gersten, J. and A. Nitzan, Electromagnetic theory of enhanced Raman scattering by molecules adsorbed on rough surfaces. The Journal of Chemical Physics, 1980. **73**(7): p. 3023-3037.

8.   Moskovits, M., Enhanced Raman Scattering by Molecules Adsorbed On Electrodes-A Theoretical Model. Solid State Communications, 1979. **32**(1): p. 59-62.

9.   Metiu, H. and P. Das, The Electromagnetic Theory of Surface Enhanced Spectroscopy. Annual Review of Physical Chemistry, 1984. **35**(1): p. 507-536.

10.   Schatz, G.C., Theoretical Studies Of Surface Enhanced Raman Scattering. Accounts of Chemical Research, 1984. **17**(10): p. 370-376.

11. Philpott, M., Theory Of Surface Enhanced Raman Scattering: A Prospective View. Le Journal de Physique Colloques, 1983. **44**(C10): p.295-303.

12. Wokaun, A., Surface-enhanced Electromagnetic Processes. Solid State Physics, 1984. **38**: p. 223-294.

13. Wokaun, A., Surface Enhancement Of Optical Fields: Mechanism And Applications. Molecular Physics, 1985. **56**(1): p. 1-33.

14. Xia, Y. and N.J. Halas, Shape-Controlled Synthesis And Surface Plasmonic Properties of Metallic Nanostructures. Material Research Society Bulletin, 2005. **30**(5): p. 338-348.

15. Campion, A., Ivanecky III, J. E., Child, C. M., & Foster, M., On the Sechanism of Chemical Enhancement in Surface-Enhanced Raman Scattering. Journal of the American Chemical Society, 1995. **117**(47): p. 11807-11808.

16. Mahajan, S., Cole, R. M., Soares, B. F., Pelfrey, S. H., Russell, A. E., Baumberg, J. J., & Bartlett, P. N., Relating SERS Intensity to specific Plasmon Modes on Sphere Segment Void Surfaces. The Journal of Physical Chemistry C, 2009. **113**(21): p. 9284-9289.

17. Perney, N., De Abajo, F. G., Baumberg, J. J., Tang, A., Netti, M. C., Charlton, M. D. B., & Zoorob, M. E., Tuning localized Plasmon Cavities for Optimized Surface-Enhanced Raman Scattering. Physical Review B, 2007. **76**(3): p. 035426.

18. Kneipp, Wang, Y., Kneipp, H., Perelman, L. T., Itzkan, I., Dasari, R. R., & Feld, M. S., Single Molecule Detection using Surface-Enhanced Raman Scattering (SERS). Physical Review Letters, 1997. **78**(9): p. 1667.

19. Nie, S. and S.R. Emory, Probing Single Molecules and Single Nanoparticles by Surface-Enhanced Raman Scattering. Science, 1997. **275**(5303): p. 1102-1106.

20. Haynes, C.L., A.D. McFarland, and R.P.V. Duyne, Surface-enhanced Raman Spectroscopy. American Chemical Society Publications, 2005, ACS Publications.

21. Wang, X., Li, M., Meng, L., Lin, K., Feng, J., Huang, T. & Ren, B., Probing the Location of Hot Spots by Surface-enhanced Raman Spectroscopy: toward uniform substrates. American Chemical Society Nano, 2013. **8**(1): p. 528-536.

22.	Li, Z. and H. Xu, Nanoantenna Effect of Surface-enhanced Raman Scattering: Managing Light with Plasmons at the Nanometer Scale. Advances in Physics: X, 2016. **1**(3): p. 492-521.

23.	Brus, L., Noble Metal Nanocrystals: Plasmon Electron Transfer Photochemistry and Single-Molecule Raman spectroscopy. Accounts of Chemical Research, 2008. **41**(12): p. 1742-1749.

24.	Hong, K.Y., Label-free Plasmonic Detection using Nanogratings Fabricated by Laser Interference Lithography. Plasmonics,2017.

25.	Zehentbauer, F.M., Moretto, C., Stephen, R., Thevar, T., Gilchrist, J. R., Pokrajac, D., & Kiefer, J., Fluorescence Spectroscopy of Rhodamine 6G: Concentration and Solvent Effects. Spectrochimica Acta Part A: Molecular and Biomolecular Spectroscopy, 2014. **121**: p. 147-151.

26.	Rycenga, M., Camargo, P. H., Li, W., Moran, C. H., & Xia, Y, Understanding The SERS Effects of Single Silver Nanoparticles and Their Dimers, one At A Time. the Journal of Physical Chemistry Letters, 2010. **1**(4): p. 696-703.

27.	Schlücker, S., Surface‐Enhanced Raman Spectroscopy: Concepts And Chemical Applications. Angewandte Chemie International Edition, 2014. **53**(19): p. 4756-4795.

28.	Ikeda, K., Surface Enhanced Raman Scattering, in Compendium of Surface and Interface Analysis. 2018, Springer. p. 661-665.

29.	Alonso-González, P., et al., Resolving the Electromagnetic Mechanism of Surface-Enhanced Light Scattering at Single Hot Spots. Nature Communications, 2012. **3**: p. 684.

30.	Wei, H. and H. Xu, Hot Spots In Different Metal Nanostructures for Plasmon-Enhanced Raman Spectroscopy. Nanoscale, 2013. **5**(22): p. 10794-10805.

31.	Cialla, D., März, A., Böhme, R., Theil, F., Weber, K., Schmitt, M., & Popp, J.., Surface-Enhanced Raman Spectroscopy (SERS): Progress and Trends. Analytical and Bioanalytical Chemistry, 2012. **403**(1): p. 27-54.

32.	Moskovits, M., Persistent Misconceptions Regarding SERS. Physical Chemistry Chemical Physics, 2013. **15**(15): p. 5301-5311.

33.	Sharma, B., Frontiera, R. R., Henry, A. I., Ringe, E., & Van Duyne, R. P., SERS: Materials, Applications, and the Future. Materials Today, 2012. **15**(1): p. 16-25.

34.   Hammond, J.L., Bhalla, N., Rafiee, S., & Estrela, P., Localized Surface Plasmon Resonance as A Biosensing Platform for Developing Countries. Biosensors, 2014. **4**(2): p. 172-188.

35.   Kneipp, J., H. Kneipp, and K. Kneipp, SERS—A Single-Molecule and Nanoscale Tool for Bioanalytics. Chemical Society Reviews, 2008. **37**(5): p. 1052-1060.

36.   Lane, L.A., X. Qian, and S. Nie, SERS Nanoparticles In Medicine: From Label-Free Detection to Spectroscopic Tagging. Chemical Reviews, 2015. **115**(19): p. 10489-10529.

37.   Álvarez-Puebla, R.n.A., Effects of the Excitation Wavelength on the SERS Spectrum. The journal of Physical Chemistry Letters, 2012. **3**(7): p. 857-866.

38.   Shiohara, A., Y. Wang, and L.M. Liz-Marzán, Recent Approaches Toward Creation of Hot Spots for SERS Detection. Journal of Photochemistry and Photobiology C: Photochemistry Reviews, 2014. **21**: p. 2-25.

39.   Mortazavi, D., Kouzani, A. Z., Kaynak, A., & Duan, W., Developing LSPR Design Guidelines. Progress in Electromagnetics Research, 2012. **126**: p. 203-235.

40.   Sepúlveda, B., et al., LSPR-based Nanobiosensors. Nano Today, 2009. **4**(3): p. 244-251.

41.   Huang, J.A., Zhang, Y. L., Ding, H., & Sun, H. B., SERS‐Enabled Lab‐on‐a‐Chip
        Systems. Advanced Optical Materials, 2015. **3**(5): p. 618-633.

42.   Chen, C., et al., Recent Advances in Electrochemical Glucose Biosensors: a Review. Royal Society of Chemistry Advances, 2013. **3**(14): p. 4473-4491.

43.   Khalil, I., Julkapli, N., Yehye, W., Basirun, W., & Bhargava, S., Graphene–Gold Nanoparticles Hybrid—Synthesis, Functionalization, and Application in a Electrochemical and Surface-Enhanced Raman Scattering Biosensor. Materials, 2016. **9**(6): p. 406.

44.   Zhu, Y., Hao, Y., Adogla, E. A., Yan, J., Li, D., Xu, K., & Lin, Q., A Graphene-Based Affinity Nanosensor for Detection of Low-Charge and Low-Molecular-Weight Molecules. Nanoscale, 2016. **8**(11): p. 5815-5819.

45.   Betz, J.F., Wei, W. Y., Cheng, Y., White, I. M., & Rubloff, G. W., Simple SERS Substrates: Powerful, Portable, and Full of Potential. Physical Chemistry

Chemical Physics, 2014. **16**(6): p. 2224-2239.

46.   Etchegoin, P.G. and E.C. Le Ru, Basic Electromagnetic Theory of SERS. Surface Enhanced Raman Spectroscopy: Analytical, Biophysical and Life Science Applications, 2010: p. 1-37.

47.   Le Ru, E.C., M. Meyer, and P.G. Etchegoin, Proof Of Single-Molecule Sensitivity in Surface Enhanced Raman Scattering (SERS) by Means Of A Two-Analyte Technique. The Journal of Physical Chemistry B, 2006. **110**(4): p. 1944-1948.

48.   McNay, Eustace, D., Smith, W. E., Faulds, K., & Graham, D., Surface-Enhanced Raman Scattering (SERS) And Surface-Enhanced Resonance Raman Scattering (SERRS): A Review of Applications. Applied Spectroscopy, 2011. **65**(8): p. 825-837.

49.   Hoppmann, E.P., W.Y. Wei, and I.M. White, Highly Sensitive and Flexible Inkjet Printed SERS Sensors on Paper. Methods, 2013. **63**(3): p. 219-224.

50.   Willets, K.A., Super-Resolution Imaging Of SERS Hot Spots. Chemical Society Reviews, 2014. **43**(11): p. 3854-3864.

51.   Song, J., J. Zhou, and H. Duan, Self-Assembled Plasmonic Vesicles Of SERS-Encoded Amphiphilic Gold Nanoparticles for Cancer Cell Targeting And Traceable Intracellular Drug Delivery. Journal of the American Chemical Society, 2012. **134**(32): p. 13458-13469.

52.   Vinokurov, V.A., Kopitsyn, D. S., Kotelev, M. S., Ivanov, E. V., Lvov, Y. M., & Novikov, A. A.., Natural Ceramic Nanotube Substrates For Surface-Enhanced Raman Spectroscopy. Jounral of Material, 2015. **67**(12): p. 2877-2880.

53.   Sharma, B., et al., High-performance SERS substrates: Advances and Challenges. Material Research Society bulletin, 2013. **38**(8): p. 615-624.

54.   Stuart, D.A., Yonzon, C. R., Zhang, X., Lyandres, O., Shah, N. C., Glucksberg, M. R., ... & Van Duyne, R. P., Glucose Sensing using Near-infrared Surface-enhanced Raman spectroscopy: Gold Surfaces, 10-day Stability, and Improved Accuracy. Analytical Chemistry, 2005. **77**(13): p. 4013-4019.

55.   Hackler, McAnally, M. O., Schatz, G. C., Stair, P. C., & Van Duyne, R. P., Identification Of Dimeric Methylalumina Surface Species During Atomic Layer Deposition Using Operando Surface-Enhanced Raman Spectroscopy. Journal of the American Chemical Society, 2017. **139**(6): p. 2456-2463.

56.   Gao, R., Z. Cheng, and J. Choo, Wash-free Magnetic Immunoassay of the PSA Cancer Marker using SERS and Droplet Microfluidics. Lab on a Chip, 2016. **16**(6): p. 1022-1029.

57.   Lee, S., Chon, H., Lee, J., Ko, J., Chung, B. H., Lim, D. W., & Choo, J., Rapid and Sensitive Phenotypic Marker Detection on Breast Cancer Cells using Surface-Enhanced Raman scattering (SERS) Imaging. Biosensors and Bioelectronics, 2014. **51**: p. 238-243.

58.   Smith, E. and G. Dent, The Theory of Raman Spectroscopy. Modern Raman Spectroscopy-A Practical Approach, 2005: p. 71-92.

59.   Raman, C.V. and K.S. Krishnan, A New Type of Secondary Radiation. Nature, 1928. **121**(3048): p. 501-502.

60.   Smekal, A., The Quantum Theory of Dispersion. Naturwissenschaften, 1923. 11: p. 873.

61.   Ferraro, J., K. Nakamoto, and C.W. Brown, Introductory Raman Spectroscopy. 2003. Academic press.

62.   Li, W., Camargo, P. H., Lu, X., & Xia, Y., Dimers of Silver Nanospheres: Facile Synthesis and their Use as Hot Spots for Surface-Enhanced Raman scattering. Nano letters, 2008. **9**(1): p. 485-490.

63.   Hu, Y., Cheng, H., Zhao, X., Wu, J., Muhammad, F., Lin, S., ... & Wang, P., Surface-Enhanced Raman Scattering-Active Gold Nanoparticles with Enzyme Mimicking Activities for Measuring Glucose and Lactate in Living Tissues. American Chemical Society Nano, 2017.

64.   Yonzon, C.R., et al., A glucose Biosensor Based on Surface-Enhanced Raman Scattering: Improved Partition Layer, Temporal Stability, Reversibility, and Resistance to Serum Protein Interference. Analytical Chemistry, 2004. **76**(1): p. 78-85.

65.   Yonzon, C., R., Lyandres, O., Shah, N. C., Dieringer, J. A., & Van Duyne, R. P., Glucose Sensing with Surface-Enhanced Raman Spectroscopy. Surface-Enhanced Raman Scattering, 2006: p. 367-379

66.   Mulvaney, S.P., Musick, M. D., Keating, C. D., & Natan, M. J., Glass-coated, Analyte-Tagged Nanoparticles: a New Tagging System Based on Detection with Surface-Enhanced Raman Scattering. Langmuir, 2003. **19**(11): p. 4784-4790.

67. Doering, W.E. and S. Nie, Spectroscopic tags using dye-embedded nanoparticles and surface-enhanced Raman scattering. Analytical Chemistry, 2003. **75**(22): p. 6171-6176.

68. Jarvis, R.M., A. Brooker, and R. Goodacre, Surface-enhanced Raman Spectroscopy for Bacterial Discrimination Utilizing a Scanning Electron Microscope with a Raman Spectroscopy Interface. Analytical Chemistry, 2004. **76**(17): p. 5198-5202.

69. Huh, Y.S., Chung, A. J., Cordovez, B., & Erickson, D., Enhanced on-chip SERS based Biomolecular Detection using Electrokinetically Active Microwells. Lab on a Chip, 2009. **9**(3): p. 433-439.

70. Culha, M., Stokes, D., Allain, L. R., & Vo-Dinh, T., Surface-Enhanced Raman Scattering Substrate based on a Self-Assembled Monolayer for use in Gene Diagnostics. Analytical Chemistry, 2003. **75**(22): p. 6196-6201.

71. Haynes, C.L. and R.P. Van Duyne, Plasmon Scanned Surface-Enhanced Raman Scattering Excitation Profiles. Material Reasearch Society, Online Proceedings Library Archive, 2002. **728**.

72. Willets, K.A. and R.P. Van Duyne, Localized surface plasmon resonance spectroscopy and sensing. Annual. Review of Physical Chemistry, 2007. **58**: p. 267-297.

73. McFarland, A.D., Young, M. A., Dieringer, J. A., & Van Duyne, R. P., Wavelength-scanned Surface-Enhanced Raman Excitation spectroscopy. The Journal of Physical Chemistry B, 2005. **109**(22): p. 11279-11285.

74. Van Duyne, R.P., Laser Excitation of Raman Scattering from Adsorbed Molecules on Electrode Surfaces. Chemical and Biochemical Applications of Lasers, 1979. **4**: p. 101.

75. Ascherl, L., Sick, T., Margraf, J. T., Lapidus, S. H., Calik, M., Hettstedt, C., ... & Auras, F., Molecular Docking Sites Designed for the Generation of Highly Crystalline Covalent Organic Frameworks. Nature Chemistry, 2016. **8**(4): p. 310.

76. Dar, A. and S. Mir, Molecular Docking: Approaches, Types, Applications and Basic Challenges. Journal of Analitical and Bioanalitical Technology, 2017. **8**: p. 2.

77. Ashtawy, H.M. and N.R. Mahapatra. Molecular Docking for Drug Discovery:

Machine-Learning Approaches for Native Pose Prediction of Protein-Ligand Complexes. in International Meeting on Computational Intelligence Methods for Bioinformatics and Biostatistics, Springer, 2013.

78.	Rauf, M.A., S. Zubair, and A. Azhar, Ligand docking and Binding Site Analysis with Pymol and Autodock/vina. International Journal of Basic and Applied Sciences, 2015. **4**(2): p. 168.

79.	Sliwoski, G., Kothiwale, S., Meiler, J., & Lowe, E. W., Computational Methods in Drug Discovery. Pharmacological Reviews, 2014. **66**(1): p. 334-395.

80.	Meng, X.-Y., Zhang, H. X., Mezei, M., & Cui, M., Molecular docking: a powerful approach for structure-based drug discovery. Current Computer-aided Drug Design, 2011. **7**(2): p. 146-157.

81.	Kumar, A., R. Goyal, and S. Jain, Docking Methodologies and Recent Advances, in Oncology: Breakthroughs in Research and Practice. 2017, IGI Global. p. 804-828.

82.	Arcon, J.P., Defelipe, L. A., Modenutti, C. P., López, E. D., Alvarez-Garcia, D., Barril, X., & Martí, M. A., Molecular Dynamics in Mixed Solvents Reveals Protein–Ligand Interactions, Improves Docking, and Allows Accurate Binding Free Energy Predictions. Journal of Chemical Information and Modeling, 2017. **57**(4): p. 846-863.

83.	Forli, S., Huey, R., Pique, M. E., Sanner, M. F., Goodsell, D. S., & Olson, A. J., Computational protein–ligand docking and virtual drug screening with the AutoDock Suite. Nature Protocols, 2016. **11**(5): p. 905.

84.	Muhammad, S.A. and N. Fatima, In silico Analysis and Molecular Docking Studies of Potential Angiotensin-converting Enzyme Inhibitor using Quercetin glycosides. Pharmacognosy Magazine, 2015. **11**(Suppl 1): p. S123.

85.	Ravindranath, P.A., Forli, S., Goodsell, D. S., Olson, A. J., & Sanner, M. F., AutoDockFR: Advances in Protein-Ligand Docking with Explicitly Specified Binding Site Flexibility. PLoS Computational Biology, 2015. **11**(12): p. e1004586.

86.	Pagadala, N.S., K. Syed, and J. Tuszynski, Software for Molecular Docking: a Review. Biophysical Reviews, 2017. **9**(2): p. 91-102.

87.	Żarów, A., Wagner, W., Lee, E., Adar, F., Zhou, B., Pinal, R., & Iqbal, Z., Raman Spectroscopy of Defected Griseofulvin in Powders and Films. Advances in Material Design for Regenerative Medicine, Drug Delivery, and Targeting/Imaging, 2009.

88.   Šašić, S., Raman mapping of low-content API pharmaceutical formulations. I. Mapping of Alprazolam in Alprazolam/Xanax tablets. Pharmaceutical Research, 2007. **24**(1): p. 58-65.

89.   Conti, C., Fustella, G., Colombo, C., Realini, M., & Zerbi, G., Micro‐Raman Depth Profiling on Polished Cross‐sections: the Mapping of Oxalates used in Protective Treatment of Carbonatic Substrate. Journal of Raman Spectroscopy, 2008. **39**(10): p. 1307-1308.

90.   Żuk, J., J. Romanek, and W. Skorupa, Micro-Raman Depth Profile Investigations of Beveled Al+-ion Implanted 6H-SiC Samples. Nuclear Instruments and Methods in Physics Research Section B: Beam Interactions with Materials and Atoms, 2009. **267**(8): p. 1251-1254.

91.   Borchert, H., Solar Cells Based on Colloidal Nanocrystals. Springer,2014.

92.   Johnson, J.A. and R.M. Wightman, Cyclic Voltammetric Measurements of Neurotransmitters. The Electrochemical Society Interface, 2017. **26**(3): p. 53-57.

93.   Adesokan, Quan, X., Evgrafov, A., Sørensen, M. P., Heiskanen, A., & Boisen, A.. Hydrodynamics Studies of Cyclic Voltammetry for Electrochemical Micro Biosensors. in Journal of Physics: Conference Series. 2015. IOP Publishing.

94.   Elgrishi, N., Rountree, K. J., McCarthy, B. D., Rountree, E. S., Eisenhart, T. T., & Dempsey, J. L., A Practical Beginner's Guide to Cyclic Voltammetry. Journal of Chemical Education, 2017. **95**(2): p. 197-206.

95.   Thomas, D., Rasheed, Z., Jagan, J. S., & Kumar, K. G., Study of Kinetic Parameters and Development of a Voltammetric Sensor for the Determination of Butylated Hydroxyanisole (BHA) in Oil Samples. Journal of food Science and Technology, 2015. **52**(10): p. 6719-6726.

96.   Benchafia, E.m., Yao, Z., Yuan, G., Chou, T., Piao, H., Wang, X., & Iqbal, Z., Cubic Gauche Polymeric Nitrogen under Ambient Conditions. Nature communications, 2017. **8**(1): p. 930.

97.   Khan, I., K. Saeed, and I. Khan, Nanoparticles: Properties, Applications and Toxicities. Arabian Journal of Chemistry, 2017.

98.   Lee, S.J., J.M. Baik, and M. Moskovits, Polarization-Dependent Surface-Enhanced Raman Scattering from a Silver-nanoparticle-Decorated Single Silver Nanowire. Nano Letters, 2008. **8**(10): p. 3244-3247.

99.   Israelsen, N.D., C. Hanson, and E. Vargis, Nanoparticle Properties and Synthesis Effects on Surface-Enhanced Raman Scattering Enhancement Factor: an Introduction. The Scientific World Journal, 2015. **2015**.

100.   Dreaden, Alkilany, A. M., Huang, X., Murphy, C. J., & El-Sayed, M. A.., The Golden Age: Gold Nanoparticles for Biomedicine. Chemical Society Reviews, 2012. **41**(7): p. 2740-2779.

101.   Mock, J., Barbic, M., Smith, D. R., Schultz, D. A., & Schultz, S., Shape Effects in Plasmon Resonance of Individual Colloidal Silver Nanoparticles. The Journal of Chemical Physics, 2002. **116**(15): p. 6755-6759.

102.   Guo, H., Xing, B., White, J. C., Mukherjee, A., & He, L., Ultra-Sensitive Determination of Silver Nanoparticles by Surface-Enhanced Raman Spectroscopy (SERS) after Hydrophobization-Mediated Extraction. Analyst, 2016. **141**(18): p. 5261-5264.

103.   Meheretu, G.M., D. Cialla, and J. Popp, Surface Enhanced Raman Spectroscopy on Silver Nanoparticles. International Journal of Biochemistry and Biophysics, 2014. **2**(4): p. 63-67.

104.   Vendamani, V., Nageswara Rao, S. V. S., Venugopal Rao, S., Kanjilal, D., & Pathak, A. P., Three-Dimensional Hybrid Silicon Nanostructures for Surface Enhanced Raman Spectroscopy based Molecular Detection. Journal of Applied Physics, 2018. **123**(1): p. 014301.

105.   Jensen, L. and G.C. Schatz, Resonance Raman Scattering of Rhodamine 6G as Calculated using Time-Dependent Density Functional Theory. The Journal of Physical Chemistry A, 2006. **110**(18): p. 5973-5977.

106.   Sugiarto, I. and K. Putri. Analysis of Dual Peak Emission from Rhodamine 6G Organic Dyes using Photoluminescence. in Journal of Physics: Conference Series. 2017. IOP Publishing.

107.   Hulteen, J.C. and R.P. Van Duyne, Nanosphere Lithography: a Materials General Fabrication Process for Periodic Particle Array Surfaces. Journal of Vacuum Science & Technology A: Vacuum, Surfaces, and Films, 1995. **13**(3): p. 1553-1558.

108.   Jensen, T.R., G.C. Schatz, and R.P. Van Duyne, Nanosphere Lithography: Surface Plasmon Resonance Spectrum of a Periodic Array of Silver Nanoparticles by Ultraviolet− Visible Extinction Spectroscopy and Electrodynamic Modeling. The Journal of Physical Chemistry B, 1999. **103**(13): p. 2394-2401.

109. McCreery, R.L., Raman Spectroscopy for Chemical Analysis. Vol. 225. 2005: John Wiley & Sons.

110. Han, X.X., Huang, G. G., Zhao, B., & Ozaki, Y, Label-free Highly Sensitive Detection of Proteins in Aqueous Solutions using Surface-Enhanced Raman Scattering. Analytical Chemistry, 2009. **81**(9): p. 3329-3333.

111. Bell, S.E. and N.M. Sirimuthu, Surface-Enhanced Raman Spectroscopy (SERS) for Sub-Micromolar Detection of DNA/RNA Mononucleotides. Journal of the American Chemical Society, 2006. **128**(49): p. 15580-15581.

112. Bell, S.E. and N.M. Sirimuthu, Surface-Enhanced Raman Spectroscopy as a Probe of Competitive Binding by Anions to Citrate-Reduced Silver Colloids. The Journal of Physical Chemistry A, 2005. **109**(33): p. 7405-7410.

113. Wang, H.-C. and A.-R. Lee, Recent Developments in Blood Glucose Sensors. Journal of Food and Drug Analysis, 2015. **23**(2): p. 191-200.

114. Heller, A., Implanted Electrochemical Glucose Sensors for the Management of Diabetes. Annual Review of Biomedical Engineering, 1999. **1**(1): p. 153-175.

115. Wilson, G.S. and Y. Hu, Enzyme-based biosensors for in Vivo Measurements. Chemical Reviews, 2000. **100**(7): p. 2693-2704.

116. McNichols, R.J. and G.L. Cote, Optical Glucose Sensing in Biological Fluids: an overview. Journal of Biomedical Optics, 2000. **5**(1): p. 5-16.

117. Steffes, P.G., Laser-based Measurement of Glucose in the Ocular Aqueous Humor: an Efficacious Portal for Determination of Serum Glucose Levels. Diabetes Technology & Therapeutics, 1999. **1**(2): p. 129-133.

118. Taguchi, M., Ptitsyn, A., McLamore, E. S., & Claussen, J. C., Nanomaterial-mediated Biosensors for Monitoring Glucose. Journal of Diabetes Science &Technology, 2014. **8**(2): p. 403-411.

119. Wang, J., D.F. Thomas, &A. Chen, Nonenzymatic Electrochemical Glucose Sensor Based on Nanoporous PtPb Networks. Analytical Chemistry, 2008. **80**(4): p. 997-1004.

120. Evans, N.D., Gnudi, L., Rolinski, O. J., Birch, D. J., & Pickup, J. C., Non-invasive Glucose Monitoring by NAD (P) H Autofluorescence Spectroscopy in Fibroblasts and Adipocytes: a Model for Skin Glucose Sensing. Diabetes Technology & Therapeutics, 2003. **5**(5): p. 807-816.

121. Shafer-Peltier, K.E., Haynes, C. L., Glucksberg, M. R., & Van Duyne, R. P., Toward a Glucose Biosensor Based on Surface-Enhanced Raman Scattering. Journal of the American Chemical Society, 2003. **125**(2): p. 588-593.

122. Schatz, G.C. & R.P. Van Duyne, Electromagnetic Mechanism of Surface-Enhanced Spectroscopy. Handbook of Vibrational Spectroscopy, 2002.

123. Xu, W., N. Mao, and J. Zhang, Graphene: A Platform for Surface-Enhanced Raman Spectroscopy. Small, 2013. **9**(8): p. 1206-1224.

124. Ling, X., Fang, Y., Xu, H., Zhang, H., Kong, J.& Liu, Z., Can Graphene be used as a Substrate for Raman Enhancement? Nano Letters, 2009. **10**(2): p. 553-561.

125. Novoselov, K.S., Geim, A. K., Morozov, S. V., Jiang, D., Zhang, Y., Dubonos, S. V., & Firsov, A. A., Electric Field Effect in Atomically Thin Carbon Films. Science, 2004. **306**(5696): p. 666-669.

126. Bai, H., C. Li, and G. Shi, Functional Composite Materials based on Chemically Converted Graphene. Advanced Materials, 2011. **23**(9): p. 1089-1115.

127. Verdejo, Bernal, M. M., Romasanta, L. J., & Lopez-Manchado, M. A., Graphene filled Polymer Nanocomposites. Journal of Materials Chemistry, 2011. **21**(10): p. 3301-3310.

128. Pumera, M., Graphene-based Nanomaterials and their Electrochemistry. Chemical Society Reviews, 2010. **39**(11): p. 4146-4157.

129. Novoselov, K.S., Geim, A. K., Morozov, S., Jiang, D., Katsnelson, M., Grigorieva, I., ... & Firsov, A. A., Two-dimensional Gas of Massless Dirac Fermions in Graphene. arXiv preprint cond-mat/0509330, 2005.

130. Allen, M.J., V.C. Tung, and R.B. Kaner, Honeycomb Carbon: a Review of Graphene. Chemical Reviews, 2009. **110**(1): p. 132-145.

131. Dreyer, D.R., Park, S., Bielawski, C. W., & Ruoff, R. S., The Chemistry of Graphene Oxide. Chemical Society Reviews, 2010. **39**(1): p. 228-240.

132.   Du, J., Yue, R., Ren, F., Yao, Z., Jiang, F., Yang, P., & Du, Y., Novel Graphene
         Flowers Modified Carbon Fibers for Simultaneous Determination of
         Ascorbic Acid, Dopamine and Uric Acid. Biosensors and Bioelectronics,
         2014. **53**: p. 220-224.

133.   Kwak, Y.H., Choi, D. S., Kim, Y. N., Kim, H., Yoon, D. H., Ahn, S. S., ... & Seo,
         S., Flexible Glucose Sensor using CVD-grown Graphene-Based Field
         Effect Transistor. Biosensors and Bioelectronics, 2012. **37**(1): p. 82-87.

134.   Shan, C., Yang, H., Song, J., Han, D., Ivaska, A., & Niu, L.., Direct
         Electrochemistry of Glucose Oxidase and Biosensing for Glucose based
         on Graphene. Analytical Chemistry, 2009. **81**(6): p. 2378-2382.

135.   Yavari, F. and N. Koratkar, Graphene-based Chemical Sensors. The Journal of
         Physical Chemistry Letters, 2012. **3**(13): p. 1746-1753.

136.   Bolotin, K., Sikes, K. J., Hone, J., Stormer, H. L., & Kim, P.., Temperature-
         Dependent Transport in Suspended Graphene. Physical Review Letters,
         2008. **101**(9): p. 096802.

137.   Turkevich, J., Colloidal Gold. Part II. Gold Bulletin, 1985. **18**(4): p. 125-131.

138.   Frens, G., Controlled Nucleation for The Regulation of the Particle Size in
         Monodisperse Gold Suspensions. Nature, 1973. **241**(105): p. 20-22.

139.   Kumar, S., K. Gandhi, and R. Kumar, Modeling of Formation of Gold
         Nanoparticles by Citrate Method. Industrial & Engineering Chemistry
         Research, 2007. **46**(10): p. 3128-3136.

140.   Fisichella, G G., Verso, S. L., Di Marco, S., Vinciguerra, V., Schilirò, E., Di
         Franco, S., ... & Ravesi, S.., Advances in the Fabrication of Graphene
         Transistors on Flexible Substrates. Beilstein Journal of Nanotechnology,
         2017. **8**: p. 467.

141.   Hsu, Y.W., Hsu, T. K., Sun, C. L., Nien, Y. T., Pu, N. W., & Ger, M. D..,
         Synthesis of CuO/graphene Nanocomposites for Nonenzymatic
         Electrochemical Glucose Biosensor Applications. Electrochimica Acta,
         2012. **82**: p. 152-157.

142. Fischer, C., Adam, M., Mueller, A. C., Sperling, E., Wustmann, M., van Pée, K. H., ... & Brunner, E., Gold Nanoparticle-Decorated Diatom Biosilica: A Favorable Catalyst for the Oxidation of d-Glucose. American Chemical Society Omega, 2016. **1**(6): p. 1253-1261.

143. Maple, S.R. and A. Allerhand, Detailed Tautomeric Equilibrium of Aqueous D-glucose. Observation of Six Tautomers by Ultrahigh Resolution Carbon-13 NMR. Journal of the American Chemical Society, 1987. **109**(10): p. 3168-3169.

144. Söderholm, S., Roos, Y. H., Meinander, N., & Hotokka, M.., Raman Spectra of Fructose and Glucose in the Amorphous and Crystalline States. Journal of Raman Spectroscopy, 1999. **30**(11): p. 1009-1018.

145. Muszynski, R., B. Seger, and P.V. Kamat, Decorating Graphene Sheets with Gold Nanoparticles. The Journal of Physical Chemistry C, 2008. **112**(14): p. 5263-5266.

146. Hao, Q., Morton, S. M., Wang, B., Zhao, Y., Jensen, L., & Jun Huang, T., Tuning Surface-enhanced Raman Scattering from Graphene Substrates using the Electric Field Effect and Chemical Doping. Applied Physics Letters, 2013. **102**(1): p. 011102.

147. van Huis, M.A., Kunneman, L. T., Overgaag, K., Xu, Q., Pandraud, G., Zandbergen, H. W., & Vanmaekelbergh, D., Low-temperature Nanocrystal Unification Through Rotations and Relaxations Probed by in Situ Transmission Electron Microscopy. Nano Letters, 2008. **8**(11): p. 3959-3963.

148. Pandey, P.A., Bell, G. R., Rourke, J. P., Sanchez, A. M., Elkin, M. D., Hickey, B. J., & Wilson, N. R., Physical Vapor Deposition of Metal Nanoparticles on Chemically Modified Graphene: Observations on Metal–graphene Interactions. Small, 2011. **7**(22): p. 3202-3210.

149. Munro, C., Smith, W. E., Garner, M., Clarkson, J. W. P. C., & White, P. C., Characterization of the Surface of a Citrate-reduced Colloid Optimized for Use as a Substrate for Surface-Enhanced Resonance Raman Scattering. Langmuir, 1995. **11**(10): p. 3712-3720.

150. MA, F., LIU, K., ZHANG, Y., & PAN, S., A Novel Silver Colloid as Substrate for Detection of Single-Molecular Level of R6G [J]. The Journal of Light Scattering, 2007. **1**: p. 002.

151. Stuart, D.A., Yuen, J. M., Shah, N., Lyandres, O., Yonzon, C. R., Glucksberg, M. R., ... & Van Duyne, R. P., In Vivo Glucose Measurement by Surface-enhanced Raman Spectroscopy. Analytical Chemistry, 2006. **78**(20): p. 7211-7215.

152. Levin, C.S., Bishnoi, S. W., Grady, N. K., & Halas, N. J., Determining the Conformation of Thiolated Poly (Ethylene Glycol) on Au Nanoshells by Surface-Enhanced Raman Scattering Spectroscopic Assay. Analytical chemistry, 2006. **78**(10): p. 3277-3281.

153. Lyandres, O., Shah, N. C., Yonzon, C. R., Walsh, J. T., Glucksberg, M. R., & Van Duyne, R. P., Real-time Glucose Sensing by Surface-Enhanced Raman Spectroscopy in Bovine Plasma Facilitated by a Mixed Decanethiol/mercaptohexanol Partition Layer. Analytical Chemistry, 2005. **77**(19): p. 6134-6139.

154. Love, J.C., Estroff, L. A., Kriebel, J. K., Nuzzo, R. G., & Whitesides, G. M., Self-assembled Monolayers of Thiolates on Metals as a Form of Nanotechnology. Chemical Reviews, 2005. **105**(4): p. 1103-1170.

155. Ferrari, A.C., Meyer, J. C., Scardaci, V., Casiraghi, C., Lazzeri, M., Mauri, F., ... & Geim, A. K.., Raman Spectrum of Graphene and Graphene Layers. Physical Review Letters, 2006. **97**(18): p. 187401.

156. Malard, L., Pimenta, M. A. A., Dresselhaus, G., & Dresselhaus, M. S., Raman Spectroscopy in Graphene. Physics Reports, 2009. **473**(5-6): p. 51-87.

157. Wang, H., T. Maiyalagan, and X. Wang, Review on Recent Progress in Nitrogen-Doped Graphene: Synthesis, Characterization, and its Potential Applications. American Chemical Soceity Catalyest. 2 (5), P:781–794 (2012).

158. Wang, Y., Shao, Y., Matson, D. W., Li, J., & Lin, Y.., Nitrogen-Doped Graphene and its Application in Electrochemical Biosensing. American Chemical Society Nano, 2010. **4**(4): p. 1790-1798.

159. Su, W.-J., Chang, H. C., Honda, S. I., Lin, P. H., Huang, Y. S., & Lee, K. Y., Nitrogen Plasma-Treated Multilayer Graphene-Based Field Effect Transistor Fabrication and Electronic Characteristics. Physica E: Low-dimensional Systems and Nanostructures, 2017. **92**: p. 41-46.

160. Jeong, H.M., Lee, J. W., Shin, W. H., Choi, Y. J., Shin, H. J., Kang, J. K., & Choi, J. W., Nitrogen-doped graphene for high-performance ultracapacitors and the importance of nitrogen-doped sites at basal planes. Nano letters, 2011. **11**(6): p. 2472-2477.

161. Rybin, M., Pereyaslavtsev, A., Vasilieva, T., Myasnikov, V., Sokolov, I., Pavlova, A., ... & Obraztsova, E., Efficient Nitrogen Doping of Graphene by Plasma Treatment. Carbon, 2016. **96**: p. 196-202.

162. Stone, H., Sensory evaluation practices. 2012: Academic press.

163. Benetti, F., Fedel, M., Minati, L., Speranza, G., & Migliaresi, C. Gold Nanoparticles: Role of Size and Surface Chemistry on Blood Proteins Adsorption. Journal of Nanoparticle Research, 2013. **15**: p. 1694.

164. Larson-Smith, K. and D.C. Pozzo, Competitive Adsorption of Thiolated Poly (ethylene glycol) and Alkane-thiols on Gold nanoparticles and its Effect on Cluster Formation. Langmuir, 2012. **28**(37): p. 13157-13165.

165. Lombardi, J.R. and R.L. Birke, A unified View of Surface-Enhanced Raman Scattering. Accounts of Chemical Research, 2009. **42**(6): p. 734-742.

166. Chen, L., Yan, H., Xue, X., Jiang, D., Cai, Y., Liang, D., ... & Zhao, B., Surface-Enhanced Raman Scattering (SERS) Active Gold Nanoparticles Decorated on a Porous Polymer Filter. Applied Spectroscopy, 2017: p. 0003702817703293.

167. Wang, Y., Ruan, W., Zhang, J., Yang, B., Xu, W., Zhao, B., & Lombardi, J. R., Direct Observation of Surface‐Enhanced Raman Scattering in ZnO Nanocrystals. Journal of Raman Spectroscopy, 2009. **40**(8): p. 1072-1077.

168. Li, W., Zamani, R., Rivera Gil, P., Pelaz, B., Ibáñez, M., Cadavid, D., ... & Cabot, A., CuTe nanocrystals: Shape and Size Control, Plasmonic Properties, and Use as SERS Probes and Photothermal Agents. Journal of the American Chemical Society, 2013. **135**(19): p. 7098-7101.

169. Alessandri, I., Enhancing Raman Scattering without Plasmons: Unprecedented Sensitivity Achieved by TiO2 Shell-based Resonators. Journal of the American Chemical Society, 2013. **135**(15): p. 5541-5544.

170. Facchetti, A., π-Conjugated Polymers for Organic Electronics and Photovoltaic Cell Applications. Chemistry of Materials, 2010. **23**(3): p. 733-758.

171. Labastide, J.A., Thompson, H. B., Marques, S. R., Colella, N. S., Briseno, A. L., & Barnes, M. D., Directional Charge separation in Isolated Organic Semiconductor Crystalline Nanowires. Nature Communications, 2016. **7**.

172. Zhang, L., Cao, Y., Colella, N. S., Liang, Y., Bredas, J. L., Houk, K. N., & Briseno, A. L.., Unconventional, Chemically Stable, and Soluble two-Dimensional Angular Polycyclic Aromatic Hydrocarbons: from Molecular Design to Device Applications. Accounts of Chemical Research, 2014. **48**(3): p. 500-509.

173. Zang, L., Y. Che, and J.S. Moore, One-dimensional Self-assembly of Planar π-Conjugated Molecules: Adaptable Building Blocks for Organic Nanodevices. Accounts of Chemical Research, 2008. **41**(12): p. 1596-1608.

174. Yilmaz, M., Ozdemir, M., Erdogan, H., Tamer, U., Sen, U., Facchetti, A. & Demirel, G., Micro-/Nanostructured Highly Crystalline Organic Semiconductor Films for Surface-Enhanced Raman Spectroscopy Applications. Advanced Functional Materials, 2015. **25**(35): p. 5669-5676.

175. Gao, X. and Y. Hu, Development of n-type Organic Semiconductors for Thin Film Transistors: a Viewpoint of Molecular Design. Journal of Materials Chemistry C, 2014. **2**(17): p. 3099-3117.

176. Kurinec, S.K. and K. Iniewski, Nanoscale Semiconductor Memories: Technology and Applications. 2013: CRC Press.

177. Macedo, E.R., P.S. Oliveira, and H.P. de Oliveira, Synthesis and Characterization of Branched Polypyrrole/titanium dioxide Photocatalysts. Journal of Photochemistry and Photobiology A: Chemistry, 2015. **307**: p. 108-114.

178. Sultan, A. and F. Mohammad, Chemical Sensing, Thermal Stability, Electrochemistry and Electrical Conductivity of Silver Nanoparticles Decorated and Polypyrrole Enwrapped Boron Nitride Nanocomposite. Polymer, 2017. **113**: p. 221-232.

179. Advincula, R.C., Conducting Polymers with Superhydrophobic Effects as Anticorrosion Coating, in Intelligent Coatings for Corrosion Control. 2014, Elsevier. p. 409-430.

180. Jang, H.Y., S.K. Kim, and S. Park, Electromagnetic Field Enhancement in the Multilayer of Metallic Nanomesh Films: Synthesis and Application as Surface-Enhanced Raman Scattering Substrates. The Journal of Physical Chemistry C, 2015. **119**(19): p. 10585-10591.

181.   Jangid, N.K., Chauhan, N. P. S., Meghwal, K., Ameta, R., & Punjabi, P. B., A review: Conducting Polymers and their Applications. Research Journal of Pharmaceutical, Biological & Chemical Sciences, 2014. **5**(3): p. 383-412.

182.   Yuan, X., Zeng, X., Zhang, H. J., Ma, Z. F., & Wang, C. Y.., Improved Performance of Proton Exchange Membrane Fuel Cells with p-toluenesulfonic Acid-doped Co-PPy/C as Cathode Electrocatalyst. Journal of the American Chemical Society, 2010. **132**(6): p. 1754-1755.

183.   Gupta, S., Hydrogen Bubble‐assisted Syntheses of Polypyrrole micro/nanostructures using Electrochemistry: Structural and Physical Property Characterization. Journal of Raman Spectroscopy: An International Journal for Original Work in all Aspects of Raman Spectroscopy, Including Higher Order Processes, and also Brillouin and Rayleigh Scattering, 2008. **39**(10): p. 1343-1355.

184.   Jones, R.A. and G.P. Bean, The Chemistry of Pyrroles: Organic Chemistry: A Series of Monographs. Vol. 34. 2013: Academic Press.